Structural and dynamical properties of hydrogen in graphene and platinum surface systems

（グラフェン及び白金表面系における水素の
吸着構造と動的挙動に関する理論的研究）

2009

Tanglaw Abat Roman
タングラウ　アバット　ロマン

Division of Precision Science & Technology and Applied Physics
Graduate School of Engineering
Osaka University
大阪大学大学院工学研究科
精密科学･応用物理学専攻

Abstract

This dissertation is an integration of several studies on the hydrogen-graphite and hydrogen-platinum systems, which are standards for reactions relevant in realizing the vision of practical hydrogen fuel systems. The studies I discuss here are carried out *ab initio*, meaning no empirical parameters are employed in the theoretical treatment of the condensed matter systems. Electronic structure calculations here are based on density functional theory, an exact theory for many-body problems which has greatly accelerated not only the understanding of physical/chemical processes at the atomic level, but also the search for new materials and the systematic design of new devices and chemical processes. Total energy calculations parametric in nuclear coordinates were then used as the potential energy term for discussing hydrogen atomic reactions of concern in these studies, in accordance with the Born-Oppenheimer picture.

More specifically, in this dissertation I discuss results on the following: (1) Hydrogen atomic adsorption & clustering on graphene: Among the most stable groups of two/three H atoms, the adsorption per H atom is found stronger as compared with the adsorption of isolated H atoms on graphene, and so favorable cluster formation of H on the graphene surface is ascertained. Results also show that the H-graphene system is an excellent example of substrate effects being much more important, compared with direct adsorbate interaction, in determining the nature of grouping/ordering of adsorbed species on a surface; (2) Effects of adsorbed hydrogen on the electronic states of graphene: The adsorption of hydrogen disrupts the π bonding network of graphene in an extended range – an event that affects the material's reactivity to subsequent hydrogen, and hence promotes cluster formation. A hydrogen atom on graphene is also shown to be easily identified and distinguished from pairs at a very local level through its effects on graphene electronic states near the Fermi level; (3) Graphene two-face hydrogenation and saturation: Calculations for the closest pairing using both faces of graphene suggest not only stronger adsorption, but also barrierless entries for the second as well as all subsequent incoming hydrogen atoms. The ensuing fully hydrogenated material is stable, and has a structure greatly distinct from graphene; (4) H-Pt(111) revisited: Calculated hydrogen states on Pt(111) within three different numerical treatments are discussed.

The ground state of atomic H on Pt(111) was found to have a localized character, physically independent of the PES construction used. All calculations support the low barrier to surface diffusion, as delocalization states start just 32 meV above the ground state for atomic H adsorption, and subsequent delocalized states are not much higher in energy. Results are discussed with relevant experimental data available; (5) The role of lattice defects – vacancies: Application to a hypothetical rough Pt surface is also discussed – a benchmark for understanding the role of vacancies on actual surfaces, which should lie between the two extremes for the Pt surface presented here. The edges of vacancies trap adsorbed H strongly, a factor that leads to increased difficulty of hydrogen diffusion as compared to that on the ideal surface. The hydrogen atom is however still more unlikely to reside at or enter a surface vacancy itself, much more the subsurface; (6) Coadsorbed H and CO interaction on platinum: A clear nonattractive interaction of hydrogen with CO is confirmed, most notably with oxygen, which retains its strong H-repulsive traits in the Pt-bound CO case. Inhibiting effects of CO greater than what is expected from simple adsorption site exclusion are discussed with regard to adsorption/desorption and mobility on platinum, as well as possibilities of surface-bound COH and HCO formation.

Keywords:
graphene, platinum, graphite, graphane, diamond-like carbon, hydrogen, deuterium, adsorption, absorption, cluster formation, diffusion, migration, desorption, substrate-mediated interactions, surface and interface chemistry, quantum effects, heterogeneous catalysis, defects, reconstruction, scanning tunneling microscopy, ab initio/first principles quantum chemical methods and calculations, density functional theory, variation method, hydrogen motion wave functions, saturation, reactivity, modeling, energy storage, fuel cell, renewable energy

Contents

1 Introduction

The biggest scientific challenge of our time is addressing the global climate crisis, and expected to play a crucial role in its solutions is hydrogen. While fossil fuels are expected to be around for some time, the reality of its limited supply and scientifically proven role in climate change are real, current concerns. Considering all available options for replacing oil, the prevalent answer is not unexpected, considering its known advantages: clean, renewable, and potentially a much more efficient source of energy. Hydrogen is the most abundant element in the universe. On our planet, it exists in great quantity as a component of water and organic compounds. It is the simplest, the lightest of all the chemical elements, and it has the unique chemical property of being both an alkali and a halogen. But most importantly, hydrogen is viewed as the major energy source for mobile applications of the future.

The so-called hydrogen economy is a state in which society's everyday energy needs come from that stored through hydrogen, produced for example through the breakdown of water by solar or nuclear power. However, serious hurdles are still present along the road to achieving this vision, as breakthroughs are needed in all key areas of achieving everyday hydrogen-based energy systems: production, storage, and practical utilization of hydrogen fuel. I do not plan to enlighten the reader with solutions by the end of this work, but rather contribute to fundamental knowledge on specific systems that are highly relevant to the theme that is being discussed here.

This dissertation is primarily an integration of several studies of mine on the hydrogen-graphite and hydrogen-platinum systems, which are standards for reactions essential in realizing the vision of practical hydrogen systems, and serve as benchmarks for materials design, for example in the pursuit of alternatives. More precisely, the hydrogenation of graphitic carbon has been seen as a possible storage solution, while platinum and its alloys are currently still the best catalysts for fuel cell related chemical reactions.

As will be discussed in more detail in the proceeding chapters, this area of research isn't what I can consider as groundbreaking as the reader may already be aware that studies concerning the hydrogenation of solid surfaces dates back decades, mostly comprised of experimental work in vacuum environments. However, despite this

long and colorful history of hydrogen-surface interactions, I believe a lot of details are still left unclear, and continuing developments in the field offer more questions that require theoretical work in finding answers. In the case of the physical systems I am focusing on for example, the clustering of hydrogen on graphene and its subsequent saturation has not yet been fully understood, which is why in the past five years this has been a very active topic of research for several materials research groups across the globe. On the side of transition metals, detailed examinations of the hydrogenation of surface vacancies and coadsorbed interaction of H with CO from the theoretical side are surprisingly very much lacking, considering that these are two very fundamental topics in understanding real situations for catalytic reactions on Pt. Along with their significance beyond academic understanding, these topics have hence been natural choices for me to tackle in my graduate school research.

The initial motivation for the works that I discuss is in line with hydrogen-based energy technology. However, I would like to emphasize that the applications covered by this research are numerous. Hydrogen in amorphous and diamond-like carbon has for example been studied for the tribological properties of the system, and studies on hydrogenation-dehydrogenation processes on graphitic surfaces have been fueled by the need to understand reactions in interstellar media. Also, the inherent lightness and reported high hydrogen uptake of carbon materials have led to much interest in using this class of materials in hydrogen-powered vehicles, and the recent attention given to graphene for novel carbon-based nanoscale devices has revived interest in the chemical modification of this carbon material. Furthermore, on a more academic perspective, hydrogenation of graphene is one direct bridge that links concepts in organic chemistry with the possibilities in solid state engineering. Platinum on the other hand, while not as hot a topic as today's two dimensional carbon sheets, it is still one of most recognized components of catalysts for processes involving hydrocarbons and water, and so I expect that valuable insights should be obtained from the more fundamental investigations discussed here. In short the availability of a considerable amount of experimental data and exciting, ongoing developments in these areas make these materials fertile ground for further theoretical surface science work.

This dissertation is organized as follows. In Chapter 2, a brief write-up on the background of the computational methods and approximations used in this study is

presented. The studies heavily involve electronic structure calculations based on density functional theory, from the determination of stable structures, to the analyses of surfaces states, to the creation of potential energy surfaces needed for further work on a more detailed description of adsorbate motion. In Chapter 3, I try to answer the question of how the steps to graphene saturation with hydrogen look like. I discuss physical mechanisms that lead toward the conversion of graphene into its fully-hydrogenated counterpart – a material which possesses properties closer to that of diamond than graphene. I firstly discuss stability trends in small clusters of adsorbed hydrogen, as well as surface structure and concurrent reactivity changes for graphene one-face and two-face hydrogenation. Effects of adsorbed hydrogen on graphene electronic states, which are essential to adsorbed hydrogen structure discrimination, are also discussed.

In a markedly distinct yet related focus, in Chapter 4, I discuss some open topics regarding the role of defects (vacancies) and unwanted coadsorbates (CO poisoning) on platinum surface-bound hydrogen atoms, topics which provide a more general picture of processes valuable to many catalytic reactions. Quantum states describing hydrogen motion were determined from wave functions expressed as a linear combination of a uniformly distributed set of Gaussian-type orbitals spanning the space within the vicinity of the topmost layer of Pt atoms, using an independent hydrogen approximation in an external periodic potential brought about by the frozen solid surface. Revisiting the clean, ideal surface was done not only to provide the standard to which I compare in my results regarding the effects of defects and coadsorption, but also as a tool to discuss previously reported data on this topic. Key findings are summarized at the end.

2 Theoretical background

2.1. Many-body systems and the adiabatic approximation

The purpose of this chapter is to provide the reader of this work with some brief explanations on (1) the theoretical concepts in which the calculations in this dissertation are based on, and (2) the approximations that are usually made in the implementation of the theory in order to minimize computational costs without sacrificing physical accuracy. Investigating the dynamics of chemical reactions, or determining the electronic structure of atomic, molecular, or large condensed matter systems *ab initio* (i.e., solely from fundamental physical principles, without empirical data) entails solving the many-body Schrödinger equation

$$\hat{H}\Phi = E\Phi \tag{2.1}$$

where the wave function Φ is a function of real space coordinates of the individual particles comprising the physical system:

$$\Phi\left(\mathbf{r}_1,...\mathbf{r}_N;\mathbf{R}_1...\mathbf{R}_M\right) \tag{2.2}$$

Here, the atomic nuclei are located in positions denoted by $\mathbf{R}_I$, while the positions of the electrons are given by $\mathbf{r}_i$ in a system with 3(N+M) degrees of freedom. The many-body Hamiltonian is given by

$$\hat{H} = \hat{T}^{Nuc} + \hat{T}^{el} + \hat{V}^{Nuc-Nuc} + \hat{V}^{Nuc-el} + \hat{V}^{el-el} \tag{2.3}$$

where the individual terms, expressed in Gaussian units for notation simplicity, are given by

$$\hat{T}^{Nuc} = -\sum_{I=1}^{M}\frac{\hbar^2}{2\mu_I}\nabla_I^2 \tag{2.4}$$

$$\hat{T}^{el} = -\frac{\hbar^2}{2m}\sum_{i=1}^{N}\nabla_i^2 \tag{2.5}$$

$$\hat{V}^{Nuc-Nuc} = \sum_{I<J}\frac{Z_I Z_J e^2}{\left|\mathbf{R}_I-\mathbf{R}_J\right|} = \frac{1}{2}\sum_{I\neq J}\frac{Z_I Z_J e^2}{\left|\mathbf{R}_I-\mathbf{R}_J\right|} \tag{2.6}$$

$$\hat{V}^{Nuc-el} = -\sum_{I,i}^{M,N}\frac{Z_I e^2}{\left|\mathbf{R}_I-\mathbf{r}_i\right|} \tag{2.7}$$

$$\hat{V}^{el-el} = \sum_{i<j}\frac{e^2}{\left|\mathbf{r}_i-\mathbf{r}_j\right|} = \frac{1}{2}\sum_{i\neq j}\frac{e^2}{\left|\mathbf{r}_i-\mathbf{r}_j\right|}. \tag{2.8}$$

Here, capital letter indices are labels for atomic nuclei, while small letters are for electrons. Also, ∇_I^2 represents the Laplacian with respect to nucleus *I* whose mass is μ_I, while ∇_i^2 is the Laplacian with respect to the electron *i*, whose mass is *m*.

The main problem with this approach in studying a system of atoms is that in almost all cases, with the exceptions being the simplest, obtaining exact solutions of the Schrödinger equation is not possible. In this view, reasonable approximations have to be implemented. The Born-Oppenheimer approximation springs from the fact that the atomic nuclei are much heavier, and slower, than the electrons. This allows us to say that the nuclei are nearly fixed with respect to electron motion. Reactions in which this approximation is valid are commonly referred to as electronically adiabatic. This situation then provides logical bases to separate the electronic degrees of freedom for any given fixed configuration of atomic nuclei, giving Eq. (2.9) which shows the case in which the electronic wave function is solved parametrically on the nuclear coordinates $\mathbf{R}_I$:

$$\hat{H}^{el}\left(\{\mathbf{R}_I\}\right)\Psi\left(\mathbf{r}_i,\{\mathbf{R}_I\}\right)=E^{el}_{\mathbf{R}_I}\left(\{\mathbf{R}_I\}\right)\Psi\left(\mathbf{r}_i,\{\mathbf{R}_I\}\right) \tag{2.9}$$

$$\hat{H}^{el}\left(\{\mathbf{R}_I\}\right)=\hat{T}^{el}+\hat{V}^{Nuc-Nuc}_{\mathbf{R}_I}+\hat{V}^{Nuc-el}_{\mathbf{R}_I}+\hat{V}^{el-el} \tag{2.10}$$

Next, according to the Born-Oppenheimer method $E^{el}\left(\mathbf{R}_I\right)$ is used as a potential energy function to examine the nuclear motion. That is, we set up a Schrödinger equation of the form

$$\left[\hat{T}^{Nuc}+E^{el}\left(\mathbf{R}_I\right)\right]\xi\left(\mathbf{R}_I\right)=E^{Nuc}\xi\left(\mathbf{R}_I\right) \tag{2.11}$$

In this dissertation, the term $E^{el}\left(\mathbf{R}_I\right)$ in (2.11) is called the *potential energy surface* (PES), which is very useful, for example, in determining activation barriers and finding optimum reaction paths in chemical reactions. While called a 'surface', the PES obviously is not limited to a dependence of only two variables (for a one-dimensional dependence on nuclear motion, the term potential energy curve is frequently used). One specific way of investigating atomic motion by solving (2.11) is discussed in Chapter 4.

While separately treating the electronic from the nuclear degrees of freedom has been shown to be a very convenient tool in a lot condensed matter systems, there is still the hurdle of obtaining the eigenvalues and wave functions of the electronic system in (2.9), for any frozen configuration of the nuclear coordinates $\mathbf{R}_I$. Even

with this simplification, the many-body problem remains an arduous task. While obtaining the Schrödinger wave functions for a system of few electrons using traditional wave function methods is tractable [1], the exponential increase in computational expenses renders dealing with more complex systems impractical considering the computational costs involved. It is in this light that alternative treatments for studying condensed matter systems have been sought even long after the onset of wave mechanics. One alternative which showed early promise (but did not gain popularity until a series of developments to the theory) revolved on a simple premise: that knowledge of the ground-state density for an electronic system uniquely determines the system.

2.2. Total energy calculations for many-electron systems

The topics that are discussed in this dissertation are theoretical/computational in nature, being largely rooted on density functional theory (DFT) [2, 3], a concept whose mathematical formalism was established in the 1960s and has greatly accelerated not only the understanding of ground state properties of many body systems and physical/chemical processes at an atomic level, but also the search for new materials and the systematic design of new devices and desired chemical processes. Under this theory, a many-electron problem uses the electronic density $n(\mathbf{r})$ (i.e., the number of electrons per unit volume) as its fundamental variable, instead of the wave function. In my studies, stable physical structures, electronic/magnetic properties, and multidimensional reaction energetics are some of the key results which I have obtained based on density functional theory. Aside from the topics covered in this thesis, some of my work which have used density functional theory include investigations on physical properties of systems involving carbon nanotubes [4-8], analyses of chemical interactions at materials interfaces [9-14], computational materials design for energy and spintronics applications [15-17], as well as the dynamics of transition metal surface abstraction/etching reactions [18-23].

In a nutshell, density functional theory states that if the ground state charge density is known for any given system of atoms, the external potential and the number of electrons can be known, and hence the full Hamiltonian H. The density $n(\mathbf{r})$ thus implicitly determines all properties derivable from H through the solution of the

time-independent or time-dependent Schrödinger equation. This conclusion arises from the straightforward proof of Hohenberg and Kohn [2] that the external potential $V(\mathbf{r})$ is uniquely determined, within a trivial additive constant, by $n(\mathbf{r})$. The same paper also established an analogous variational principle: the variational principle in quantum mechanics states that for any normalized trial wave function, the expectation value of the Hamiltonian for this wave function must be greater than or equal to the actual ground state energy. It was shown that the energy functional assumes its minimum value for the correct $n(\mathbf{r})$. Hence, combining this with the fact that the total energy of an electron gas, including exchange and correlation, is a unique functional of the electron density, we then have

$$E_{tot}^{el}[n] = \min_{n(\mathbf{r})} E[n] = \min_{n(\mathbf{r})} \left(T[n] + V_{ext}[n] + V_H[n] + E_{xc}[n] \right) \tag{2.12}$$

or more explicitly,

$$E_{tot}^{el}[n] = T[n] + \int d\mathbf{r}\, v_{\mathbf{R}_I}(\mathbf{r}) n(\mathbf{r}) + \int d\mathbf{r} \int d\mathbf{r}' \frac{e^2 n(\mathbf{r}) n(\mathbf{r}')}{2|\mathbf{r}-\mathbf{r}'|} + V_{\mathbf{R}_I}^{nuc-nuc} + E_{xc}[n] \tag{2.13}$$

.

The total energy of an electron gas, including exchange and correlation E_{xc} as defined in Eq. (2.13), is a unique functional of the electron density. Kohn and Sham in a subsequent paper showed how it is possible, formally, to replace the many-electron problem by an exactly equivalent set of self-consistent one-electron equations by extracting the Hartree equations [24] from the variational principle for the energy functional:

$$n(\mathbf{r}) = \sum_{j=1}^{N} |\psi_j(\mathbf{r})|^2 \tag{2.14}$$

$$\left[-\frac{\hbar^2}{2m} \nabla^2 + v_{eff}(\mathbf{r}) \right] \psi_j(\mathbf{r}) = \varepsilon_j \psi_j(\mathbf{r}) \tag{2.15}$$

$$v_{eff}(\mathbf{r}) = v_{ext}(\mathbf{r}) + \int \frac{n(\mathbf{r}')}{|\mathbf{r}-\mathbf{r}'|} e^2\, d\mathbf{r}' + \frac{\delta E_{xc}[n]}{\delta n}(\mathbf{r}) \tag{2.16}$$

where the integral in (2.16) is the Hartree energy $v_H(\mathbf{r})$ and the final term is the exchange-correlation potential $v_{xc}(\mathbf{r})$. While the Pauli exclusion principle is an integral part of the method, the problem with Hartree theory is that it treats *noninteracting* electrons moving in the external potential v_{eff}, i.e., neglecting quantum statistics. Not only do the Kohn-Sham equations (2.14) to (2.16) show a more general picture from Hartree theory, but the set also presents a tractable tool for

an exact theory, since knowledge of the exact $E_{xc}[n]$, in principle, includes *all* many-body effects. This term takes into account the *exchange energy*, which is the reduction in the energy of the electronic system due to the antisymmetry of the wave function, and the *correlation energy*, which is defined as the remaining difference with the exact many-body energy of the system (i.e., all other contributions beyond Hartree-Fock), brought about by electronic correlations not yet taken into account by the inclusion of the exchange term, like that due to spatially separated electrons of opposite spins. I must add that in some definitions the correlation energy is comprised of both the exchange energy defined above and the remaining error in energy (i.e., all other energy terms beyond the Hartree model).

As mentioned earlier from the discussion on the Hohenberg-Kohn variational principle, the immediate goal is finding the ground state electron density. Computationally, this can be achieved by simply iterating the Kohn-Sham equations until self-consistency is achieved – a process more clearly explained through the flowchart shown in Fig. 2.1.

In contrast to the Hartree and Hartree-Fock approximation, the ground-state energy (2.13) is exact. However, for an arbitrary $n(\mathbf{r})$, one can give no simple exact expression for $E_{xc}[n]$, and so the reliability of any practical implementation of density functional theory crucially depends on the accuracy of the expression for the exchange-correlation functional. What is exactly calculable is the exchange-correlation energy for the spatially homogeneous electron gas, i.e., for the case in which $n(\mathbf{r})$ is the same at all $\mathbf{r}$. This is exactly what is done in the simplest representation for $E_{xc}[n]$: the so-called local density approximation (LDA),

$$E_{xc}^{LDA}[n] = \int \varepsilon_{xc}^{LDA}\left(n(\mathbf{r})\right) n(\mathbf{r})\, d\mathbf{r} \tag{2.17}$$

where at any point $\mathbf{r}$, the local exchange-correlation energy of the *homogeneous* electron gas is used for the corresponding electron density, ignoring the general nonlocality of the true exchange-correlation energy. This crude approximation not surprisingly leads to significant differences of predicted values when compared with experimental data, a common example being the known overbinding flaw of LDA. The next significant attempt to improve $E_{xc}[n]$ comes from the generalized gradient approximations (GGA) [25-27], implemented in light of knowing that any real system has a spatially varying density $n(\mathbf{r})$, and so it would clearly be useful to also

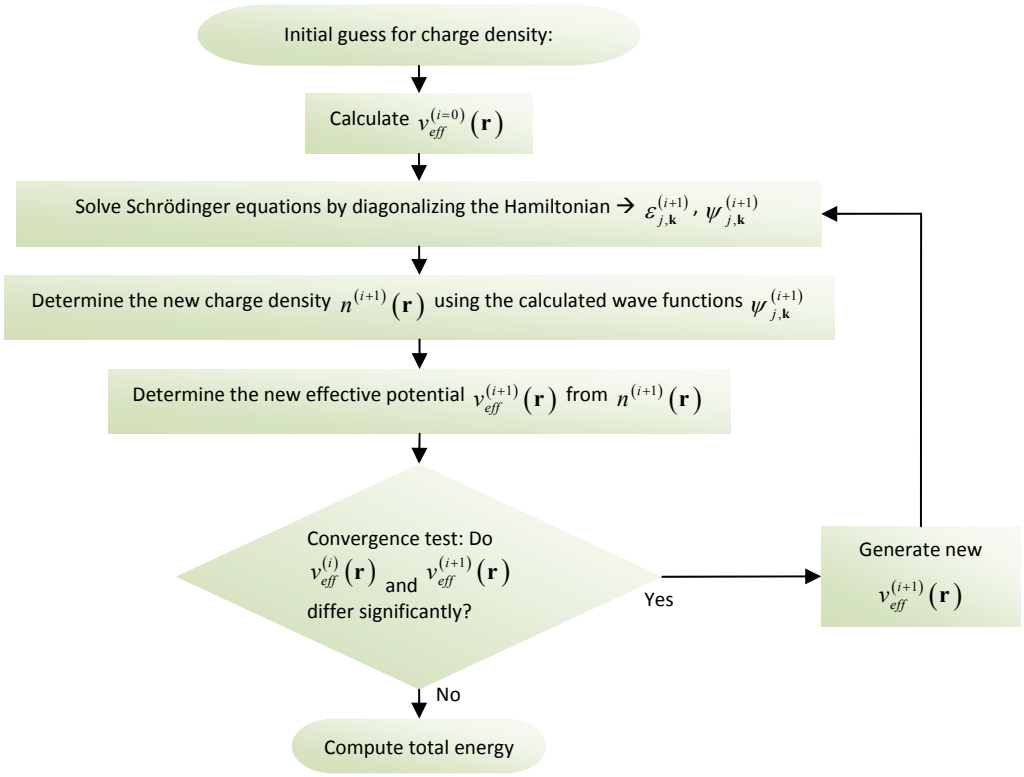

Fig. 2.1. Flowchart for the self-consistent calculation of the ground state electron density using the Kohn-Sham equations.

include information on the rate of this variation. Here, the value of the exchange correlation potential at a point **r** depends not only on the value of the density at **r**, but also on its variation close to **r**, taken into account through systematic gradient expansions:

$$E_{xc}^{GGA}[n] = \int \varepsilon_{xc}^{GGA}\left(n(\mathbf{r}), |\nabla n(\mathbf{r})|\right) n(\mathbf{r})\, d\mathbf{r} \qquad (2.18)$$

In general, GGA improves on LDA in terms of predicting binding energies and structure geometries. GGA was particularly found to be better than LDA in hydrocarbon systems and in transition metals in general, hence my choice of GGA for the exchange-correlation energies in the computations in this work. However, failures of both the LDA and current available GGA implementations in predicting some band gaps for example, especially in strongly correlated electron systems, are the reasons why improving the term $E_{xc}[n]$ is still an active area of research in condensed matter theory as of the time of writing of this paper. This is however beyond the scope of this thesis. In the next section, some specific points in the

practical implementation of density functional theory for studying crystalline systems are discussed.

2.3. Implementing density functional theory in condensed matter systems

Over popular cluster implementations which commonly use a basis set of Gaussian orbitals [28], I have chosen to use supercell implementations of Fig. 2.1 for the studies that are discussed in the proceeding chapters. In the calculations, one of the main concerns of anyone using density functional theory is how to minimize computational cost (i.e., minimizing the amount of hardware and time used) without compromising the accuracy of the calculated physical properties of the system being studied. There are many other tools that are useful in implementing density functional theory in periodic systems, but in this section I only deal with the most important methods that are currently being used by theoretical surface scientists.

Since a supercell implementation is periodic in three dimensions, the only way to get around this for modeling surfaces (which are two-dimensional) is to use infinitely repeating, periodic slabs of atoms with vacuum layers separating the slabs large enough in order to avoid significant interaction between slab images. Of course, the slabs should also be thick enough (for example, five or more atomic layers for transition metal surfaces) to accurately represent a material's surface. In general, the asymmetry in surface-adsorbate systems creates a net dipole moment in the direction of the surface normal, and causes the energy to converge slowly with respect to the size of the super cell. This is where the use of dipole corrections [29, 30] is beneficial. Moving away from the surface normal, caution must also be exercised in choosing the unit cell size along lateral directions in order to avoid unwanted interactions between adsorbate images, for example, or even longer-ranging substrate-mediated interactions. Of course the disadvantage for surface unit cells would be the increase in atoms, hence much more hardware-demanding and time-consuming calculations. Finally, I would like to point out that for consistency, the surface normal direction is always oriented along the z direction for the studies discussed in this dissertation.

An alternate statement of Bloch's theorem asserts that for an electron in a periodic potential (which is an intrinsic property of the supercell approach to DFT), the

electronic wave functions at each **k** point can be expanded in terms of a discrete plane-wave basis set, as in

$$\psi_{j,\mathbf{k}}(\mathbf{r}) = \sum_{\mathbf{G}} c_{\mathbf{k}+\mathbf{G}} e^{i(\mathbf{k}+\mathbf{G})\cdot\mathbf{r}} \tag{2.19}$$

where **G** is a reciprocal lattice vector and **k** is set to lie within the first Brillouin zone, noting that any given wave vector **q** in all of the reciprocal space can be represented by an appropriate **k** differing by a reciprocal lattice vector. Substituting (2.19) into Eq. (2.15) and taking the inner product, the Kohn-Sham eigenvalue equation in the plane-wave representation becomes

$$\sum_{\mathbf{G}'} \left[\frac{\hbar^2}{2m} |\mathbf{k}+\mathbf{G}|^2 \delta_{\mathbf{G}\mathbf{G}'} + v_{eff}(\mathbf{G}-\mathbf{G}') \right] c_{j,\mathbf{k}+\mathbf{G}'} = \varepsilon_j c_{j,\mathbf{k}+\mathbf{G}} \tag{2.20}$$

In principle, an infinite plane-wave basis set is required in expanding the electronic wave functions. However, the coefficients $c_{j,\mathbf{k}+\mathbf{G}'}$ for the plane waves with small kinetic energy $\left(\hbar^2/2m\right)|\mathbf{k}+\mathbf{G}|^2$ are more important than those with large kinetic energy. Knowing this, the size of the matrix can be reduced, up to a certain kinetic energy *cutoff* for the plane waves which defines the size of the matrix to be setup for diagonalization. Numerical convergence for the basis set often refers to the point in which physical properties such as the binding energy of a system does not change significantly (say, to within 0.01 eV) even if the plane wave cutoff is increased.

However, an extremely large plane wave basis set would still be required to perform an all-electron calculation, especially in order to accurately take into account the tightly-bound core orbitals. In order to be able to further reduce computational expenses, *pseudopotentials* have been introduced. The concept of pseudopotentials is simply based on the well-known observation that the physical/chemical properties of solids are dependent on the valence electrons to a much greater extent than on the core electrons. The pseudopotential approximation exploits this fact by removing the core electrons and by replacing them and the strong ionic potential with a weaker pseudopotential v^{ps} that acts on a set of pseudo wave functions ψ^{ps} rather than the true valence wave functions ψ^{v}, giving

$$\left[-\frac{\hbar^2}{2m}\nabla^2 + v^{ps}(\mathbf{r}) \right] \psi^{ps}_{j,\mathbf{k}}(\mathbf{r}) = \varepsilon^{v}_{j} \psi^{ps}_{j,\mathbf{k}}(\mathbf{r}) \tag{2.21}$$

Asymptotically, a pseudopotential should be able to correctly reproduce the long-range interaction of the core. Outside the core region of radius r_c, a good

pseudopotential should exactly match the all-electron ionic potential, and ψ^{ps} should coincide with the full wave function. Smooth, weakly oscillating pseudopotentials are ideal since these would require less Fourier coefficients, and consequently a lower cutoff energy. This property of a pseudopotential is often referred to its *softness*, and very soft ("ultrasoft") pseudopotentials [31] can be created that enable a dramatic reduction in size of the basis set.

Under the Born-von Karman boundary conditions for any given bulk crystal, the density of allowed **k** points is proportional to the volume of the crystal. For infinite periodic systems, the infinite number of **k** points thus ideally requires integration over the first Brillouin zone, over all occupied energy bands, in determining the total energy of a crystal. Some ways have been devised in order to avoid calculating electronic states at too many (infinite!) **k** points, based on the fact that the electronic wave functions at **k** points that are very close together are almost identical. Thus only a finite number of these "special" **k** points are required, belonging to sets more concretely defined in Refs. [32, 33], and have been shown to approximate the full integration rather accurately. Numerical convergence with respect to **k** point sampling refers to the point where physical properties such as the binding energy of a system do not change significantly even if the number of **k** points is increased.

There is still a number of details and related topics that can be added into the present discussion, but what I have just briefly gone through should already cover most of the underlying theory for the portions in the proceeding chapters related to electronic structure calculations.

3 Hydrogen on graphitic carbon

3.1. Background

Graphene is an atom-thin sheet of sp^2-bonded carbon atoms. Its most basic unit cell has a basis of two carbon atoms, with lattice constants of length 2.462 Å separated by a 60° angle, creating what's usually known as a two-dimensional honeycomb structure of atoms since the bonding network resembles the structure which honey bees build. Considered the limit for large aromatic molecules, graphene has recently gained a lot of attention for its unique physical properties, being one of the best two-dimensional materials that physicists can use to test theories. In relation to other carbon allotropes, *carbon nanotubes* are simply rolled graphene sheets, while the stable material that is formed by an ordered stacking of these sheets is *graphite*. As shown in Fig. 3.1, the most stable three-dimensional structure is a Van der Waals-bonded alternating stacking of graphene sheets, which

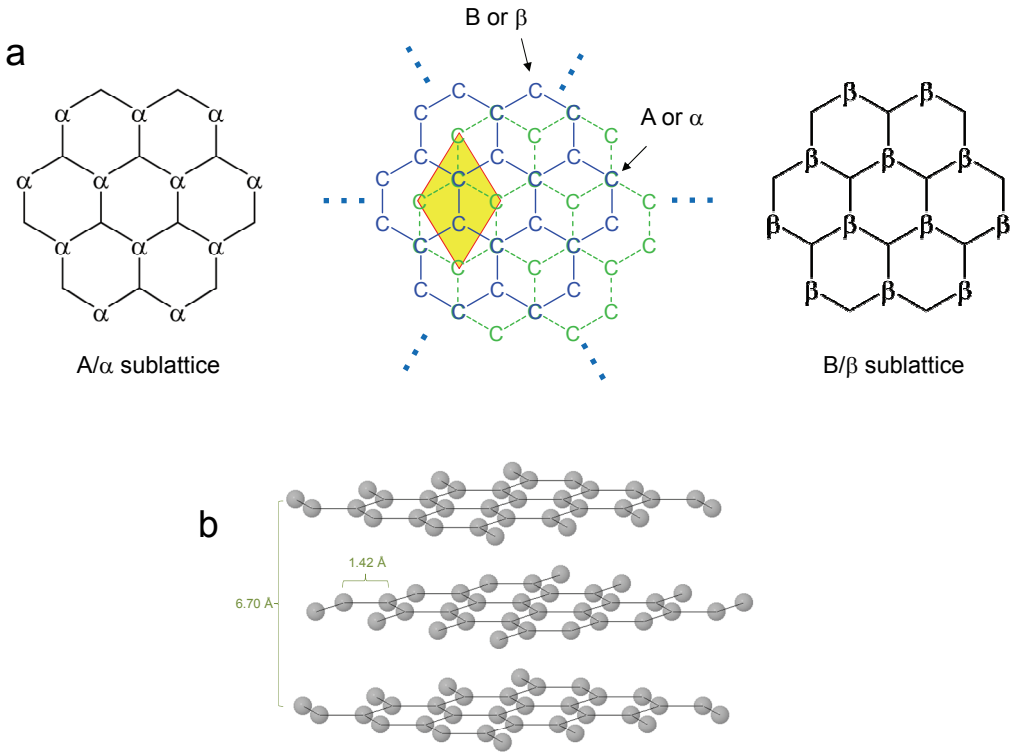

Fig. 3.1. (a) sublattices in graphite sheets. (b) ABAB stacking of graphene sheets in the bulk graphite structure. A primitive cell is drawn in the center panel of (a).

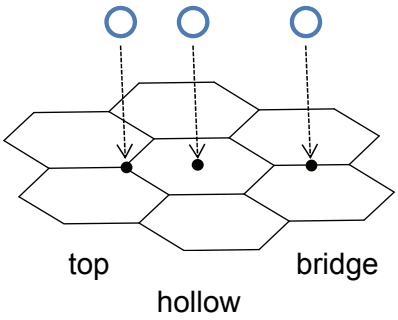

Fig. 3.2. High-symmetry sites on graphene

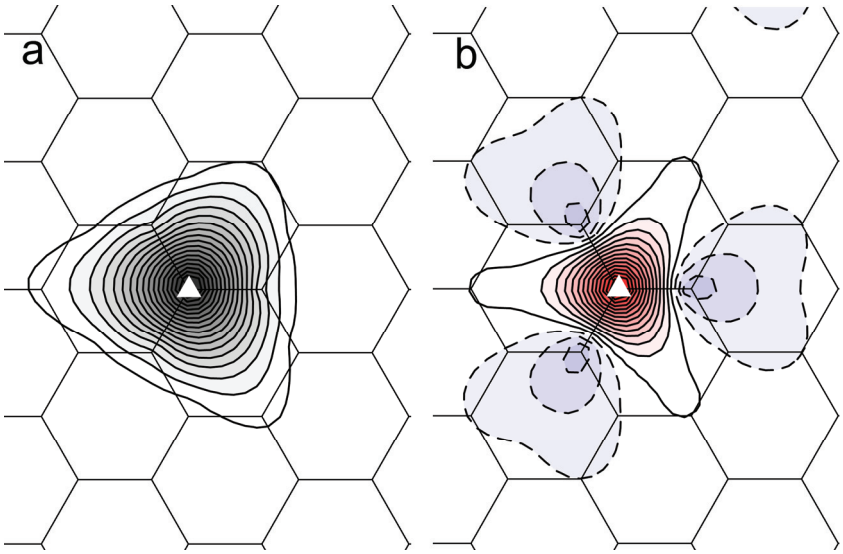

Fig. 3.3. Contour maps describing adsorbed H-induced graphene reconstruction. (a) displacement of C atoms from the original graphene plane, and (b) local planar distortion. For (b), dashed (solid) contours indicate downward (upward) local planar distortion. Contours are separated by 0.02 Å. Positions of H atoms are marked by the white triangles.

inevitably leads to physical differences between the two sublattices of graphene (here noting once again the basis of two carbon atoms).

My primary motivation in investigating hydrogen in carbon systems is realizing high hydrogen uptakes on surfaces for practical hydrogen storage in solid-state materials. In order to achieve this, it is always beneficial to know how the road to adsorption saturation on the surface looks like in terms of the physical mechanisms involved, and how one can control required reactions given this knowledge. Much theoretical and experimental work has been done globally in this area in the past

decade, and in this study I revisit some key concepts that I have reported in the past few years. This study discusses systems involving hydrogen in chemisorbed states on graphene, which have been studied with density functional theory. I outline my recent findings crucial to understanding graphene defects brought about by hydrogen, which serves as a benchmark for covalently-adsorbed species on the carbon surface. Emphasis is given to the underlying mechanisms related to the growth of defect structures, which have been shown to drastically change the properties of graphene.

3.2. Hydrogen atom adsorption & clustering on graphene

Investigations on the physical/chemical modification of graphene by the addition of adsorbed species on one or both faces of graphene have been carried out for a wide range of reasons. Reactions with NO and NH_3, for example, have been studied for sensing applications, while studies involving adsorbed metals have been carried out in light of addressing the demands of post-silicon electronics. On the latter, recent studies [34-37] have predicted the tendency of metal atoms to attach onto graphene through the hexagonal C ring centers (i.e., the hollow sites, Fig. 3.2), with binding energies ranging from about 0.1 to 2.0 eV. It was shown that strong changes in the carbon sheet's properties can indeed be induced by such attachments to graphene, the extent dependent on the bonding mechanisms involved.

In the case of hydrogen, an atom approaching graphene preferentially ends up at top sites, i.e., H prefers single-coordination, and given appropriate time to relax, it reaches a very stable chemisorbed state, albeit having to go through a barrier of about 0.2 eV [38]. This barrier arises from the need to disrupt C-C bonds (which raises the system energy) in the process of creating a stable C-H bond (which lowers the system energy). Reported H atom adsorption energies vary slightly across computational studies (roughly in the range of –0.6 to –0.8 eV, the negative sign denoting adsorption exothermicity), the values primarily depending on how isolated the H atom is treated on graphene. Bridge-site adsorption is endothermic (~0.1 eV), while the hollow-site is not a local energy minimum for the H atom on graphene. The chemisorption is associated with the receiving carbon atom being pulled out by about 0.33 Å from the initial planar geometry of graphene. Reconstruction due to the adsorption of a single H atom is however not limited to the receiving C atom, as clearly described in Fig. 3.3(a), which plots the displacement of C atoms from the original graphene plane along *z*, taken to be the direction normal to the graphene

plane. Local planar distortion, which is the distance a C atom moves out of the plane determined by its three nearest neighboring C atoms, is shown in Fig. 3.3(b). It becomes apparent that C-C bonds within a certain range of the adsite are strained out of their initial planar geometries in order to minimize the energy of the system. Even longer ranging is the H atom's effects on the graphene electronic states – but let's firstly consider the behavior of small groups of hydrogen adsorbed on graphene, starting with hydrogen pairs.

Stable hydrogen molecule adsorption on graphene [39] requires molecular dissociation. Breaking up the incoming molecules requires a large amount of energy (in particular, the H_2 binding energy from my calculations is 4.48 eV), but graphene reconstruction reduces the barrier to reaching stable adsorbed states to about 3.3 eV. The configuration with atoms attaching to opposite corners of a graphene hexagon (i.e., in the para configuration) was found to be the most stable configuration for an adsorbed pair, and from the constructed potential energy surface was additionally found to be the most accessible.

On the experimental side, Zecho et al. characterized graphite basal plane-adsorbed hydrogen, verified with electron energy loss spectra and reasonable agreements with density functional theory calculations [40]. Prominent peaks from thermal desorption spectroscopy (TDS) measurements were furthermore confirmed to be contributions from adsorbed deuterium (D) atoms at terraces [41]. Analyses of the spectra through numerical simulations of first order desorption kinetics suggest from the separate TDS profile contributions the presence of relatively solitary adsorbed deuterium atoms, close-pairing deuterium dimers, and mixtures of these on the graphite surface. Very recent scanning tunneling microscopy (STM) measurements [42, 43] confirm this, in particular showing four distinct pair configurations on graphene. Adsorbed clusters of four hydrogen atoms ordered along the perimeter of a graphite hexagon, in addition to the presence of pairs, have furthermore been proposed from a comparison of high-resolution electron energy loss spectroscopy with simulated vibrational spectra [44].

Understanding the stability of small groups of hydrogen adsorbed on graphene is fundamental in tracing succeeding steps to achieving levels of saturation. It is with this motivation that the stability of adsorbed two-hydrogen [45] and three-hydrogen [46] clusters on graphene were investigated. Geometries for these clusters, which span H-H separations approximately within the bounds of two graphitic hexagons,

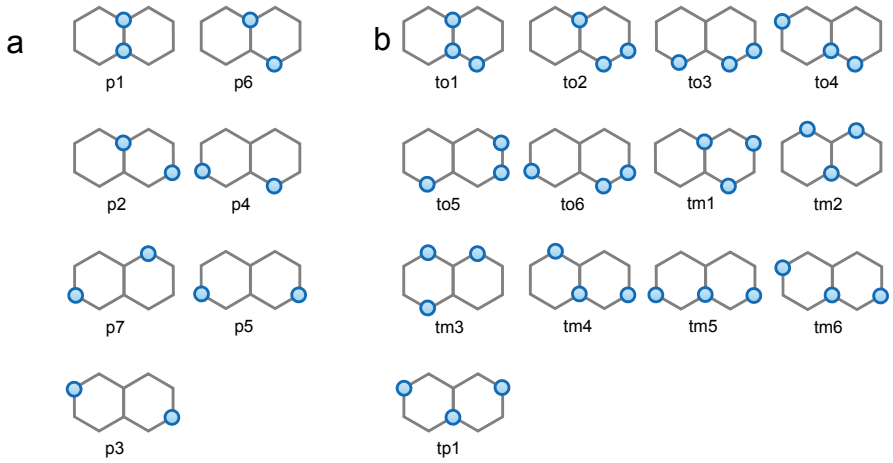

Fig. 3.4. Closest-packing hydrogen clusters: (a) seven pairs, and (b) thirteen trios adsorbed on one face of graphene.

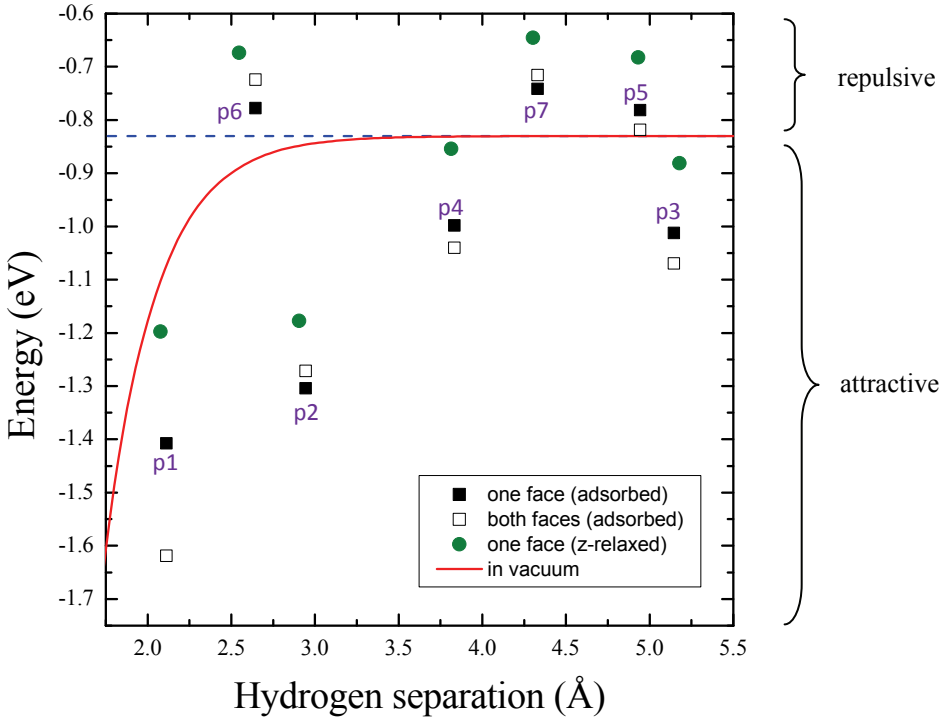

Fig. 3.5. Adsorption energy per H atom of single face-adsorbed two H clusters (E_{ads} = ½[$E_{gr+2H(ads)}$ − (E_{gr} + 2$E_{H(g)}$)]), plotted against hydrogen atom separation. The reference dashed line (E_a = –0.83 eV) corresponds to the binding energy of an isolated hydrogen adatom on graphene. The solid red line shows the interaction of two H atoms in a vacuum, i.e. the formation/dissociation of H_2 far from the graphene surface, adjusted to the above-mentioned energy reference. Both single-face and both-face pairings are shown (squares), as well as results of partially constrained optimization calculations which were published in Roman et al., Carbon 45 (2007) 218 (circles).

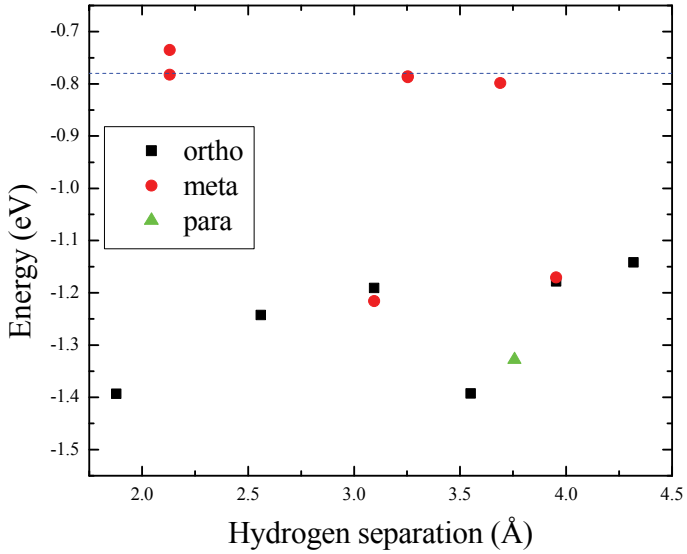

Fig. 3.6. Adsorption energy of a three-H cluster (per H atom, single face, E_{ads} = ⅓[$E_{gr+3H(ads)}$ − (E_{gr} + 3$E_{H(g)}$)]) plotted against hydrogen separation. The reference dashed line (E_a = –0.77 eV) corresponds to the binding energy of an isolated hydrogen adatom on graphene. Hydrogen separation in this case is defined as the distance of the third H atom from the center of its component (ortho/meta/para) pair.

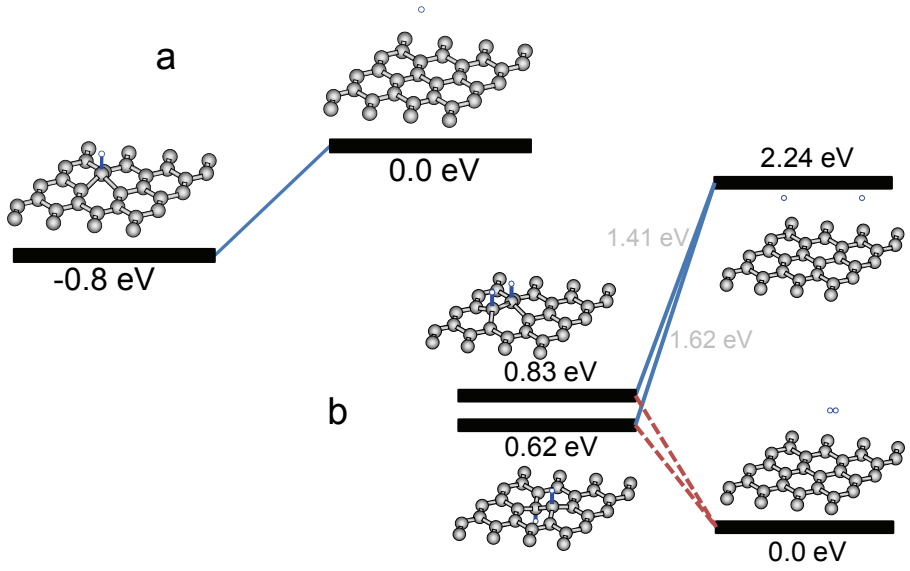

Fig. 3.7. Energy/stability of adsorbed H atoms/molecules: (a) atomic H adsorption on graphene, (b) adsorbed pair formation from two H atoms or from a H_2 molecule.

are shown in Fig. 3.4, and the corresponding adsorption energies for the adsorbed pairs and trios are shown in Figs. 3.5 and 3.6, respectively. Schematics comparing single atom adsorption with that of pair adsorption from H atoms/an H_2 molecule are shown in Fig. 3.7. Reference energies for adsorbed, but individually isolated H

atoms, are indicated by the broken lines in Fig. 3.5 and 3.6. Asymptotically – that is, as hydrogen separation approaches infinity – I expect all three plots to merge into this reference level. Hydrogen atoms in a vacuum merge into this reference at around 4.0 Å separation. The fact that the data points in the graphs deviate from the reference levels shows the non-negligible clustering effects even at large interatomic separations.

Results shown here were obtained from unconstrained structure optimization calculations. Differences in the employed supercell size led to slight differences in isolated H atom adsorption energy. For the hydrogen pair stabilities, structural optimization calculations were performed using the Dacapo code [31, 47], which implements a supercell approach to density functional theory, using ultrasoft pseudopotentials for the frozen atom cores. I used a 400 eV cutoff for the expansion of the one-electron wave functions, and the generalized gradient approximation [12] for the electronic exchange-correlation term. The Brillouin zone was sampled using a 4×4×1 grid through the Monkhorst and Pack scheme [33]. In general I expect hydrogen on solid surfaces to have non-negligible magnetic properties, which is why calculations here and for most of this dissertation are spin-polarized. A pair of hydrogen atoms on 32 substrate carbon atoms comprise the unit cell ("isolated" adsorbed atoms were treated at half the coverage), using a single, isolated graphene sheet with C-C nearest neighbor distances of 1.42 Å and a 15 Å vacuum separating sheets in the periodic supercell scheme. While surface reconstruction was extensive in terms of the substrate area affected, it is most prominent within the immediate vicinity of the adsorbed hydrogen atoms. The carbon atoms closest to the attached hydrogen (i.e. the receiving carbons) expectedly pucker up the most, moving to positions up to around 0.8 Å above the lowest-lying substrate atoms. Note that pairs p1, p2 and p6 are similar to the T-B-T, T-H-T, and T-C-T final geometries of Ref. [39], respectively. The pairs have been labeled in decreasing order of adsorption strength. Stable hydrogen pair positions obtained after geometry optimization only slightly differ (<0.1 Å increase in H-H separation) from the exact on-top positions shown in the figure, save for pair p1 where the repulsion is much stronger.

For the trimer stabilities, stable hydrogen adsorption configurations were determined through geometry optimization calculations using the VASP code [48], which implements the projector augmented-wave method [49] for density functional theory-based electronic structure calculations. All calculations were also spin-

	E_s	E_o	E_m	E_p
to1	-1.39	-1.45	-2.60	–
to4	-1.39	-1.45	–	-1.43
tp1	-1.33	–	–	-1.23
to2	-1.24	-1.00	-2.15	-0.98
tm3	-1.22	–	-2.07	-0.90
to3	-1.19	-0.84	-1.99	–
to5	-1.18	-0.81	–	–
tm6	-1.17	–	-1.93	-0.76
to6	-1.14	-0.70	–	–
tm5	-0.80	–	-0.82	–
tm4	-0.79	–	-0.78	–

Table 3.1. H trio adsorption energies on graphene. Cells without numeric values indicate that the specific pair (o=ortho, m=meta, p=para) is not part of the given trio.

polarized, and utilized the exchange-correlation functional based on the PBE version of the generalized gradient approximation [25]. I applied a 400 eV cutoff to limit the plane-wave basis set without compromising computational accuracy, and a 4×4×1 Monkhorst-Pack special **k** point grid for Brillouin zone sampling. Three H atoms on a 48-C atom single sheet comprise the unit cell, with C-C nearest-neighbor distances of 1.42 Å before relaxation. All atoms were completely unrestricted in the geometry optimization. Likewise, a 15.0 Å vacuum separating adjacent sheets was used. I specifically choose the thirteen most closely-packed combinations of three atoms adsorbed on C atom "top" sites. Upon reconstruction, hydrogen atom lateral positions generally do not deviate much from the positions on receiving C atoms shown in Fig. 3.4. A trio is named based on its smallest H pairing component (o=ortho, m=meta, p=para) and distance of the third member of the trio from the pair center. This means, for example, that the trio labeled to1 is the three-hydrogen cluster comprised of a pair of adjacently adsorbed (ortho) hydrogen, and a third H atom adsorbed in the closest possible distance from the aforementioned pair.

Pair energies were computed using $E_s = [E_{gr+2H(ads)} - (E_{gr} + 2E_{H(g)})]/2$, where the terms E_{gr}, $E_{H(g)}$, and $E_{gr+2H(ads)}$ are the total energies for the graphene sheet, a gas phase H atom, and the system comprised of an adsorbed H pair and graphene, respectively. Table 3.1 shows the trios arranged by adsorption energy, starting with the most stable geometry. Table values were computed using the following

expressions: $E_{ads} = E_{gr+3H(ads)} - (E_{gr} + 3E_{H(g)})$; $E_s = E_{ads}/3$; $E_o = E_{gr+3H(ads)} - (E_{gr+2H(ortho)} + E_{H(g)})$; $E_m = E_{gr+3H(ads)} - (E_{gr+2H(meta)} + E_{H(g)})$; and $E_p = E_{gr+3H(ads)} - (E_{gr+2H(para)} + E_{H(g)})$, where the terms E_{gr}, $E_{H(g)}$, $E_{gr+3H(ads)}$, and E_{gr+2H} are the total energies for the graphene sheet, a gas phase H atom, the system comprised of an adsorbed H trio and graphene, and the system comprised of an adsorbed H pair and graphene, respectively. The adsorption energy of an isolated H atom on graphene $E_{iso} = E_{gr+H(ads)} - (E_{gr} + E_{H(g)})$ is –0.77 eV, a value which differs slightly from previous calculations [38, 45] due to the different adsorbate coverage used in these studies. For the same reason pair and trio adsorption energies reported here also differ slightly from corresponding values reported in Refs. [50, 51].

The closest pairing, most commonly labeled in related literature as the ortho pair given that its hydrogen atoms are directly attached to adjacent carbon atoms, is found to be the most stable pairing, in contrast to findings at a higher coverage [38], and hence suggesting one specific coverage effect on pairing stability. The para pair however does not come too far behind in energy. A comparison with analogous yet more restricted calculations (very localized relaxation) suggests that the increased stability of p1 over p2 arises from the inclusion of carbon atoms beyond the hydrogen's immediate neighbors in the substrate reconstruction. The two most stable pairs are followed by that with the farthest atomic separation among pairings considered, and then by a not immediately foreseeable sequence of the rest of the pairings. Despite this apparent irregularity with regard to H-H separation, results noticeably favor hydrogen pair attachment to locations involving carbon atoms from different sublattices, i.e. the case in which the two adatoms are separately attached to an α and a β carbon atom. The preference arises from the unavoidable disruption of the stable sp^2/π-bonding of the neighboring carbon atoms brought about by the receiving carbon tetrahedrization required by the attaching H.

As seen in Fig. 3.5, the four most stable adsorbed pair configurations are more stable than the state comprised of two isolated H adatoms, while the remaining pairings are not. Bound pairs are all chemically stable with respect to free hydrogen atoms, but the results support the greater likelihood of odd-neighbored pairs (Fig. 3.8) being present on hydrogenated graphite surfaces. This is in exact agreement with experiments involving different deuterium atom dosages. More specifically, pairs p2, p3, and p4 of the current study correspond exactly to observed pairs c, e and d of Andree et al. [42], respectively, while pairs p1 and p2 correspond to dimers A

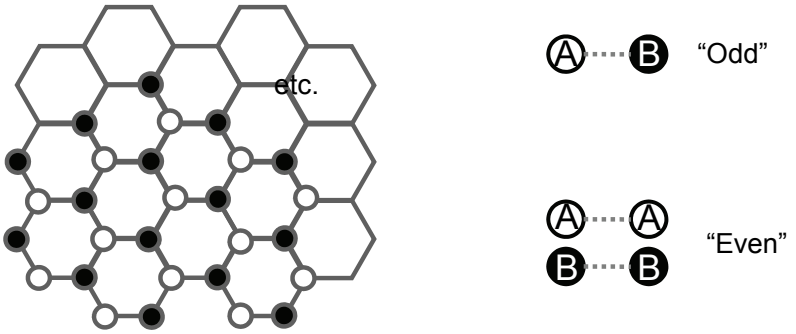

Fig. 3.8. The adsorption of a first H selectively modifies the reactivity of nearby graphite atoms, leading to drastic differences between the stabilities of "odd" and "even" pairs.

and B of Hornekaer et al. [43]. Thermal desorption spectroscopy (TDS) data [40, 41] for a deuterium coverage that favors formation of deuterium pairs on the surface show three key features – two peaks (500 K and 580 K) with a shoulder in between (540 K). Assuming that the numbers for each specific pair type simultaneously existing on the carbon surface do not vary greatly, the features at 580 K, 540 K, and 500 K can then be tentatively assigned as originating from p1, p2, and the combination of p3 and p4, respectively, if based solely on the pair adsorption energies. A more detailed treatment of the simultaneous dynamics of two adatoms desorbing from graphene would be needed in order to give finality to these assignments. Nonetheless, the initial rise in sticking probability with hydrogen exposure [42] and reduced barriers to hydrogen sticking [50] are in agreement with the lower energy for clustering which I have reported.

This trend I expect should hold for pairs with adatom separations beyond that covered by two graphite rings, but should weaken with increasing H-H interatomic separation. The results do not imply that the p5, p6 and p7 pairs cannot form – they can. However, given sufficient energy, the hydrogen atoms may diffuse out to form lower energy pair configurations, if not moving into isolation. Barriers to diffusion between H atom chemisorption sites on graphite are relatively large [52], but I expect that moving out of the metastable states should generally be easier, as in the I→B transition of Ref. [43].

These results also suggest that the first adsorbed hydrogen can induce nearby neighbor reactivity: it is clearly shown here that the presence of adsorbed hydrogen on graphene has a significant effect on the adsorption of a second one, even to a

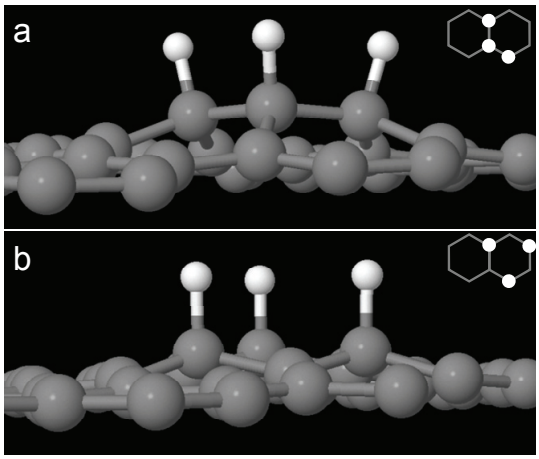

Fig. 3.9. Closely packed but different. The closest-packed cluster (to1, upper panel) is most stable, while the threefold-symmetric group (tm1, bottom) is not.

relatively distant H-H separation of 5 Å. Energetics of multiple adsorbates on surfaces can in most cases be described by direct coadsorbate interaction and electronic screening effects, but the case of pairs on graphene shows one of the clearest examples of substrate effects being much more important in determining the nature of clustering. In particular, I have associated the reported stability trends with the high stress due to bonds involving both sp^2 and sp^3 carbon atoms. Certain configurations for example leave the C atoms located in between receiving C atoms strained, leading to higher system energy.

Adsorbed groups of three hydrogen atoms are generally stable: the E_{ads} and associated E_s values are all negative, meaning all adsorbed three-hydrogen groups are stable with respect to hydrogen atoms located far from the graphene surface. If E_s for a given trio is less than E_{iso}, the trio is more stable compared with a system comprised of three isolated adsorbed H on graphene. In other words it would be more energetically favorable for the hydrogen atoms to clump together than to separate from each other on the surface, i.e., the net interaction shows an 'attractive' character. Only one trio – tm1 – is found unstable when compared with separately adsorbed atoms (Fig. 3.6, 3.9). As with the hydrogen atom and pair on graphene cases, the extent of the sheet reconstruction is rather substantial. For the most stable trio to1, which also is the most closely-grouped among all the considered geometries, the receiving C atoms all move out from the plane, consequently forming a local puckered-up island on the graphene sheet.

Comparing these with the pair adsorption [46], one can see that most of the trios are unlikely to dissociate into a pair and an atom on the surface, especially when one considers the high barriers to H atom diffusion. These results further affirm the likelihood of clustering of hydrogen adatoms on graphene. Also, while I expect that the probability for meta pairs existing on graphene is low, it is shown here that a third H adatom attaching nearby in most cases stabilizes that pair. The general trend is that the clusters of three have stronger binding per H atom compared to the pairs, and so experimental work should be able to find these.

It's also worthwhile mentioning the stabilities of adsorbed hydrogen trios in terms of component pairs. It has been earlier shown that the 'odd' ortho (p1) and para (p2) pairs are stable, while 'even' pairs such as the meta (p6) pair are higher in energy. Enhanced reactivity for the formation of the former kind of pairs has earlier been suggested [45, 46, 50]. Table 3.1 values clearly show that adding a third H atom to the surface, no matter how far/close it is to a pre-adsorbed pair, is never an endothermic process. A more important question to answer here however is: would it be more favorable to have a cluster of three, or a pair and single H atom separately adsorbed on graphene? Table 3.1 can be used straightforwardly to provide answers to this: if E_o (or E_m, E_p) for a given trio is less than E_{iso}, then the trio is more stable than having a separately adsorbed pair and atom. From this criterion it can be seen that most of the trios are unlikely to dissociate into a pair and an atom on the surface, especially when one considers the reported high barriers to H atom diffusion. These results once again affirm the likelihood of clustering of hydrogen atom adsorbates on graphene. Also, while I expect that the probability for meta pairs existing on graphene is low, it is shown here that a third H atom adsorbing nearby in most cases stabilizes the pair.

Comparing the stabilities of trios with that of pairs, another trend is obvious. The most stable pairs, the ortho and para pairs, are components of the most stable trios in the set considered in this study. The configuration to1 for example is a combination of two ortho pairs and one meta pair. It may be useful to note that it's geometrically impossible to have a trio comprised of purely odd pairs. Less stable trios such as tm3 contain the stable pair p3 or p4, which while less stable than the ortho and para pairs, are nonetheless favored pairing geometries. The least stable trios are entirely comprised of the three least stable pairs discussed earlier on, and thus one may

actually make good qualitative estimates on the stability of adsorbed groups of three based on the knowledge of pair and single atom adsorption.

As a final note on this section, the threefold-symmetric configurations of three hydrogen atoms are shown to be the least stable, and so scanning tunneling microscopy (STM) structures with threefold/sixfold symmetry are not likely originating from closely-clustered H trimers. This fact is advantageous for more precise H adatom identification, which is discussed in more detail in the succeeding section.

3.3. Effects of adsorbed hydrogen on the electronic states of graphene

Detecting and discriminating singly adsorbed and small groups of adsorbates is an essential step to knowing how saturation is reached, as in the case for hydrogen adsorption on graphite. Despite the difficulty associated with the size of the hydrogen atom, structures attributable to the presence of hydrogen in pairs or in relative isolation have been recently reported in two independent studies [42, 43] employing STM at high resolutions. Four distinct pairs have been suggested, all involving odd-neighbor adsites, in agreement with the results I presented in the previous section. One point from Ref. [42] that particularly interested me was the difficulty of clearly recognizing adsorbed pairs with atomic separations less than that of a *para* pair, noting that the close proximity of the atoms of these pairings casts sensible doubt on clear discrimination not only from each other, but also from an isolated atomic adsorbate.

In this section, I comment on the surface electronic states in the presence of adsorbed hydrogen, which are important in the identification of adsorbed hydrogen structures [51], as well as in providing fundamental knowledge on how graphene electronics can be tailored by hydrogenation. Related theoretical descriptions of defect-induced effects on the electronic states of graphite have pointed out useful ways of describing the nature of point defects on the surface [53-55], but have been primarily concerned with vacancies, substitutions, or arbitrary adsorbates, and so I believe more specificity to effects of H/D atoms is necessary. As important references, I include in this study the adsorbed *ortho* and *meta* hydrogen atom pairs (referred to as p1 and p6), which are the pairs of closest spacing. It should be further noted that while simple stability calculations predict that the p6 pair is not likely to

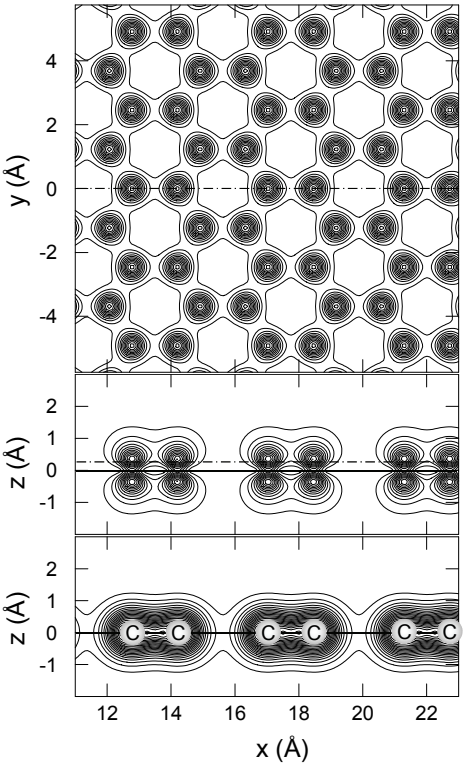

Fig. 3.10. A representative electronic state ($|\psi|^2$) near the Fermi level: pristine graphene. The figure shows slices (dash-dotted lines) along (a) z=0.31 Å (b) y=0.0 Å. The surface normal is oriented along the z direction. A total charge density plot for (b) is provided in (c), indicating atomic nuclei positions.

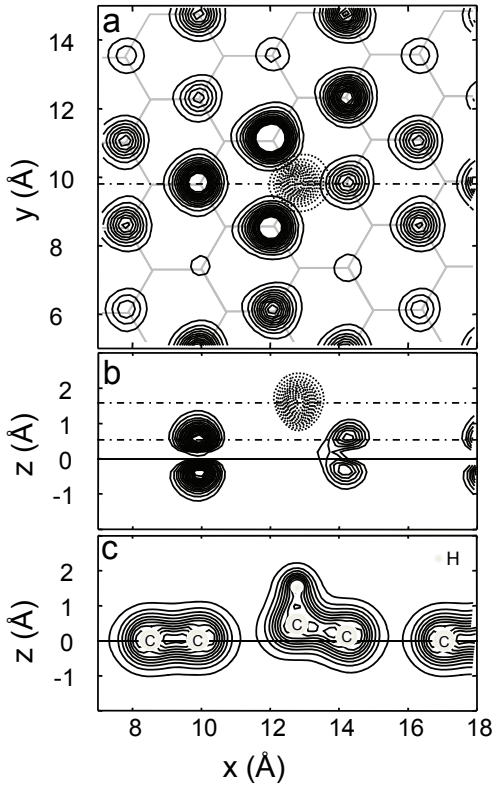

Fig. 3.11. A representative electronic state ($|\psi|^2$) near the Fermi level: atomic H on graphene. The figure shows slices (dash-dotted lines) along (a) z=0.56 Å (solid line wave function contours), z=1.69 Å (broken line contours) and (b) y=9.84 Å. The surface normal of pristine graphene is oriented in the z direction. A total charge density plot for (b) is provided in (c), indicating atomic nuclei positions frozen at the optimized coordinates.

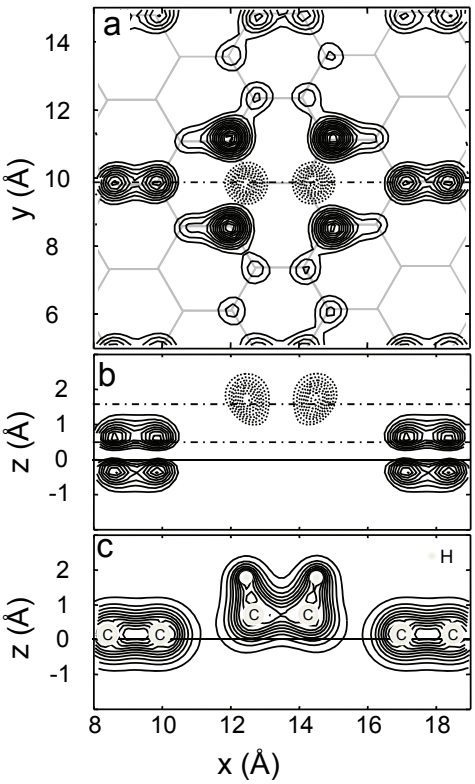

Fig. 3.12. Same as Fig. 3.11, but for pair p1 on graphene. (a) top view, (b) cross sectional side view, (c) total charge density.

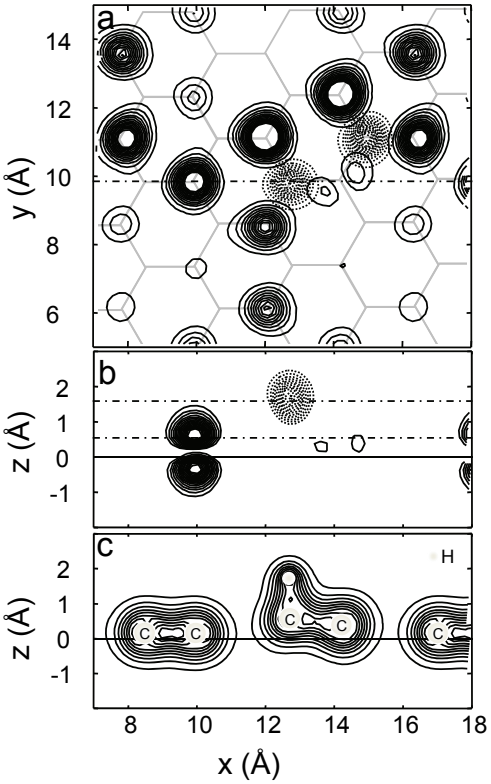

Fig. 3.13. Same as Fig. 3.11, but for pair p6 on graphene. (a) top view, (b) cross sectional side view, (c) total charge density.

exist, especially when compared with p1, I do not refute the mere possibility of its existence on the graphite surface.

Figures 3.10, 3.11, 3.12, and 3.13 show two dimensional cross-sections of representative electronic states near the Fermi level for pristine graphene and the systems involving an H atom, an ortho pair, and a meta pair adsorbed on graphene, respectively, where all C and H atom nuclei are frozen at their optimized coordinates. To be consistent with sample-positive STM measurement bias voltages, I chose the lowest states for which $E–E_F > 0$. For reference, the total charge density distributions are given as well in the lowermost panels. Complementing the results shown in Fig. 3.11, panels d and e of Fig. 3.14 show the atomic orbital-projected density of states for a free hydrogen atom and a component carbon atom of graphene, separately, while panels a, b and c describe those for the combined system. Nonzero magnetization is apparent. Consistent with Fig. 3.11, the density of states in the vicinity of the Fermi level for the graphene-H atom system is large for the hydrogen and varies per carbon atom on the graphene sheet, giving easy insights on what can

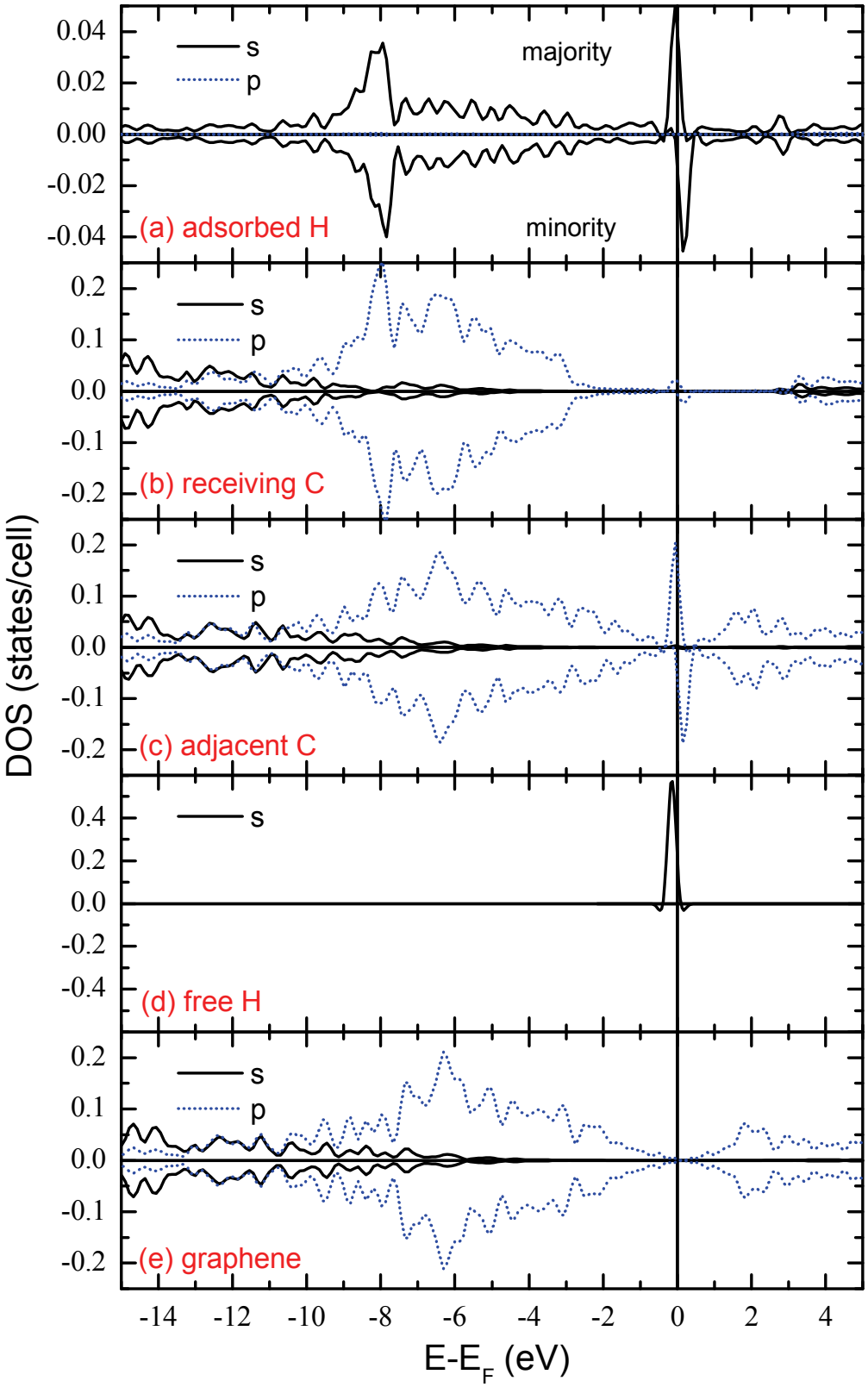

Fig. 3.14. Spin-polarized density of states projected onto atomic orbitals: panels (a)-(c) are for the graphene-H adatom system, while (d) and (e) are isolated systems. (a) DOS projected on the H adatom orbitals, (b) for the receiving C atom, (c) for a C atom next to the receiving C atom, (d) for a H atom in the gas phase, and (e) for a C atom of clean graphene.

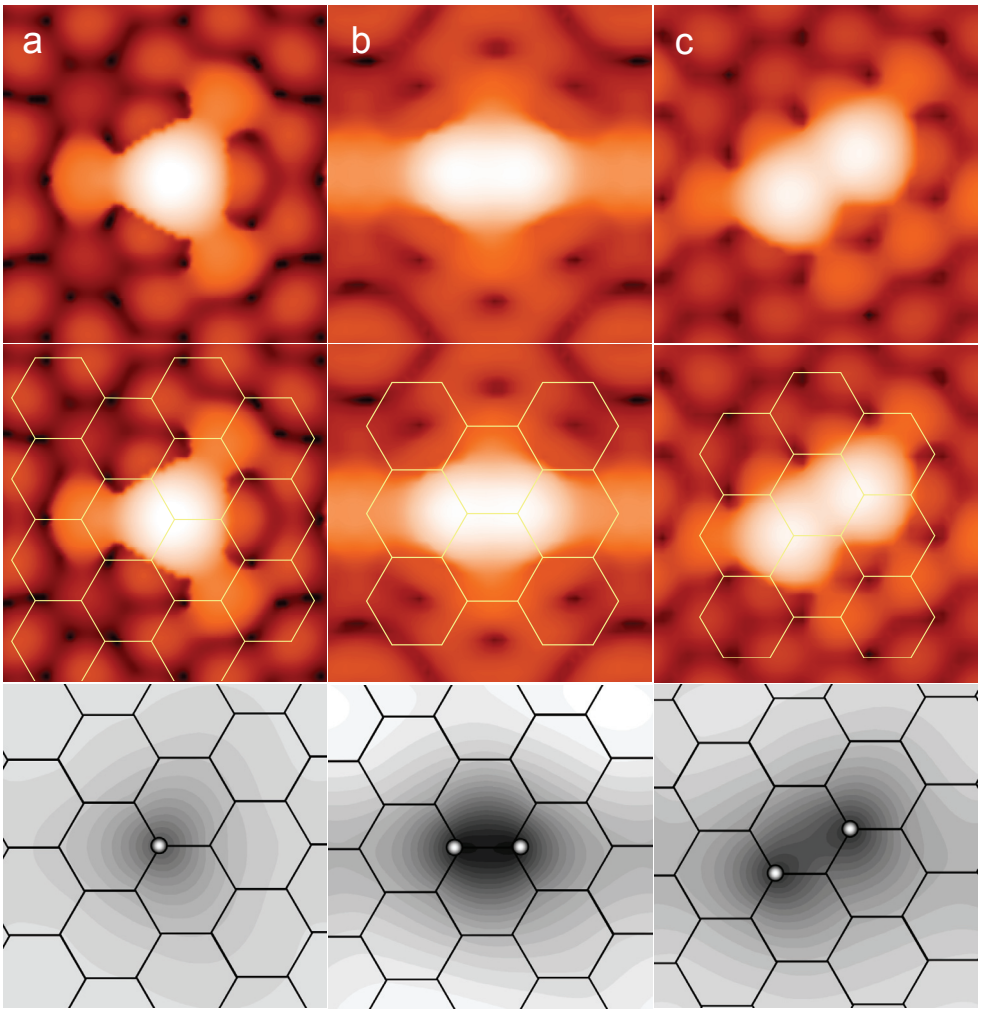

Fig. 3.15. (top row) Simulated STM images (tip z position plots). (a) H atom on graphene, (b) p1 pair on graphene, and (c) p6 pair on graphene. All images are shown using the same scale. The LDOS value used for the p1 pair on graphene image is 5.0×10^{-5} Å^{-3}eV^{-1}, while the rest used 1.0×10^{-3} Å^{-3}eV^{-1}. The middle row shows the approximate position of the C atoms. Bottom panels show the hydrogen structures together with reconstruction extents for comparison.

be easily probed via STM. Simulated constant-current STM images are shown in Fig. 3.15. Calculations were based on the theory of Tersoff and Hamann [56] for constant-current STM imaging, which in a nutshell states that the STM tip position map follows the contours of a local density of states (LDOS) isosurface. Assuming an s-wave probe tip, I use the states closest to the Fermi level. The isosurfaces used here (both for atom and pair adsorption) were chosen solely to get a topography that is quantitatively consistent with the reported tip position corrugation in Ref. [42], i.e., "bright spots" are about 2 Å above the clean sections of the surface.

Figure 3.11 indicates that the presence of adsorbed hydrogen atom should be very well observable from the strong disruption of the graphene surface electronic states: the presence of the H atom breaks the resonance of the original π-network at the Fermi level of clean graphene. An obvious manifestation of this effect is that every other p_z orbital on the C lattice is skipped by the wave function, i.e. the electronic state has maxima only in the graphene sublattice which does *not* include the receiving C atom, aside from the maximum at the location of the H atom itself. This causes the original honeycomb lattice to form a triangular one. In contrast to this, the charge density distributions for all three systems do not discriminate graphene C atoms, and show that both the puckering up of the receiving carbon atom and the presence of the hydrogen adsorbate itself should contribute to an observable topography change over the position of the adsorbed atom, which should be relevant, for example, in atomic force microscopy measurements. The proximity of the H atom with its images in the periodic model I used here unfortunately makes me unable to comment more on larger superstructures associated with the adsorption, but such is not of much significance in this discussion. I limit the analysis to the immediate vicinity of an adsorbed atom, which would be more useful in identifying adsorbed structures for intermediate to high adsorbate coverages.

The corresponding simulated STM image for H atom adsorption is shown in Fig. 3.16, which can be compared with the high resolution image attributed to adsorbed D (type a) in Ref. [42]. In that report, it was assumed that a D atom was at the center of a bright spot. It should be noted that H and D are electronically equivalent. The simulation reproduces the image from experiment satisfactorily in terms of its size and general shape and symmetry. The tripod extensions of the central spot in the simulation come from p_z orbitals from third-nearest neighboring (*para*) C atoms (shown in black in the schematics of Fig. 3.16).

While the H atom adsorption on graphene exhibits a distinct threefold symmetry, the pairs, by their very nature, have to break such symmetry completely. A similar means for discriminating paired from single point defects has been pointed out in a previous study [54], using a superlattice. Another point that should be emphasized here is the fact that the two closest pairs show a marked difference in disrupting graphene electronics. The ortho pair has its hydrogen atoms separately attached to C atoms of both substrate sublattices, and hence the electronic states in the vicinity of the Fermi level reveal the complete honeycomb network. Do note however that this

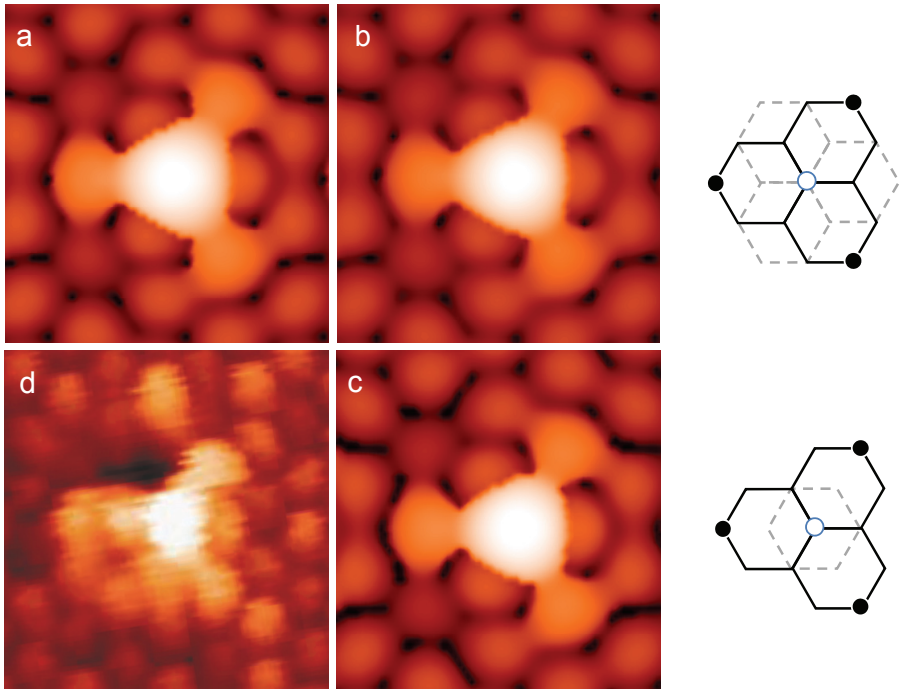

Fig. 3.16. Simulated STM (i.e., tip z corrugation for constant current imaging) for H atom adsorption on graphene. Clockwise: (a) H atom adsorbed on single-sheet graphene, (b) H atom adsorbed on an A carbon atom on a two-layer graphite surface, (c) same as (b) but on a type B carbon, (d) actual STM image from A. Andree et al., Chem. Phys. Lett. 425, 99 (2006), where $U = -0.2$ V (sample positive). The inset in (a) shows the position/orientation of substrate atoms with respect to the adsorbate (white circle).

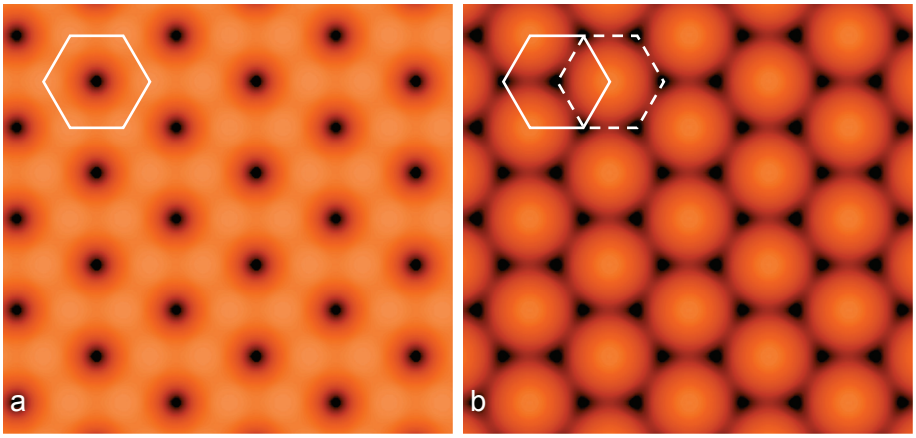

Fig. 3.17. Calculated STM images for pristine carbon sheets: (a) graphene, (b) graphite (bilayer graphene). The hexagons at the upper left of the panels are guides for locating carbon atoms (dashed for the subsurface C layer).

translated to a significant loss in C atom resolution in the corresponding simulated STM image at the chosen parameters.

The appearance of substrate atoms from both sublattices is in agreement with a previous STM simulation of the closest pairing p1 (dimer A) [43], but the spatial extent of the prominent STM features differ. The adsorbed pair is represented as two distinguishable bright spots in Ref. [43], but the image presented in this study is more of a single yet elongated bright spot, with extensions in four directions. Several factors may contribute to these differences, including surface unit cell size (pair adsorption coverage) and density of states isosurfaces used, as well as electronic states chosen with respect to the Fermi level. The meta pair on the other hand reproduces the cloaked sublattice effect found in the atomic adsorption. These two pairs have been shown to differ significantly in terms of adsorption strength, and are shown here to differ as well on how they modify the graphene electronic states (and thus how they would look like under the STM).

The electronic wave function features at elevated positions (marked by the dashed contours in Figs. 3.11 to 3.13) suggest that the exact positions of adsorbed H atoms are at the centers of the bright spots. Hence one may actually say that an adsorbed hydrogen atom on graphene is not really transparent to the STM based on these results. This of course works under the important assumption that the hydrogen atom remains localized on its adsorption position, which should not be unreasonable considering the high barriers involved in chemisorbed H hopping, and the standard use of D atoms in related experimental work. An equally important concern is: can the H atoms in the close pairings be resolved? The wave functions in Figs. 3.12 and 3.13 do not say no, though actual experimental conditions may not be as ideal. If at this scale individual hydrogen atom resolution is poor, one can at least expect that more elongated bright spots at specific orientations for the closely-spaced adsorbed pairs, as in Figs. 3.15(b) and 3.15(c), and the surrounding C atom contributions to the STM image should provide supporting clues as well.

On an actual multilayer graphite system without defects, it is well-known that electronic differences on A and B site atoms are very significant, to the point that it's common to observe only the surface B-site atoms (i.e., C atoms that do not have neighbors in adjacent sheets) under scanning tunneling microscopy [57]. This is affirmed by straightforward calculations using a two-atom basis for graphene (four atoms for bilayer graphene), as shown in Fig. 3.17. Here the case for a single

graphene sheet shows the hexagonal arrangement of carbon atoms, but the bilayer graphene model clearly shows the difference between A and B carbon atoms. One may then wonder about what should happen when a second perturbation – that from an adsorbed H atom – is present. Similar calculations using a two-layer system were subsequently performed: a second graphene sheet was placed at a distance 3.35 Å below the reconstructed sheet of Fig. 3.15(a), with its lateral position set to make the adsite of Fig. 3.13(a) fall on an A site (Fig. 3.16(b)), then a B site (Fig. 3.16(c)). STM images were recalculated from the surface electronic states of H on bilayer graphene. The images were found practically identical to that on (single sheet) graphene, regardless of the adsite type, indicating that H atom adsorption, within the approximations and coverage used, affects graphene electronics much more strongly.

It should be noted that Ref. [42] suggests that single atom adsorption images look different, depending on its location on the graphite surface. Given the size and position of the STM feature assigned the type b structure with respect to its surroundings, interpreting it as a single adsorbed atom at the site indicated in the inset indeed is plausible. However I think that the clear lack of threefold symmetry alone eliminates the type b feature as a singular defect, regardless of whether it's a vacancy, atom adsorbate, or substitution. Given the feature's size, shape, and orientation on the surface, I think it's more consistent to associate the type b feature of Ref. [42] to the closest pairing, p1. The extensions at the sides of the simulated bright spot may have been made more prominent due to the close proximity of adjacent adsorbed pair images in the periodic model.

The calculations suggest that the characteristic feature in Fig. 3.16(a) and Fig. 3.16(b) should then hold for atomic adsorbates on the graphite basal plane, no matter which type of site (A or B) the H atom is attached onto. One can however easily see two factors which could tell these two adsites apart: (1) a 60° rotation of the prominent structure, following the different orientations of the substrate threefold symmetries at the two inequivalent sites (a similar conclusion is pointed out for a vacancy-induced superlattice in Ref. [53]), and (2) a more disrupted substrate atom visibility for B-site adsorption. An adsorbed atom's strong electronic perturbation becomes weaker as one moves farther from the adsorbate location, and so there will have to come a point where the effects of the subsurface layers would be more dominant, showing what's expected from a clean graphite surface. The interesting case comes with B-site adsorption, as A-site C atom visibility is enhanced by the

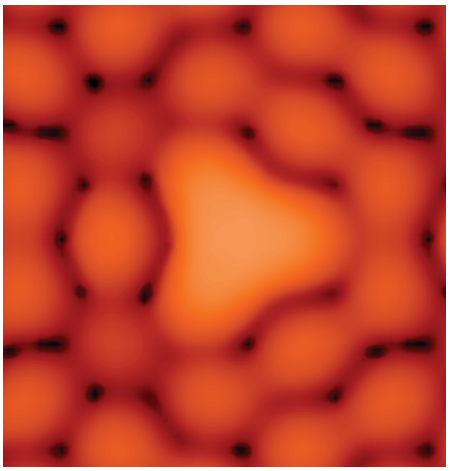

Fig. 3.18. Probing the clean (opposite) face of hydrogenated graphene

presence of the adsorbed H, creating a region centered at the adsite wherein the C atom visibility should be different with respect to the surrounding clean surface. The size of this region depends on the relative strengths of the two perturbations to the single-layer graphene electronic states, but its mere presence should already be of practical use.

Lastly, it's also interesting to see if scanning tunneling microscopy is powerful enough to detect subsurface hydrogen in graphite, since proof for entry of hydrogen inside graphitic structures is needed. In particular, here I focus on hydrogen atoms that are adsorbed just below a graphene sheet. A simulation performed on the opposite face of the system used for Fig. 3.15(a) is shown in Fig. 3.18, using similar parameters. Results show a much less pronounced feature for the unpopulated face, but it is important to note that (1) the honeycomb lattice is still incomplete, and (2) accessing electronic states farther from the Fermi level might improve the central feature.

The electronic effects of H adsorption also provide fundamental insights on clustering stability. More precisely, the location of the wave function maxima in Figs. 3.11 to 3.13 are not coincidentally the most preferred locations for the additional H atoms if one were to create a strongly adsorbed pair from an initially adsorbed H atom, or a strongly adsorbed trio from initially adsorbed ortho and meta H pairs. This is in agreement with a recent study which also tackled H pairing on graphene, attributing pairing stability from their magnetic properties [58]. Considering the high stress due to strained C-C bonds, changes in surface electronics,

and the presence of magnetism, in a rather simplified statement, even pairs create dangling bonds, odd pairs do not, which is directly manifested in the cluster stabilities.

3.4. Graphene two-face hydrogenation and saturation

When compared with the graphite terraces that have been given emphasis so far, the edges of graphite show much more reactivity to hydrogen atoms. On the experimental side, mechanical alloying has been used to prepare defective structures of graphite under hydrogen atmosphere [59, 60], and the reported 7.4 wt% hydrogen stored in the resulting nanocrystalline (finely ground, in other words) graphite was partly attributed to the formation of a vast number of edge dangling bonds resulting from the rupture of graphite intralayer linkages. One previous work [61] done in the same research group on hydrogen molecule dissociative adsorption on the zigzag edge of graphite has agreed with the aforementioned observations, as a quick check of the potential energy surface for H_2 indicates a non-activated process. Adsorption onto bare armchair edges [62], however, has been shown to be a slightly less favored route, suggesting the possible utility of the zigzag edge over the armchair edge as a reaction channel. Quantum dynamics calculations on the obtained potential energy surfaces on these two distinct edges naturally showed different scattering behaviors for approaching H_2 of different incident energies [63], affirming the expected graphite edge reactivities.

The clear trend goes: the more defects you have, the more chances you get for hydrogen chemisorbing onto a C atom. An alternative to increasing the number of dangling bonds by creating more edges is increasing the sp^3 character of the substrate atoms on the sheet itself, which should be a viable option for achieving a high hydrogen uptake in carbon-based materials. As a reference, hydrogenated tetrahedral amorphous carbon (ta-C:H), a diamond-like carbon material with a high sp^3/sp^2 ratio, is known to be capable of reaching a hydrogen/carbon atomic ratio of about 60% (4.6 wt%) . A higher uptake value (i.e., >6.5 wt%) is however desired for practical use, and explicit control of the uptake and release of hydrogen is necessitated in actual situations. Taking full advantage of graphite for this specific purpose should involve the exploitation of every single section possible, hence the need to promote adsorption on the faces of each sheet of the graphite lattice.

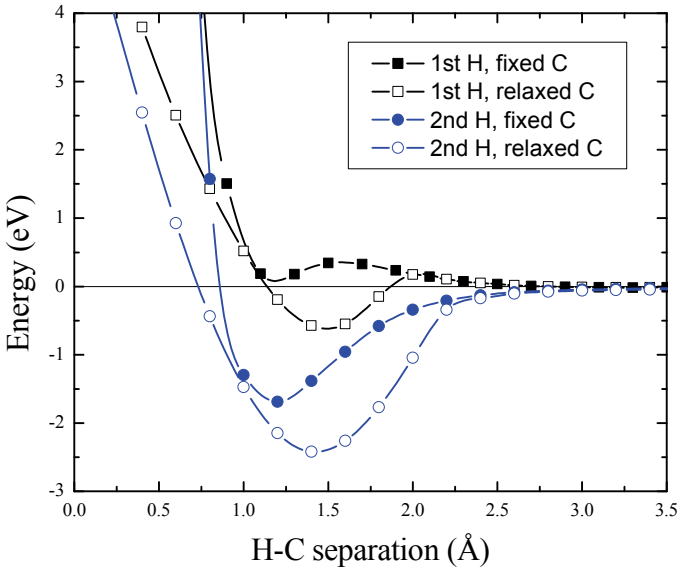

Fig. 3.19. Calculated potential energy curves showing increased substrate reactivity brought about by adsorption of the first hydrogen. Adsorption of a single hydrogen atom on frozen (relaxed) graphene is shown as filled (open) squares, while that for the second hydrogen atom is shown in circles.

While one-face hydrogenation of graphene is itself a fertile ground for academic discussion, the problem with one-face hydrogenation when considering practical applications is that a full monolayer hydrogen coverage is impossible to achieve, since there is no way for the carbon atoms to be in sp^3 configurations all at the same time. This is disadvantageous, for example, if one needs to maximize the hydrogen content on graphene. The situation however changes drastically when both faces of graphene can have access to hydrogen [64]. This is best illustrated with a pair of hydrogen atoms adsorbed closely, but on opposite faces of graphene, i.e. in a way forming the two-face analogue of the ortho pair discussed earlier.

Results for relevant adsorption pathways are shown in Fig. 3.19, which unambiguously show that atomic hydrogen adsorption on a graphene sheet with pre-adsorbed hydrogen on the opposite side can proceed much more easily compared to that onto a plain graphene sheet, since the difficulty of overcoming the energy barrier to chemisorption on graphene is removed. The final state for this pair is also a very stable one, significantly lower in energy as compared with any of the same-face pairs I discussed earlier. Regarding this, it is interesting to note that recent ab initio calculations [65] have shown that the entry of atomic H into the region between

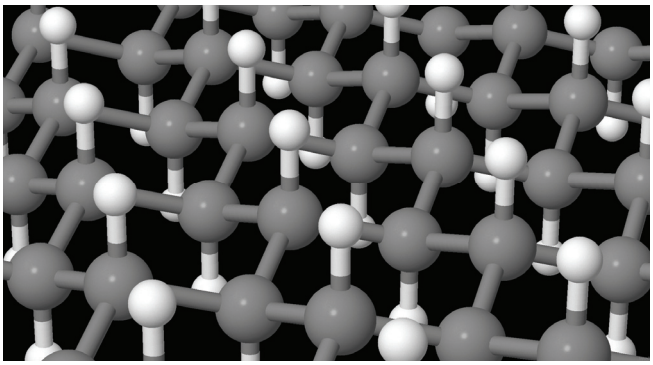

Fig. 3.20. Stable form of fully hydrogenated graphene. Hydrogen atoms are shown in white.

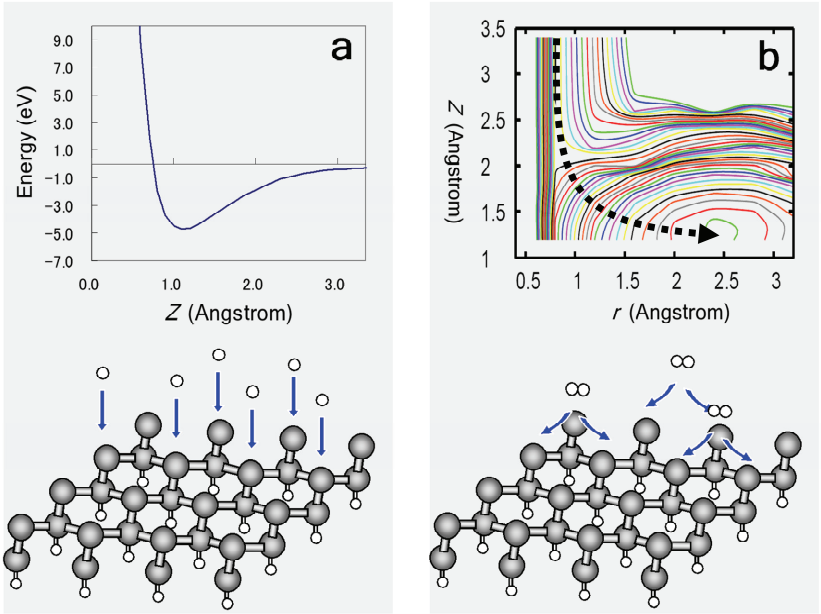

Fig. 3.21. Adding more hydrogen onto a graphene sheet pre-adsorbed with hydrogen on one face. The energy vs. hydrogen-carbon separation Z relationship for incoming atomic hydrogen is presented in the left panel (a), showing strong chemisorption at Z =1.1 Å. The right panel (b) shows the calculated potential energy contours for H_2 dissociation, as a function of the H-H separation r, and the distance Z of the H_2 molecule centre-of-mass from the surface. The adsorbed atoms for this particular case (constrained to the T-C-T dissociation geometry described in Y. Miura et al., J. Appl. Phys. 93, 3395 (2003)) are separated by about 2.5 Å, and located around 1.2 Å from the nearest carbons.

bilayer graphene is not an endothermic process, and so population of both sides of sheets of graphite is possible.

One implication of these results is that the chemisorption of a first hydrogen atom actually has the potential of setting off a series of subsequent adsorption reactions,

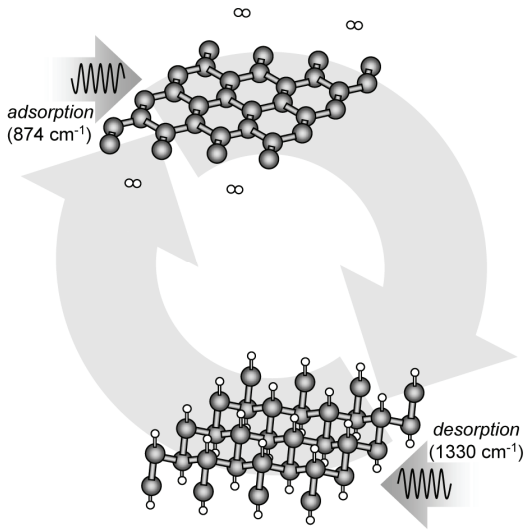

Fig. 3.22. Schematic on controlling graphite for hydrogen storage. Pristine graphite (top) has been shown to have a low reactivity to approaching hydrogen, but adsorption is expected to be promoted when the C atom planar arrangement is perturbed through infrared radiation-induced vibrations. Ideal hydrogen uptake in the final assembly is shown in the lower section. Infrared radiation at distinct frequencies can and should be used for separately promoting the two processes.

which, upon saturation of the substrate, forms the final assembly shown in Fig. 3.20. An independent study with similar conclusions is given in Ref. [66]. Such a network of fully covered sheets, with its hydrogen-to-carbon ratio of unity, can hold hydrogen to a commercially-practical storage capacity of 7.7% by weight [64]. This assembly has also been shown to be the more stable conformation of hydrogen-saturated graphene (graphane), which has a 1:1 C-H stoichiometry [67].

On a related note, though hydrogen can occupy both faces of a graphite layer once the process for hydrogen storage is initiated, adding more hydrogen onto a sheet covered with a half monolayer of hydrogen (adsorbates attached only to next-nearest carbon atoms) on the opposite face is worth examining. For this situation, isolated sheets modeled through a fully relaxed structure composed of eight carbon atoms and four pre-adsorbed hydrogen atoms in the supercell were used, with hydrogen atoms, and a hydrogen molecule approaching from the gas phase (Fig. 3.21). As expected, geometry optimization favored restructuring of the carbon lattice into an atomically non-flat carbon sheet, in which the hydrogenated carbons are separated from the plane of the upper carbon layer by 0.24 Å. Equipotential contours pertaining to the adsorption of hydrogen molecules on the unpopulated graphite sheet face are shown

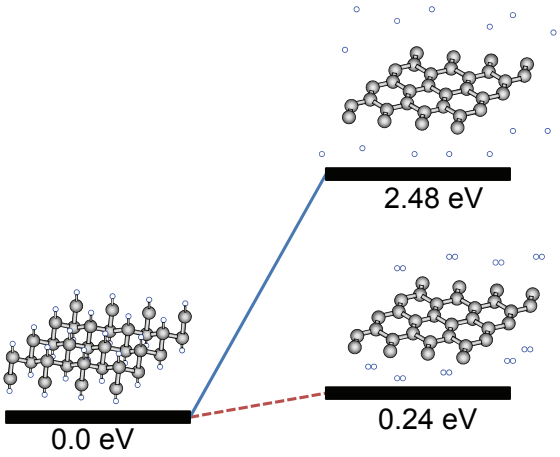

Fig. 3.23. Stability of the fully-hydrogenated graphene (graphane).

in Fig. 3.21(b), indicating that the unpopulated surface can very easily break up incoming hydrogen molecules during adsorption, given their barrierless reaction routes. Further calculations [64] on vibrational modes of pristine and hydrogenated graphene also suggest the possibility of controlling the reversible hydrogenation reactions, as depicted in Fig. 3.22.

An expansion of the graphene lattice parameter by a factor of about 3% was observed, producing C-C bonds with lengths of 1.54 Å when fully hydrogenated – and a structure closer to that of diamond than graphene (also, C-C bond lengths in diamond are 1.54 Å). This is somewhat in agreement with recent experimental work characterizing graphane [68], as local regions with in-plane expansion have been reported, albeit to a much greater extent. Along the *xy* plane, the hexagonal lattice is maintained. Finally, the hydrogen-saturated graphene is found to be more stable than graphene and hydrogen atoms (molecules) by 2.48 eV (0.24 eV), in terms of chemisorption energy per hydrogen atom (Fig. 3.23).

4 Hydrogen on platinum

4.1. Case studies for Pt-bound hydrogen atom states

Diffusion comprises an essential aspect of catalytic processes as it bridges the initial adsorption of reactants with eventual reactions at other locations. In the context of fuel cells for example, hydrogen, upon reaching the anode, would require moving along the catalyst surface, say that of platinum or its alloys, and traveling through a proton conducting membrane before reacting with ambient oxygen at the other end to complete the process. It is primarily in light of describing these processes at the atomic scale, particularly those involved at the anode, that the H-Pt system has created its own following (see for instance Refs. [69-73]), with a quantum mechanical picture of the behavior of a hydrogen atom on the platinum surface examined as well. The simplest and most widely used approach here is an electronically adiabatic treatment of the hydrogen motion near the solid surface, usually beginning with the creation of an *n*-dimensional PES. In a lot of cases this term is expressed in terms of fitting functions using input parameters from 'static' total energy calculations for given atomic nuclei positions, orientations, etc. As with related studies on the subject [74-81], in this work the PES is used in the Schrödinger equation for H atom motion Eq. (2.11) under the periodic boundary conditions of the model surface.

The significance of quantum effects on hydrogen atom motion on solid surfaces has long been suggested. For example, DiFoggio and Gomer found that the surface diffusion coefficient for hydrogen remained constant for temperatures below 140 K on the W(110) surface, suggesting hydrogen tunneling that is not shown by the heavier deuterium [82]. Furthermore, helium scattering on Pd(111) [83] and electron energy loss spectroscopy studies on Rh(111) [84], Pd(110) [85] and Cu(110) [86] show results that can only be explained by delocalized models of hydrogen. More recently, STM imaging of hydrogen atoms on copper provided a window on tracking the motion of a single H atom, and the weak temperature dependence of the H hopping rate that was found suggests H atom tunneling along the copper surface [87]. Finally, finite zero-point energy values for hydrogen atoms adsorbed on Si(111) and Pt(111) were directly measured from nuclear reaction analysis (NRA) [88], suggesting yet another quantum mechanical effect observable for hydrogen atoms on

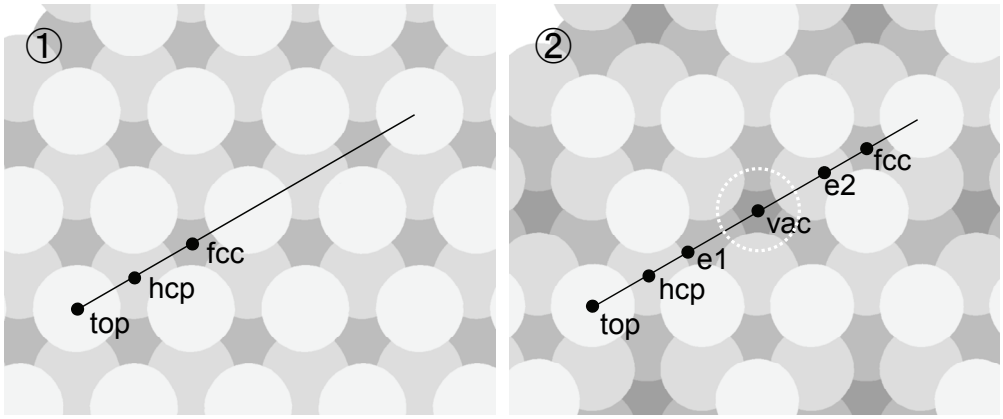

Fig. 4.1. Important sites on the (1) clean Pt surface (2) Pt surface with vacancies.

metals. These findings cannot be explained by adiabatic potential energy surfaces alone.

The small mass of hydrogen and the relatively flat corrugation of its potential energy surface on the (111) surface of platinum makes a departure from a classical analysis a necessity. This is in marked contrast with the hydrogen atom on a graphite system discussed in the previous chapter, which has a very stable energy minimum, when compared with possible adsorption on other sites. Results in ref. [38] for instance suggests a diffusion barrier in the order of 0.7 eV for hopping between adjacent C atoms, while density functional theory calculations on platinum suggests a barrier about an order of magnitude lower.

In this section, I firstly return to a benchmark system, the hydrogen atom on an ideal platinum surface, commenting firstly on how the three-dimensional potential energy surface treatment leads to differences in physical results pertaining to hydrogen atom motion. I work with the case in which the eigenstates describing hydrogen motion are determined from wave functions expressed as a linear combination of a uniformly distributed set of Gaussian-type functions spanning the space within the vicinity of the topmost layer of Pt atoms. Hydrogen atom behavior on two distinct platinum systems are discussed: a perfectly smooth (111) surface, and a hypothetical surface representing the opposite extreme, in which a periodic presence of vacancies is brought about by taking out one of four top-layer atoms on the Pt surface. Schematics for both surfaces are shown in Fig. 4.1, with special adsites labeled. These sites are high-symmetry sites on the surface, except for e1 and e2 which are vacancy edge sites on the Pt surface which have strong affinities for H

adsorption. The difference between e1 and e2 lie on their relative positions with respect to the second layer of Pt atoms – e2 is more directly above a second layer Pt atom.

4.1.1. H atom states on Pt: formalism

The potential energy surfaces for atomic H on platinum were constructed from calculations using density functional theory on a five atomic layer slab of platinum using lattice parameters consistent with experimental data. For the case of the flat Pt surface, sampling came from about 500 different positions of the hydrogen atom, while the larger space for H on the defective Pt system which will be discussed later on required about 6,200 to maintain the same sampling point density. The computations work on an adiabatic description of the atom motion on the substrate, and can thus be seen as divided into two parts: the construction of a model potential energy surface for the motion of hydrogen in three dimensions, and solving the Schrödinger equation for H atom motion under the periodic boundary conditions of the surface.

Obtaining an increasingly accurate PES goes hand in hand with the addition of more ab initio points, to the point in which there is a very fine mesh of data enough for a smooth numerical integration. This however would be way too computationally expensive to be practical, hence the employment of interpolation schemes is usually sought, for example, by finding analytic fits that are physically consistent with the data. This is very critical in the computations since the V matrix calculations are the most time consuming. Completely analytical forms were chosen in some of the calculations presented in the following section: the finite PES sampling was supplemented with surface-normal Morse and harmonic fits, both with lateral coordinate-dependent parameters interpolated from plane wave expansions. Results from these are compared with calculations from a potential energy surface created from three dimensional splines connecting the ab-initio energy data.

Real-space wave functions describing hydrogen atom motion on this system were calculated in order to comment on quantum mechanical aspects of H adsorption: relative probabilities of site occupancy, zero-point corrections to adsorption energies, as well as wave function delocalization, which is directly related to the diffusion process on the solid surface. Working within the variation method, the eigenstates describing hydrogen motion were numerically determined from wave functions

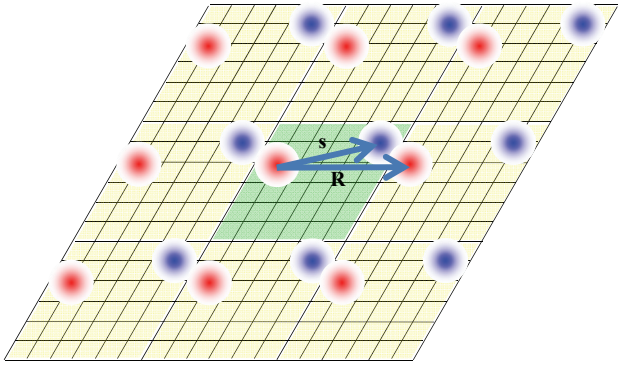

Fig. 4.2. Schematic for determining wave functions for H atom motion.

expressed as a linear combination of a uniformly distributed set of Gaussian-type functions – density of 720 (12×12×5) and 1152 (12×12×8) per surface Pt atom on the flat and defective Pt(111) surfaces treated here, respectively – spanning the space immediately above the first layer of Pt atoms. Finer meshes of orbitals would have been more ideal, but one must take into consideration the fact that computational time and memory allotment is proportional not just to the basis set size, but its *square*. Nevertheless, a reasonable compromise was found with the grid dimensions just stated.

Working within variation methods, the quantum states for hydrogen atom motion for any given wave vector **k** on an external periodic potential (here from the Pt surface) were computed numerically based on wave functions expressed as a linear combination of Gaussian functions. Gaussian functions for the basis set were chosen in view of the large plane wave basis set needed for describing localized states, especially along the surface normal direction which is not periodic (and can be severely anharmonic). I use slightly different notation in this section: the H atom position is given by **r**, and $E^{el}\left(\mathbf{R}_I\right) \to V\left(\mathbf{r}\right)$ since Eq. (2.9)'s total energy for the electronic system now serves as the potential term. Starting with the Hamiltonian,

$$\hat{H} = -\frac{\hbar^2}{2m_H}\nabla^2 + V(\mathbf{r}) = -\frac{\hbar^2}{2m_H}\left(\frac{\partial^2}{\partial x^2} + \frac{\partial^2}{\partial y^2} + \frac{\partial^2}{\partial z^2}\right) + V\left(x, y, z\right) \tag{4.1}$$

where m_H is the protonic mass, a convenient way of solving Eq. (2.11) is through wave functions for hydrogen motion on the Pt surface expressed as

$$\xi(\mathbf{k}, \mathbf{r}) = \sum_i^N c_i \Phi_i(\mathbf{k}, \mathbf{r}) \tag{4.2}$$

under the periodic potential term, where the basis set functions are LCAO Bloch functions,

$$\Phi_i(\mathbf{k},\mathbf{r}) = \sum_m e^{i\mathbf{k}\cdot\mathbf{R}_m}\phi\left(\mathbf{r}-\left(\mathbf{R}_m+\mathbf{s}_i\right)\right) \tag{4.3}$$

Here, **R** is a translational lattice vector, and **s** the position of a basis function (Fig. 4.2). Gaussian functions in three dimensions were used for orbitals:

$$\phi\left(\mathbf{r}-\left(\mathbf{R}_m+\mathbf{s}_i\right)\right) = \phi\left(\mathbf{r}-\mathbf{r}_{m,i}\right) = e^{-\frac{1}{2}\sigma_{xy}\left[\left(x-x_{m,i}\right)^2+\left(y-y_{m,i}\right)^2\right]-\frac{1}{2}\sigma_z\left(z-z_{m,i}\right)^2} \tag{4.4}$$

Band structures for the hydrogen atom can then be evaluated from **k**-dependent eigenvalues given by

$$\varepsilon_{\mathbf{k}} = \varepsilon\left[\xi(\mathbf{k},\mathbf{r})\right] = \frac{\left\langle \xi(\mathbf{k},\mathbf{r})\middle|\hat{H}\middle|\xi(\mathbf{k},\mathbf{r})\right\rangle}{\left\langle \xi(\mathbf{k},\mathbf{r})\middle|\xi(\mathbf{k},\mathbf{r})\right\rangle} \tag{4.5}$$

Inserting (4.1) and (4.2) into (4.5), we then have

$$\varepsilon_{\mathbf{k}} = \frac{\left\langle \sum_i^N c_i\Phi_i\middle|\hat{H}\middle|\sum_j^N c_j\Phi_j\right\rangle}{\left\langle \sum_i^N c_i\Phi_i\middle|\sum_j^N c_j\Phi_j\right\rangle} = \frac{\sum_{i,j}^N c_i^* c_j\left\langle \Phi_i\middle|\hat{H}\middle|\Phi_j\right\rangle}{\sum_{i,j}^N c_i^* c_j\left\langle \Phi_i\middle|\Phi_j\right\rangle} \equiv \frac{\sum_{i,j}^N H_{ij}c_i^* c_j}{\sum_{i,j}^N S_{ij}c_i^* c_j} \tag{4.6}$$

which, in matrix form, reduces to evaluating

$$\left(\mathbf{H}-\varepsilon_{\mathbf{k}}\mathbf{S}\right)\mathbf{c} = 0 \tag{4.7}$$

It should be noted that for N Gaussian orbitals, the matrices have dimensions $N\times N$, and have N distinct solutions for each **k**. The term $\varepsilon_{\mathbf{k}}$ is thus more appropriately labeled $\varepsilon_{n,\mathbf{k}}$. The matrix elements H_{ij} can be expressed as

$$\begin{aligned} H_{ij}(\mathbf{k}) &= \left\langle \Phi_i\middle|\hat{H}\middle|\Phi_j\right\rangle = \int \Phi_i^*(\mathbf{k},\mathbf{r})\left(-\frac{\hbar^2}{2m_H}\nabla^2+V(\mathbf{r})\right)\Phi_j(\mathbf{k},\mathbf{r})\,dV \\ &= \int \Phi_i^*(\mathbf{k},\mathbf{r})\left(-\frac{\hbar^2}{2m_H}\nabla^2\right)\Phi_j(\mathbf{k},\mathbf{r})\,dV + \int \Phi_i^*(\mathbf{k},\mathbf{r})V(\mathbf{r})\Phi_j(\mathbf{k},\mathbf{r})\,dV \\ &= T_{ij}(\mathbf{k})+V_{ij}(\mathbf{k}) \end{aligned} \tag{4.8}$$

and so the bulk of the computations come down to evaluating the following three terms:

$$V_{ij}(\mathbf{k}) = \int\left(\sum_m e^{-i\mathbf{k}\cdot\mathbf{R}_m}\phi\left(\mathbf{r}-\mathbf{r}_{m,i}\right)\right)V(\mathbf{r})\left(\sum_n e^{i\mathbf{k}\cdot\mathbf{R}_n}\phi\left(\mathbf{r}-\mathbf{r}_{n,j}\right)\right)dV \tag{4.9}$$

$$T_{ij}(\mathbf{k}) = -\frac{\hbar^2}{2m_H}\sum_m\sum_n e^{i\mathbf{k}\cdot(\mathbf{R}_n-\mathbf{R}_m)}\int\phi\left(\mathbf{r}-\mathbf{r}_{m,i}\right)\nabla^2\phi\left(\mathbf{r}-\mathbf{r}_{n,j}\right)\,dV \qquad (4.10)$$

$$S_{ij}(\mathbf{k}) = \left\langle\Phi_i\middle|\Phi_j\right\rangle = \sum_m\sum_n e^{i\mathbf{k}\cdot(\mathbf{R}_n-\mathbf{R}_m)}\int\phi\left(\mathbf{r}-\mathbf{r}_{m,i}\right)\phi\left(\mathbf{r}-\mathbf{r}_{n,j}\right)\,dV \qquad (4.11)$$

Fortunately, both **T** and **S** have exact solutions for a basis set of Gaussian orbitals, leaving the numerical integration job solely to the **V** term (in these studies, to further reduce computational time, a partially parallel implementation was used in calculating the **V** matrix elements). Similar methods were also used in some studies I have also worked on regarding quantum effects of hydrogen on transition metal surfaces and subsurface entry [89-92]. Due to the very computationally demanding nature of calculating full band structures, I only focus on **k**=0 states.

4.1.2. Clean Pt

For this section I return to the ideal, clean (111) surface, here represented by a five atomic layer slab with all Pt atoms fixed at bulk interatomic separation, as suggested in several studies [93-97]. I should also note that unlike the graphene case in which experimental and DFT calculations-based C-C bond length values are identical, the Pt-Pt separation used here (2.77 Å) is slightly different from my computed value of 2.83 Å. Platinum is an fcc close-packed solid, and the (111) face is most stable among low-index surfaces. This is exactly why the (111) surface was chosen. I use a hydrogen surface coverage of one-fourth, i.e. the unit cell contains twenty Pt atoms (four per layer) and a single H. Calculations for a coverage of 1.0 were also done for comparison. In essence, the number of layers used to represent the surface is the key difference from some previous calculations from our research group [77-79], with the increased H-Pt interaction energy point sampling as a secondary addition. Energy calculations were performed in a periodic supercell approach to density functional theory, employing pseudopotentials. For this particular system I used a 508 eV cutoff for the expansion of the electron wave functions, generalized gradient approximation [27] for electronic exchange-correlation, and a 4×4×1 Monkhorst-Pack [33] mesh for the Brillouin zone sampling, which showed good adsorption energy convergence.

Eighty-one total energy surface-normal scans across the 1×1 surface primitive cell were the bases of the potential energy surface (PES) constructed. Fig. 4.3(a) shows the minimum-energy corrugation along the surface (i.e. $V(x,y)$ at $\partial V(r)/\partial z = 0$), with the corresponding trace along indicated paths connecting the minima at the top and

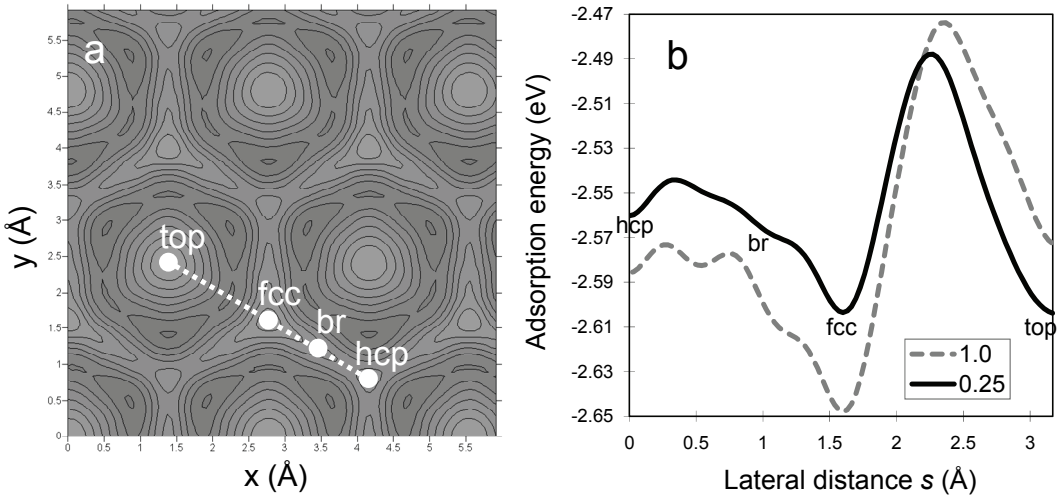

Fig. 4.3. Potential energy minimized along the *z*-direction for the (111) surface of platinum, sampled on a 6Å×6Å area. Contour lines are separated by 0.02 eV, and lighter shades denote regions of stronger adsorption. (right panel) Potential energy along the path indicated by the dashed line in the left panel for two hydrogen coverages (θ = 0.25, 1.0).

hollow sites. Fig. 4.3(b) shows a one dimensional cut along the energy topography. Top site and fcc site adsorption are found to be, in practical terms, energetically equivalent, with an adsorption energy of 2.61 eV. The slight energetics differences as compared with related computational literature, especially on the relative adsorption strength on the hollow and top sites, arises from factors including adsorbate coverages used, differences in the slab thickness, and the choice of equilibrium bulk lattice constants.

The full potential energy term $V(x,y,z)$ for the hydrogen atom on the (111) surface of clean platinum may be expressed analytically in Morse form (4.12) or harmonic (4.13):

$$V(x,y,z) = D(x,y)\left\{\left[e^{-\beta(x,y)[z-z_0(x,y)]}-1\right]^2-1\right\} \tag{4.12}$$

$$V(x,y,z) = \frac{1}{2}\alpha(x,y)\left[z-z_0(x,y)\right]^2 - D(x,y) \tag{4.13}$$

with the terms $D(x,y)$, $\alpha(x,y)$, $\beta(x,y)$, and $z_0(x,y)$ interpolated through Fourier expansions. I have specifically chosen these forms in order to compare results with previous studies on this same topic.

Figure 4.4(a) shows a surface-normal cross section of the potential energy surface (i.e. $V(x,z)$ along the axes drawn in Fig. 4.1) for the total energy calculations supplemented with cubic spline interpolations in all directions while taking into

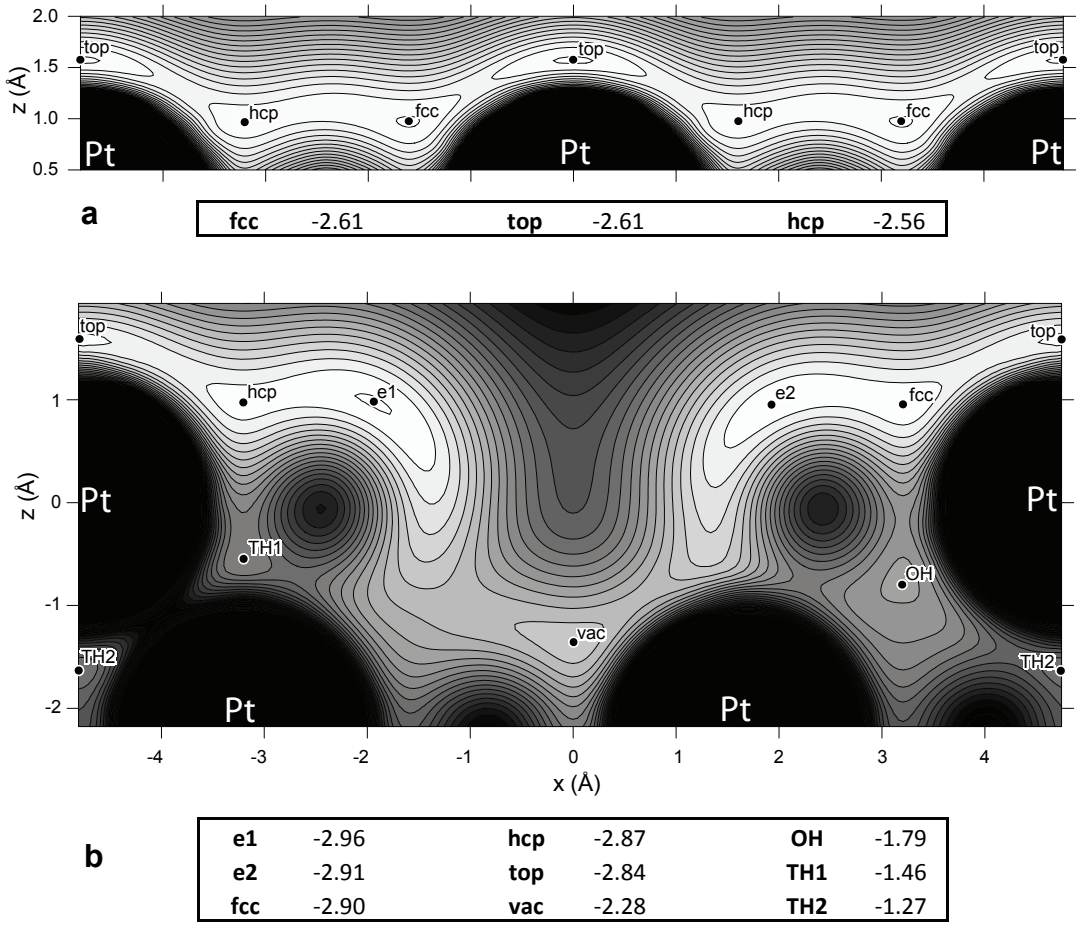

Fig. 4.4. Surface-normal cross sections of (a) the potential energy surface for flat Pt(111) and (b) for the surface with vacancies. Isoenergy contours are separated by 0.1 eV in (a) and 0.15 eV in (b). Lighter shaded regions denote lower energy (stronger adsorption). PES values at the labeled local minima are expressed in eV.

account the periodic boundary conditions along surface-parallels. Figure 4.5 on the other hand shows that in regions away from top site-adsorption, the Morse fits tend to exaggerate the Pt-H repulsion extent when the hydrogen atom is in regions near the surface but far from the top site. Correspondingly, the harmonic approximation for the *z*-component of the potential energy surface is good for hydrogen on hollow sites, wherein subsurface entry is more probable, but weak for top site adsorption. Three-dimensional cubic spline interpolations are arguably more exact since data points are connected more smoothly and contours followed more closely, although eigenstate calculations can be more time consuming, and care must be taken in some cases to avoid unphysical interpolations when the sampling is few.

Figure 4.6 shows the wave functions for **k**=0, *n*=0 to 5 for the PES constructed with Morse forms along the surface normal direction. The corresponding states

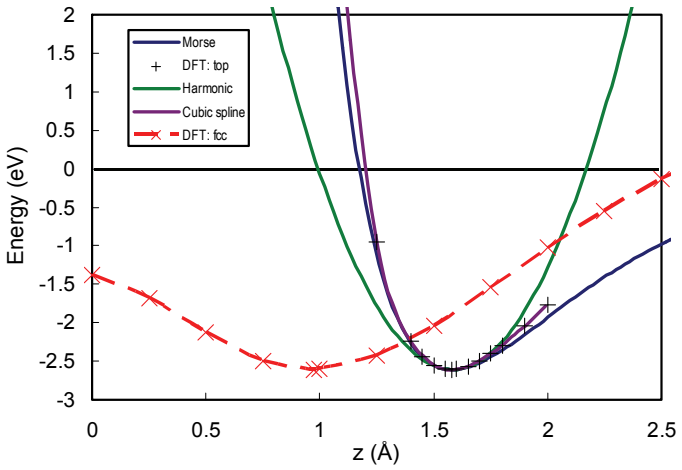

Fig. 4.5. A comparison of fitting methods for the potential energy term.

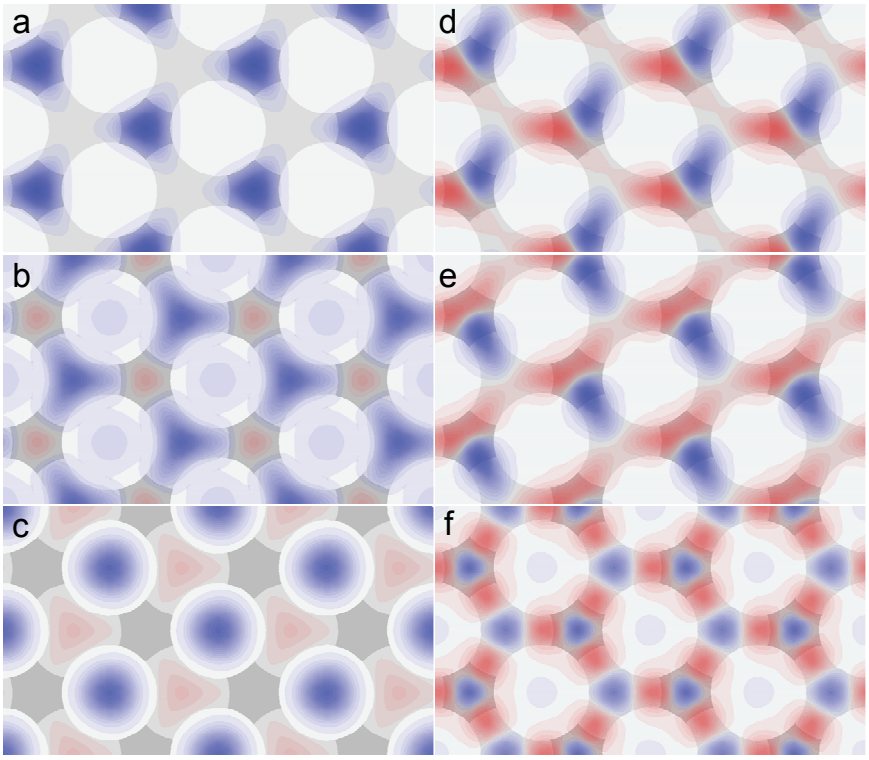

Fig. 4.6. Periodic plot of real-space wave functions describing hydrogen atom motion on the flat Pt surface, using Morse fits along the surface normal direction. Red and blue regions denote different signs for the wavefunction value. The ground state is shown in (a), while states 30 meV, 32 meV, 34 meV, 34 meV and 55 meV above the ground state are shown in (b) to (f), respectively.

describing hydrogen atom motion on the (111) surface of platinum calculated using the potential energy surfaces from a harmonic approximation and supplemented with splines, respectively, are shown in Figs. 4.7 and 4.8. Panels are ordered such that

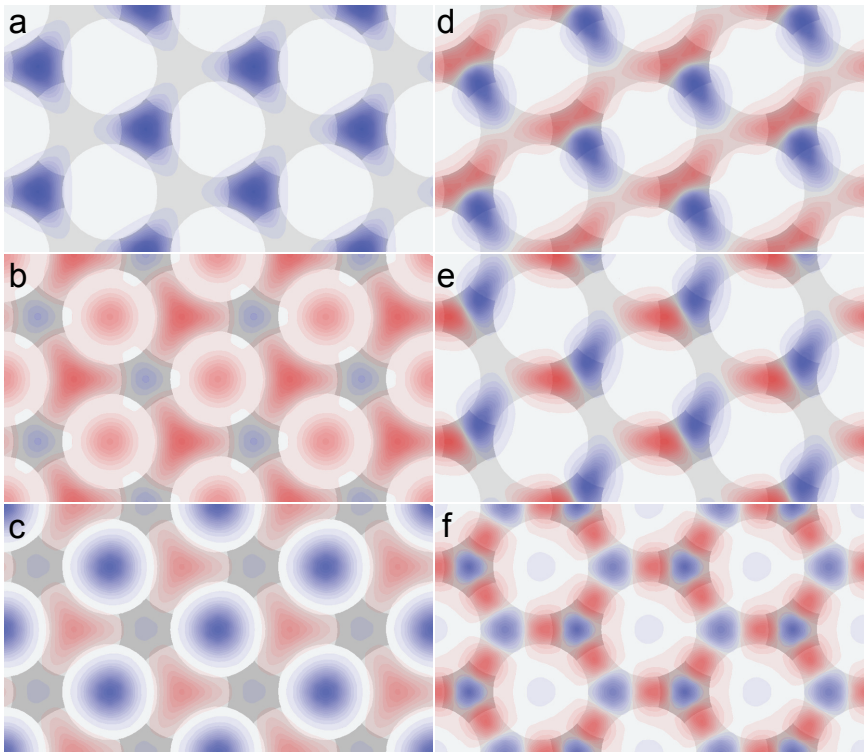

Fig. 4.7. Periodic plot of real-space wave functions describing hydrogen atom motion on the flat Pt surface, using harmonic fits along the *z*-direction. Red and blue regions denote different signs for the wavefunction value. The ground state is shown in (a), while states 30 meV, 31 meV, 33 meV, 33 meV and 54 meV above the ground state are shown in (b) to (f), respectively.

the n=0 ground state is shown in (a) and the state highest in energy among wave functions shown in panel (f), differing in energy by less than a tenth of an electronvolt.

Focusing firstly on the results for the Morse functions-based PES construction, the n=0 state (E = –2.46 eV, Fig. 4.6(a)) of hydrogen shows an important difference with previous results for a coverage of 0.25 on the Pt(111) surface modeled using three atomic layer-thick slabs [79]: the ground state wave function is clearly more localized in the vicinity of the fcc threefold hollow site in the current calculations – a distinction that should be attributed to the differences in the potential energy surfaces constructed, since the computational methods are identical. The thicker surface slab and denser PES sampling used here thus improves on the description of the interaction of an H atom with a real Pt surface. Comparing results to that reported in Refs. [75, 76], agreement is found with regard to the location and highly localized character of the ground state wave function. While being more close to Ref. [75],

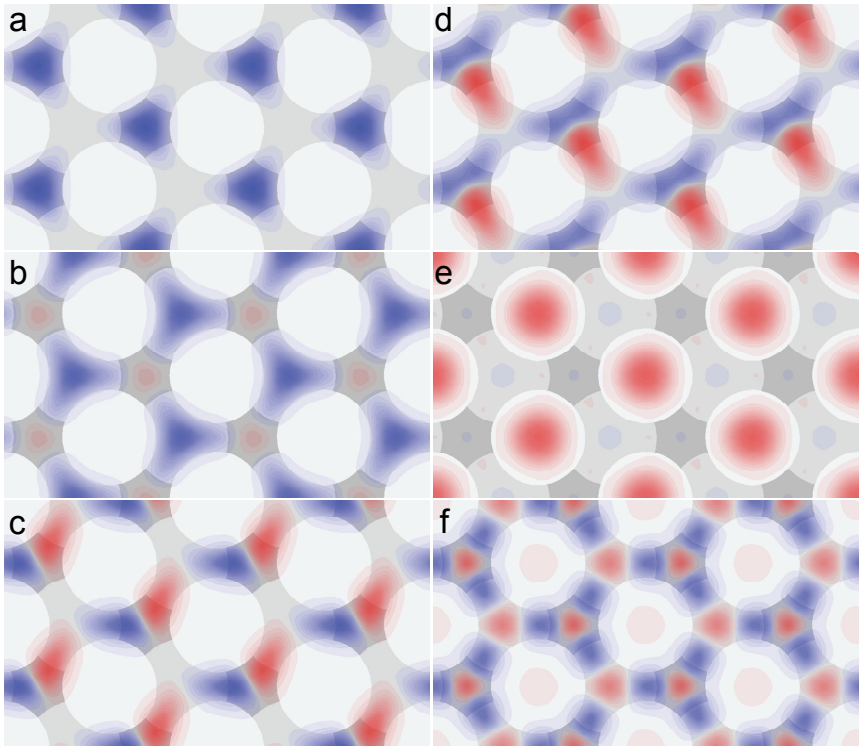

Fig. 4.8. Periodic plot of real-space wave functions describing hydrogen atom motion on the flat Pt surface, using three-dimensional spline interpolations. Red and blue regions denote different signs for the wavefunction value. The ground state is shown in (a), while states 32 meV, 38 meV, 39 meV, 48 meV and 58 meV above the ground state are shown in (b) to (f), respectively.

results deviate starting from the first higher band. I attribute these differences to the different treatments/approximations used in obtaining the wave functions. The n=1 state (Fig. 4.6(b)) is 30 meV above the ground state, and while primarily located at the hcp site, already exhibits significant delocalization, having vibrational extrema at all three high-symmetry sites. This delocalization is attributed to the intrinsic anharmonicity of the potential energy term in the surface parallel direction (in contrast to delocalization associated with the increase in wave function nodes/extrema for excited states in a harmonic oscillator). This then suggests that, assuming the hydrogen atom is initially at the ground state, quantum surface diffusion is likely to occur even at half the barrier obtained straight from the PES, as the H atoms can be widely distributed along the surface. The n=2 state shown in Fig. 4.6(c) has its extrema at the top and hcp sites, while bridge sites are accessed in the degenerate n=3 and 4 states (Fig. 4.6(d) & 4.6(e)), which as well show considerable delocalization. As we go on higher in energy to the state shown in Fig. 4.6(f),

vibrational states get more complex as the number of wave function extrema increases, translating to even greater delocalization.

The n=0 wave functions of hydrogen for the other PES constructions are physically similar to their counterpart using the Morse-fitted PES, and have practically the same zero-point corrected adsorption energy ($E_0 \approx -2.46$ eV). The states shown in Fig. 4.7 have strong physical resemblances to those shown in Fig. 4.6. In particular, considerable delocalization is seen starting from the state 30 meV above the ground state, Fig. 4.7(b). Wave functions shown in Figs. 4.8(b) to 4.8(d) also suggest the possibility of surface diffusion right above the ground state. While primarily located at the hcp site, the n=1 state 32 meV above the ground state is noticeably more spread out than the ground state, and the presence of a vibrational peak at the fcc hollow site suggests the onset of delocalization. However, a noticeable difference compared with the results within the Morse and harmonic potential constructions is the absence of the wave function extremum at the top site. Figure 4.8(e) shows that the top site is not favorably occupied until reaching a state 16 meV higher in energy, bypassing delocalized vibrational states at hollow/bridge sites (Figs. 4.8(c),(d)).

Based on adsorption energies from the potential energy surface, one can conclude that atomic hydrogen will adsorb on the fcc hollow site or the top site with near-equal preference. However, the much stronger repulsion profile at the top site as the H atom moves towards the surface suggests that these two adsites should be quantum mechanically non-degenerate, explaining the fcc-localized ground state. The use of harmonic approximations (or Morse approximations) all throughout the surface however reduces the potential energy profile differences between fcc hollow site and top site adsorption, and I see this as the primary factor that leads to the differences between figures 4.6/4.7 and 4.8, especially with regard to occupancy of the top site.

One obvious similarity though among the results is the expected increase in delocalization extent with energy. The state 58 meV above the ground state (Fig. 4.8(f)) is worth mentioning, as vibrational extrema of the wave function are observed at all high-symmetry (i.e., top, hcp, fcc, and bridge) sites. Vibrational characters of the lower states are generally parallel to the surface plane, and get more mixed with increasing energy. However, the vibrational characters perpendicular to the surface are much more associated with the corrugation of the PES itself, i.e., not particularly localized at a specific adsite. It is only in much higher states not shown here that a perpendicular character shows prominence.

Results on the numerical methods employed here once again support having a low barrier to H atom diffusion on the ideal (111) surface of platinum. To get from the localized ground state to considerable delocalization, the energy needed is less than the barrier predicted from the potential energy surface.

This section's results can be compared with some relevant experimental work. High resolution electron energy loss spectroscopy (HREELS) is an experimental technique used to obtain information concerning vibrational modes of a surface or of adatoms and admolecules. Being able to resolve energy losses in the meV range, this method is thus useful in describing adsorbed hydrogen on platinum. While the loss intensity for vibrations of atomic H on surfaces is acknowledged to be low, several peaks could still be recognized: at 31 meV [74, 75], 67-68 meV [74, 75, 98, 99], 112-113 meV [74, 99], and 152-153 meV [74, 98, 99]. Comparisons of specular and off-specular geometries suggest dipole characters for all but the 68 meV peak. The prominence of these energy loss peaks were however shown to be considerably dependent on the hydrogen coverage on the Pt surface, with the 68 meV, 112 meV and 152 meV energy peaks losing prominence as H coverage decreases [74]. At the same time however, the 31 meV peak gains more prominence, meaning that this is the only feature that is worth comparing with at the low adsorbate coverage considered in my model. Assuming hydrogen atoms on the surface are in the ground state, the 31 meV peak excellently fits the $n=0\rightarrow1$ transition (Fig. 4.8) as these states are separated by 32 meV. The agreement of these results may even be improved more by an explicit treatment of hydrogen atom motion band structure for the $n=1$, in which a little dispersion may be present.

There have also been studies quantifying the diffusion barrier for atomic hydrogen on Pt(111). Laser-induced thermal desorption (LITD) measurements [100] of the barrier to the diffusion of H on the flat Pt surface showed values in the range of 300 to 520 meV for coverages of 0.33 to 0.001 ML, although it has been pointed out that defects created on the surface may have significantly affected the reported results. Data from quasielastic helium atom scattering [101] yielded an average activation energy of 68±5meV at a coverage of 0.1 ML, while linear optical diffraction results [102] yielded values ranging from 104 to about 185 meV for the entire spectrum of coverages studied (around 157 meV for $\theta=0.1$), found generally higher than those observed on stepped surfaces, and exhibiting a different coverage-dependence trend when compared with the previous two studies mentioned. While the current

capabilities for probing hydrogen at coverages as low as 0.1 ML is encouraging, the very dissimilar values at a finite coverage of 0.1 ML from the latter two studies is a point of concern in which I can at best make only conjectures with regard to any attempt in harmonizing the two, given the fact that I from my results actually expect much lower values for the diffusion barrier of an isolated H atom on Pt(111).

The 0.15 eV zero-point energy I got from my calculations seems rather large compared to data from nuclear reaction analysis [88], but I for now tentatively attribute the significant discrepancy to the effects of neighboring hydrogen atoms in the high hydrogen coverage (θ=1 ML) used in the experiments.

4.1.3. Vacancy effects

It's worth a discussion comparing the previous section's results to a (111) surface of Pt wherein one in four first-layer surface atoms is removed, creating a surface with an ordered arrangement of vacancy defects. Physically, this system represents an extreme case for the presence of surface defects. Calculations employing density functional theory have revealed several local adsorption minima on this rough Pt surface, most notably at the edges of the vacancy (the two types which I call e1 and e2, the former being the global minimum). In terms of the PES construction, the advantages of splines become much more obvious since Morse or harmonic approximations would have grave shortcomings in describing the more complex area within the surface vacancy. It is with this reason that hydrogen motion eigenstates are pursued only from the PES constructed with cubic spline interpolation. Splines also show a very significant improvement over the 2D sinusoid-fitted case, especially when complemented with a reasonable potential term cut very close to substrate atoms in order to avoid unphysical features brought about by the repulsive singularity. The resulting potential energy cross-section surrounding a vacancy site is shown in Fig. 4.4(b).

From the symmetry of the system, total energy calculations were performed to build 324 surface-normal scans on a 2×2 area, i.e., on an 18×18 grid. All computational parameters are held the same as with the discussion in the previous section, save for the choice of the GGA functional [25] and the energy cutoff, which was done to optimize calculations without compromising accuracy. Fig. 4.9(a) shows the potential energy minimized along the *z* (surface normal) direction, while

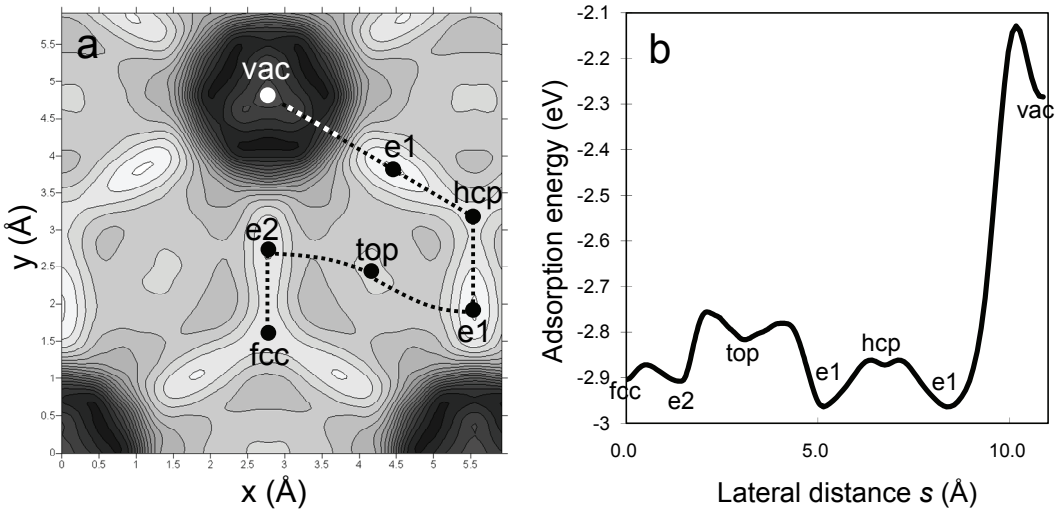

Fig. 4.9. (a) Potential energy minimized along the *z*-direction for the (111) surface of platinum with vacancies, sampled on a 6Å×6Å area. Contour lines are separated by 0.05 eV, and lighter shades denote regions of stronger adsorption. (b) Potential energy along the paths of least potential indicated by the broken curves in (a).

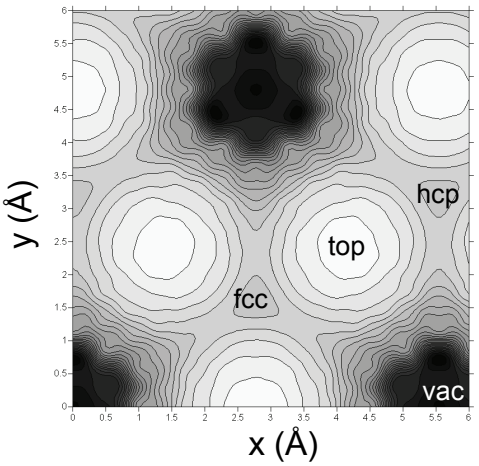

Fig. 4.10. H atom surface normal (*z*) position of the H atom at minimum energy. Contour lines are separated by 0.12 Å, and lighter shades being farther from the Pt surface.

Fig. 4.10 shows the corresponding stable-position corrugation $z_0(x,y)$ for this system, which essentially follows the contours of the surface itself.

These results show the following key details/trends: First, strongest adsorption occurs at the bridge centers on vacancy step edges, with that on the e1 step slightly preferred over the more close-packed edge site e2. The adsorption energy from DFT, i.e., without zero-point correction, at this position is –2.96 eV – stronger than that on the flat surface, attributed to the lower stability of the rough surface modeled in this

study. Adsorption at high-symmetry sites (and at all points directly above the first layer) is stronger as compared to data shown in Fig. 4.3, although the relative stability of the top site with respect to the threefold hollow sites is noticeably decreased.

There is a clear difficulty in entering the vacancy. My calculations show that vacancy entry requires surmounting a wall about 0.84 eV high, and is thus expected to prevent hydrogen from settling at the positions left vacant by the removed substrate atoms. The slight stability of the vacancy center from its immediate surroundings is expected partially from being a high-symmetry site on the second layer of the (111) surface, but the magnitude of the barrier is worth noting. This wall arises from the relative stability of the second layer atoms at the vacancy, associated with their higher coordination, and is expected to hold true in general for regions at the immediate bottom of steps, as in [80].

While H adsorption in the Pt(111) vacancy is stable relative to the system with the H atom in the vacuum region, the difficulty for a hydrogen atom in entering the area left vacant by a missing surface Pt atom may seem surprising since settling inside the hole seems to be the most logical process at first glance, like a golf ball settling into the hole of a putting green. In order to explain the energetics of a H atom near the vacancy, it is important to note the following trends one can readily obtain from a systematic study of H atom interaction with smaller Pt structures. Firstly, interaction with an H atom is much more short-ranged, i.e. H-Pt bonding is more short-ranged compared with Pt-Pt bonding and so the H atom does not directly form bonds with the first-layer atoms when it is placed at the center of a vacancy, but with the second layer (subsurface) atoms. Secondly, subsurface entry of a hydrogen atom is endothermic, consistent with the tendency of H to bind more favorably to low-coordinated substrate atoms. To illustrate this concretely, the binding energy for the H-Pt diatomic molecule, which has an interatomic separation of 1.53 Å, is 3.64 eV – much stronger than that on the surface of Pt(111). Substrate atoms with lower coordination are more reactive to adsorbates, an effect I attribute to having more electron density present for forming new bonds. It is with these reasons that the energy of the system with H at the center the vacancy is higher than when it is on the edge of the vacancy. It should be finally noted that H atom adsorption on Pt at high-symmetry adsites are generally lower in energy, which is why e1 is at a bridge center,

and the center of the vacancy, which is a second-layer analogue of an fcc threefold hollow surface adsite on ideal Pt(111), is a local potential energy minimum.

At 208 meV, the surface diffusion barrier derived directly from the PES is higher, for the defective system. The path of least potential along the surface passes through the top site, as compared with the network connecting only hollow sites in the ideal (111) surface, which has a 60 meV barrier. But it's also interesting to consider the question: does a vacancy open the way for subsurface H atom adsorption? In terms of diffusion into the subsurface, Fig. 4.4 shows several other local minima aside from the energy minima at surface sites labeled in Fig. 4.1: the tetrahedral sites TH1 (E=–1.46 eV), TH2 (E=–1.27 eV), and the octahedral site OH (E=–1.79 eV). These are rather big jumps in energy considering how strongly bound the H atom is on the surface. To put things into perspective it would be good to compare these results with that on Pd(111), as palladium is known for its high hydrogen absorption capability. Referring to a recent study by Ozawa et al. [92], the potential energy surface value for atomic H motion at the 1st TH1 subsurface site of Pd(111) is –2.38 eV, while those on the 1st OH and 1st TH2 sites are –2.55 eV and –2.30 eV, respectively. In contrast, the potential energy value at the vac site in the current study is –2.28 eV, higher than any of the aforementioned subsurface sites in palladium. On the surface of Pd(111), the PES global minimum (fcc site adsorption) is –2.92 eV, which coincidentally is very similar to the adsorption energy at e1 for the current study. Considering this, the large differences in subsurface energies for the H atom in the two systems being compared here suggest that atomic H entry into the Pt subsurface with the presence of vacancies is unlikely.

Figure 4.11 shows the real-space wave functions describing hydrogen atom behavior on the Pt surface with vacancies. States in (a) to (e) show probabilities for localized adsorption on the different adsorption local minima as we go up in energy. Panel (f) shows a considerably delocalized wave function 178 meV from the ground state. Strongest adsorption occurs at the bridge centers on vacancy step edges, with that on e1 slightly preferred over the other vacancy edge potential energy minimum, e2. The adsorption energy with zero-point correction at this position is –2.79 eV – considerably stronger than that on the flat surface, which can be expected from the lower stability of the rough surface. Subsequent higher states suggest the localized occupation at the fcc-e2 region (e.g., Fig. 4.11(b,c)) and the hcp-e1 region (e.g., Fig. 4.11(d)), separately, while the favorable occupation of the top site starts from a state

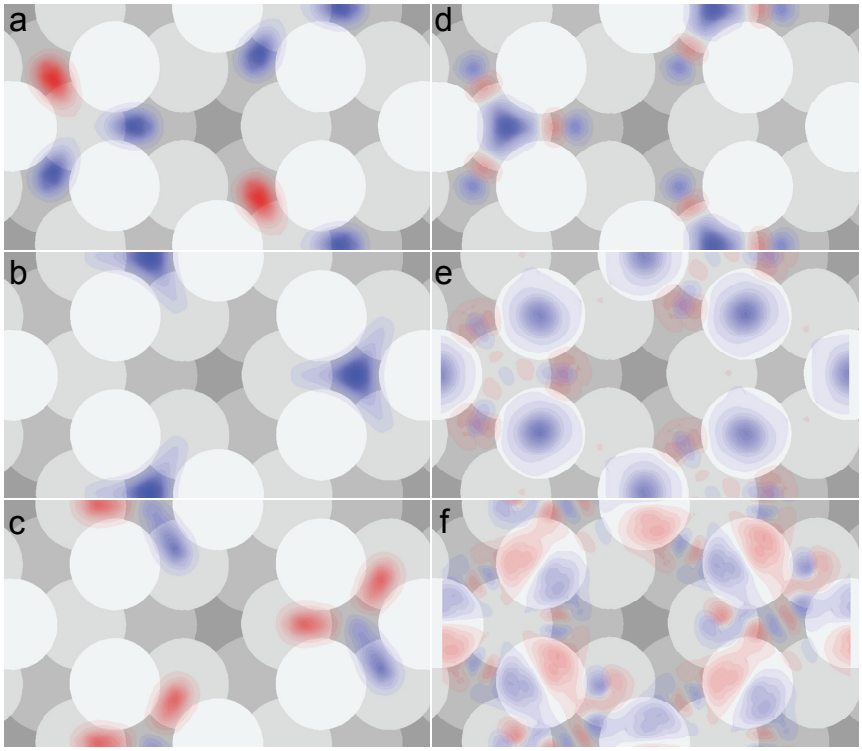

Fig. 4.11. Periodic plot of real-space wave functions describing hydrogen atom motion on the Pt surface with vacancies. Positive (negative)-valued regions are plotted in red (blue). A superposition of the lowest energy states is shown in (a), while states 35 meV, 50 meV, 53 meV, 159 meV and 178 meV above the ground state are shown in (b) to (f), respectively.

about 160 meV above the ground state (Fig. 4.11(e)). More significant wave function delocalization is manifested from thereon (Fig. 4.11(f)), implying considerably easier surface diffusion.

Lastly, these calculations also show that the hydrogen atom is highly unlikely to enter a vacancy (and subsurface sites), and hence replacing the removed Pt atom in its original position is not expected. From the potential energy surface, settling at the vacancy is a state about 680 meV higher than adsorption on e1, and wave functions showing a significant vacancy occupancy are located much higher in energy as compared to the states I have discussed in this study. For comparison, significant occupancy of a subsurface site in Pd(111) was shown for a state 0.31 eV above n=0 [89]. For the Pt system currently being discussed, I expect a much higher jump in energy. It would be good to confirm its actual value through further analyses of the higher states for H atom motion, which has not yet been done at this point because of the large number of states that need to be individually examined. This section has

anyway shown that the mere presence of vacancies holds the hydrogen at the Pt surface more strongly, and in this manner the vacancies indeed serve as trapping centers that contribute to weaker hydrogen diffusion.

4.2. Coadsorbed hydrogen and carbon monoxide on platinum

The coadsorbed hydrogen and carbon monoxide on Pt system has been the subject of a number of experimental studies [103-113] for its high relevance in heterogeneous catalysis, particularly in relation with hydrogen fuel cells. Several of these studies have looked into the limit in which hydrogen pressure is very much increased that adsorbed CO site occupancy and adsorption geometry is significantly affected [104, 106, 109, 110]. Thermal energy atom scattering and LEED studies [104] of the coadsorption system formed after H_2 exposure on Pt(111) preadsorbed with a low CO coverage revealed some of the first evidence of CO island formation, emphasizing that homogeneous islands would not form without the coadsorbed hydrogen because of CO-CO repulsion on the solid surface. Surface site occupancy is correlated with local coverage, as bridge site-adsorbed CO has been reported even for average CO coverages of less than 1/4 ML [106]. An increase in hydrogen pressure leads to opposite trends in the number of bridge-bonded and top-bonded CO admolecules, suggesting hydrogen-induced CO displacement at high hydrogen pressures that can ultimately lead to segregation into areas of high local CO coverage [106] and even decrease the CO desorption energy due to the repulsive interactions [110] between adsorbed species.

On the other hand some reports have provided evidence of mixed adsorbates/overlayers existing on the platinum surface, suggesting an attractive side to the on-surface H-CO interaction. One of the early studies on coadsorbed H and CO on Pt(111) has shown multiple binding sites for the adsorbed species, and suggested the possible formation of surface species that contained both H and CO, citing similarities with the formaldehyde-dosed surface [103]. Further evidence for the formation of H-CO surface complexes was suggested in a later thermal desorption study [105], as well as a mixed overlayer [111]. Whether or not H and CO tend to completely segregate on the Pt(111) surface may seem different across literature, but one should note the differences in experimental conditions of these studies: dosages/pressures of the adsorbing species, as well as initial surface conditions, i.e., the order of introducing CO and hydrogen to the surface.

The reader may also find interest in related experimental work on the interaction of H and CO on other metals [114-122], which have primarily been motivated by catalyzing the Fischer-Tropsch reaction. Similar to findings on Pt, studies on close-packed metal surfaces have frequently reported repulsive coadsorbate interactions associated with possible segregation into homogeneous groups, and that the presence of preadsorbed CO greatly reduces subsequent hydrogen intakes. A lesser H-CO repulsion extent has however been reported on Ni [114], which is consistent with the fact that Ni is considered an efficient catalytic component in methane conversion from CO.

There exists a good number of theoretical studies on the behavior of the hydrogen atom on Pt(111) [71, 74-79, 81], CO on Pt [123-129], as well as studies on the formyl (HCO) radical [130-140], but theoretical work specifically addressing the H/CO coadsorption system on Pt [111, 141] is however surprisingly limited. It would be good for example to quantify the extent to which H and CO interaction on Pt is repulsive knowing that H-CO interaction in the gas phase is actually partly attractive, and comment on possibilities for H and CO closely coexisting on Pt. It is in this light that I in this study try to describe in more detail the hydrogen-carbon monoxide interaction on platinum by firstly mapping out an effective potential energy term a mobile H atom experiences. From this potential energy term V_H hydrogen atom adsorption and surface diffusion are discussed, noting differences with analogous results on H-Pt(111) and the simpler three-atom CO/H systems. In the last section of this study I briefly comment on H-CO interaction with respect to the stability of adsorbed formyl on the Pt surface.

4.2.1. Computational model

Working within the electronically adiabatic H atom motion approximation, the main computational work of this study is a three-dimensional potential energy term V_H constructed from a pool of H atom position-dependent calculations based on density functional theory. For this purpose I used the VASP code [48, 49] for its periodic supercell implementation of DFT. Energy calculations covered almost 6,500 sampling points in the space spanning a 2×2 (111) surface cell laterally, and up to 5.0 Å away from the first layer of Pt atoms into the vacuum region. All calculations were spin-polarized and use the generalized gradient approximation [25, 26] for electronic exchange-correlation. An energy cutoff of 400 eV was used to

limit the plane wave basis set while retaining excellent numerical accuracy, while Brillouin zone sampling used a 4×4×1 mesh [33]. For this given set of **k** points, the potential energy converges within 0.06 eV at the PES global minimum, which is reasonably good when compared with the actual adsorption energy magnitudes. Lesser-interacting regions of the PES show much better convergence, within 0.01 eV. A vacuum region of around 16 Å between repeating Pt sheets was used to accurately represent the solid surface-vacuum interface. The same unit cell was used for adsorbed HCO calculations. Supplementary calculations for a higher CO coverage were implemented with a c(4×2) structure, using similar DFT parameters and two CO admolecules in a surface unit cell. On this topic, I received comments that relativistic effects should be taken into account. However, it must firstly be noted that relativistic effects were not found conclusive in giving light to the CO/Pt(111) puzzle. Furthermore, relativistic effects were not found necessary for theory-experiment agreement on H-Pt(111) (or H-metals in general) and H-CO, so there is reason to believe such effects would have minimal contributions in this study.

I assumed an unreconstructed (111) surface represented by a five atomic layer-thick Pt sheet with atoms fixed at interatomic separations consistent with experimental data. A single CO molecule and a hydrogen atom are included in the calculation unit cell, and contains four metal substrate atoms in each atomic layer, giving rise to a representative model for a Pt(111) surface with an intermediate CO admolecule coverage, i.e., CO-CO repulsion is still weak. The periodic model used provides a hypothetical ordering of CO on the surface which I believe is not necessarily unphysical, and nonetheless provides us with information that should prove useful in discussions with more elaborate models. The CO molecule in the surface cell was placed on a top site, as CO has experimentally been observed to preferentially adsorb on top sites with decreasing CO coverage [97, 142-152]. The topic of which site is the global energy minimum for CO adsorption is not part of this study. The chief approximation used in these calculations is the assumption of frozen CO molecule and Pt surface atoms in the presence of hydrogen. Physically this is closest to the case of hydrogen atoms moving significantly faster when compared to the motion of metal substrate and CO atoms, which is not unreasonable given the lighter mass of hydrogen and considerable differences in measured diffusion parameters of these two species on transition metal surfaces [101, 115, 153, 154]. I leave the task of describing the coupled H and CO motion on the Pt surface

Table 4.1. Bond lengths of CO on Pt(111)

Theory

	θ = 0.25	θ=0.5
Pt-C (top)	1.86 Å	1.88 Å
Pt-C (brg)	---	2.04 Å
C-O (top)	1.16 Å	1.16 Å
C-O (brg)	---	1.18 Å

Experiment

(D.F. Ogletree, et al. Surf. Sci. 173 (1986) 351)

Pt-C (top)	1.85±0.1 Å
Pt-C (brg)	2.08 ±0.07 Å
C-O (both)	1.15± 0.05 Å

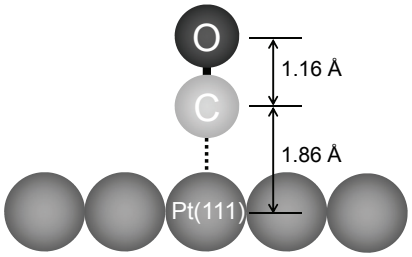

Fig. 4.12. Calculated geometry for stable CO molecule adsorption on the Pt(111) surface.

to later studies. Meanwhile, towards the end of this section, the C and O atoms are relaxed together with H in order to comment on stable states arising from the possible reaction of the coadsorbates.

The CO molecular axis is aligned parallel to the surface normal, with the molecule anchored via the carbon atom, in line with well-known experimental results. Upon relaxing the CO molecule along the direction normal to the surface (the *z* coordinate axis), Pt-C and C-O bond lengths of 1.86 Å and 1.16 Å were obtained, respectively. These values change by only less than 1% for the top-adsorbed CO in c(4×2)-2CO structure calculations, which is in excellent agreement with estimates of Ogletree et al. [97]. More details on this are given in Table 4.1 and Fig. 4.12. The magnitude of CO adsorption energy on Pt (E_{ads} = 1.54 eV) also finds very good agreement with experimental data, particularly closest to the value of 1.50 eV reported in Ref. [151]. It's helpful to note that while the usefulness of DFT in binding site prediction of CO on Pt(111) has been much discussed, the excellent agreement of the actual binding energy magnitude and geometry predictions for CO top-site adsorption with experimental data are much more relevant to this study's focus, evaluating H-CO interaction on Pt.

4.2.2. Results and discussion

Potential energy plots describing H-CO interaction on the Pt(111) surface are shown in Figs. 4.13 and 4.14. High-symmetry adsites on the surface farthest from the adsorbed CO are identified in Fig. 4.13(a) with terminology borrowed from adsorption on the clean (111) case. The two types of hcp and fcc threefold hollow sites, which differ in distance from the CO admolecule, are distinguished from each other. Calculated energy values shown in these plots have been adjusted with respect

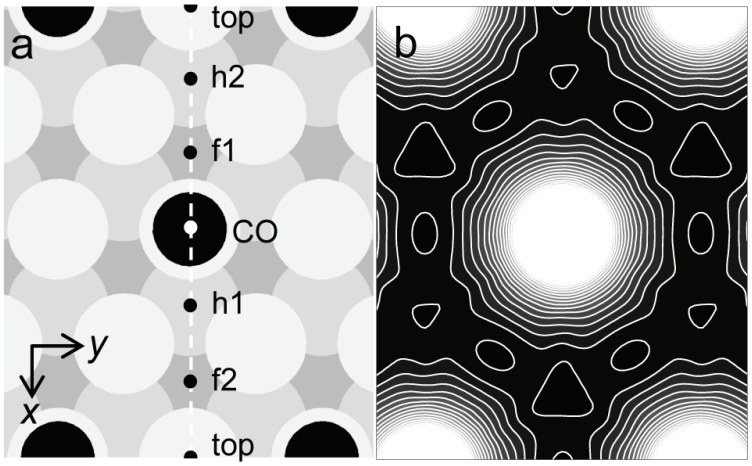

Fig. 4.13. (a) CO coverage and adsorption geometry, as viewed from the (111) direction (top view). Analogues to Pt(111) high-symmetry sites are labeled accordingly: fcc threefold hollow (f1 and f2), hcp threefold hollow (h1 and h2), and top (top) sites. Gray circles with increasing shading depth are visual guides for Pt atom positions going into the subsurface; black indicates CO. (b) H atom motion potential energy minimized along z, sampled over the area shown in (a). For prominently repulsive regions, i.e, near CO, energy minima within the range 0.0 Å < z < 1.8 Å were used. Equipotential contours are separated by 0.15 eV, and darker regions indicate lower energy, i.e., more attractive interaction with H.

to $E_{ref} = E_{Pt+CO(ads)} + E_{H(g)}$ so that the energy of the system with the H atom far from the surface is zero. This reference is particularly convenient in defining regions where the adsorption of atomic H on the Pt+CO(ads) system is favored ($V_H < 0$) and not ("repulsive", $V_H > 0$).

Potential energy continuously increases as a hydrogen adatom approaches a CO molecule adsorbed on the platinum surface. In contrast to the free CO case [132, 136, 138], there is a noticeable absence of an energy minimum near the carbon atom, overshadowed by the more strongly attractive H-Pt interaction near the metal surface. This lack of an attractive character to H-CO interaction on Pt is consistent with experimental speculations, affirming that regions comprised of mixed adsorbates on Pt are unlikely to spontaneously form.

The interaction with the adsorbed CO molecule is highly asymmetric: the lateral repulsion radius is greater for H atoms approaching O than for adatoms near C, visually depicted through the mushroom-shaped isoenergy contours in Fig. 4.14(a). And so even before an incoming hydrogen atom reaches the Pt surface, it already experiences a hindrance to adsorption when approaching within a considerable region (~2 Å) around O. Barrierless pathways to the Pt surface are still available at

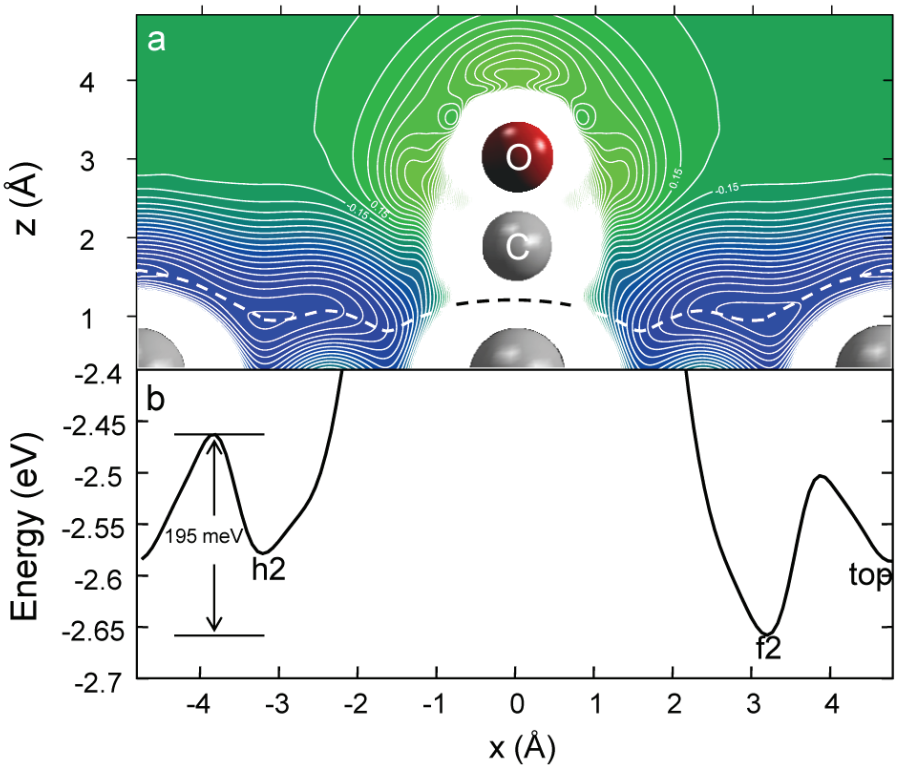

Fig. 4.14. (a) Potential energy cross section along the surface-normal plane passing through the dashed line in Fig. 4.13. The coordinate *x* is the distance along the dashed line in Fig. 4.13, with the origin set at the CO position. Equipotential contours are separated by 0.15 eV, and darker-shaded intercontour regions indicate lower energy. (b) Potential energy along the path connecting the local minima (fcc, top and hcp sites) on the exposed Pt surface. A *z*-contour corresponding to this path is given by the broken line in (a).

the coverage used in the PES calculation, but it would not be unreasonable to speculate that higher CO coverages should provide situations which would favor more scattering, and may prove even more detrimental to incoming hydrogen molecules.

One may compare the PES to energy maps on the interaction of an H atom with an isolated CO molecule previously obtained from ab-initio [132, 136, 138] and semi-empirical [134] calculations. The most obvious similarity is a predominantly repulsive O, which may initially seem surprising considering that the formation of the stronger OH bond should actually lower the system energy. On a quantitative level, the calculated binding energy of diatomic OH is 4.87 eV, compared to the CH bond's 3.68 eV, a difference that can be most attributed to the greater electronegativity of oxygen. It has been suggested that the high extent of CO bond

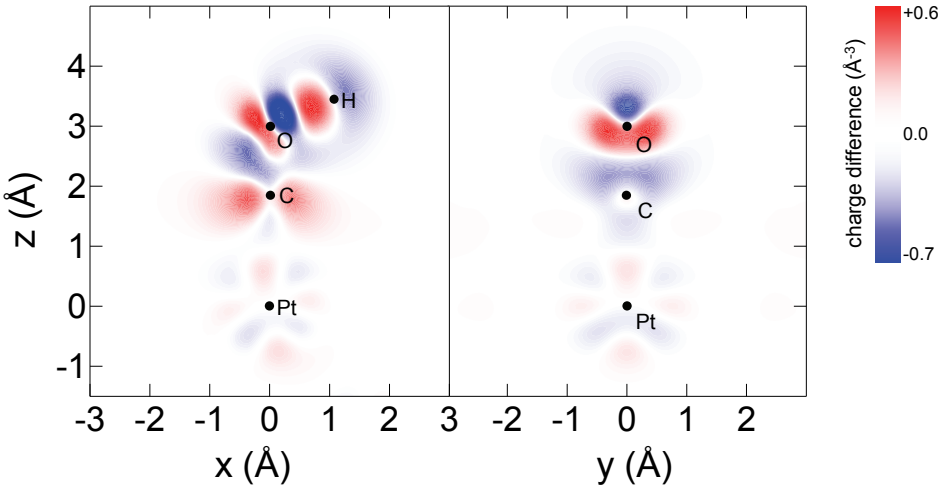

Fig. 4.15. Cross-section plots of changes in charge density distribution $n_{diff}(\mathbf{r}) = n_{Pt+COH(ads)}(\mathbf{r}) - [n_H + n_{Pt+CO(ads)}(\mathbf{r})]$ for H atom position near the Pt-COH(ads) metastable minimum. Regions in red (blue) indicate an increase (decrease) in charge density. Black dots denote positions of atomic nuclei. (a) cut along the same plane (*xz*) as Fig. 4.14, (b) along another surface-normal plane, which is perpendicular to (a).

breaking associated with the O-H bond formation is responsible for the repulsion extent of H around the oxygen atom [139]. For my system, charge accumulation/depletion for H near O shown in Fig. 4.15 is consistent with this, as a decrease in charge overlap for the C-O bond is discernible, particularly for the π interaction involving p_x orbital electrons. For H near O, the only effect of the Pt surface is a small decrease in the repulsion magnitude. The favored bent geometry of COH associated with the electronic ground state has an on-Pt analogue, as seen through the presence of the local energy minimum when the H atom is 0.98 Å from the oxygen atom, with a COH bond angle of 121°. This minimum has a local energy depth of about 0.3 eV with respect to the CO–H dissociation saddle point, opening a possible shallow anchorage for a hydrogen atom. But the metastable nature of this adsorption state ($V_H \approx +0.4$ eV) still suggests that there is a low likelihood of hydrogen spontaneously adsorbing on CO, and safely rules out an easy pathway for dissociative adsorption of H_2 on CO. Results also suggest that it would be easier for an adatom to desorb into the vacuum region than migrate up to O given the absence of a favorable local route for the latter process.

While the top and h2 adsites on the surface are local energy minima, the most stable adsorption location for the H atom is at f2. The adsorption energy of H

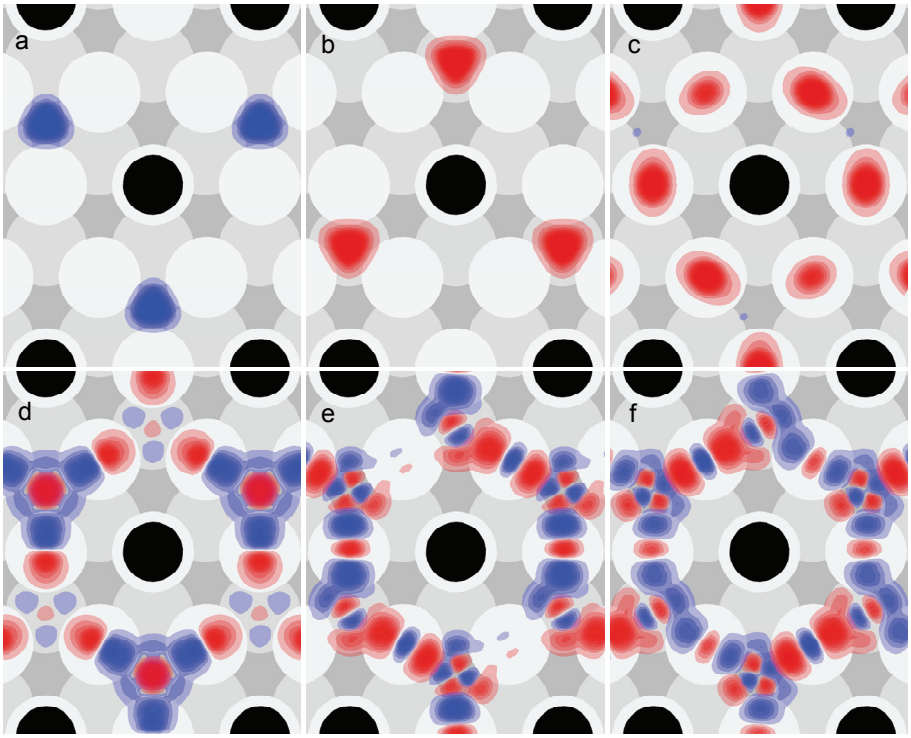

Fig. 4.16. Three-dimensional real-space wave functions describing hydrogen atom motion on the Pt surface with CO. CO admolecules are depicted by filled black circles. The ground state (E_0 = –2.50 eV) is given in panel (a). The states in panels (b) to (f) are 70 meV, 120 meV, 162 meV, 186 meV and 187 meV higher in energy from the ground state, respectively.

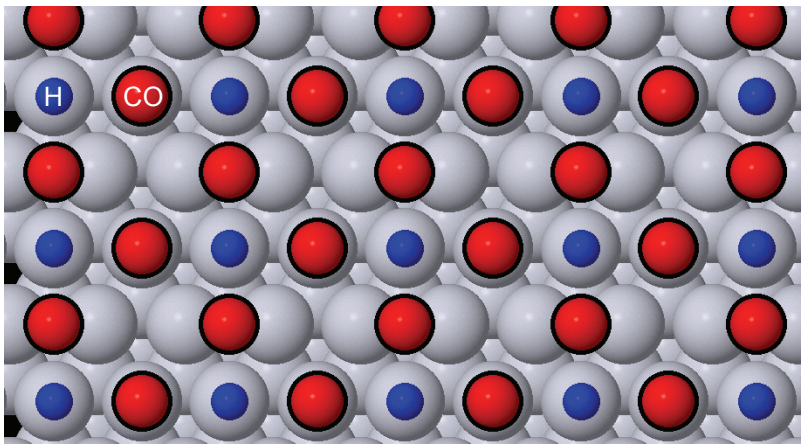

Fig. 4.17. H and CO coadsorption with high CO coverage. H atoms are in blue, while CO is in black/red (labeled in upper left).

calculated from DFT at this point on H/CO-Pt(111) is –2.65 eV, while the corresponding values at the top and h2 sites are –2.58 eV and –2.57 eV, respectively. These results show that while H-CO repulsion evidently prevents H atom adsorption

on the nearest hollow sites h1 and f1, defining an adsorption exclusion region around CO, adsorption on the next-nearest hollow sites are not significantly affected: the relative energetic difference between the top and fcc sites is more emphasized, but the values themselves do not differ much from previous results (i.e., ΔE<2%) for H adsorption on the clean Pt surface [81], which is rather surprising given the rather close proximity of these adsites to the adsorbed CO.

Real-space wave functions describing hydrogen atom motion on this system were calculated in order to comment on quantum mechanical aspects to H adsorption on this representative system of Pt with CO. Working within the variation method, the **k**=0 eigenstates describing hydrogen motion were numerically determined from wave functions expressed as a linear combination of a uniformly distributed set of Gaussian-type functions (density of 720 per surface Pt atom) spanning the space immediately above the first layer of Pt atoms. Adsorption states on the O atom were neglected in order to reduce computational costs, which can be justified with the fact that V_H at this metastable position is ~3 eV above that of H adatom minima. The finite V_H sampling was supplemented with cubic spline interpolations in all directions for smooth numerical integration, applying periodic boundary conditions along the surface-parallel directions. The ground state of hydrogen in the present calculations (Fig. 4.16(a)) is evidently one that is localized on the f2 hollow site, while high probabilities of finding hydrogen on the h2 hollow and top sites are at states 70 meV and 120 meV higher in energy. I reaffirm the possibility of finding H with an adsorption strength very close to that on the clean Pt surface: the zero-point corrected energy of the adsorbed H atom here is –2.50 eV, which again is only <2% different from its clean surface counterpart [81].

On the experimental side, a previous study showed that the presence of CO has a mixed effect on the adsorption strength of H atoms on Pt(100) [107], while another suggested, from the lower desorption temperature of hydrogen, the weakening of the hydrogen-metal surface bond when CO is around [111]. I attribute the difference of these findings and that of the latter experimental study to the fact that they used a very high CO coverage, one which is enough to decrease the H adsorption stability due to the higher inter-adsorbate repulsion. Supplementary calculations I performed for the coadsorption system including an H atom and two adsorbed CO molecules in a c(4×2) geometry support the possibility of H intercalated within CO islands, showing that at least two stable H adsorption states (with respect to unbound H) exist

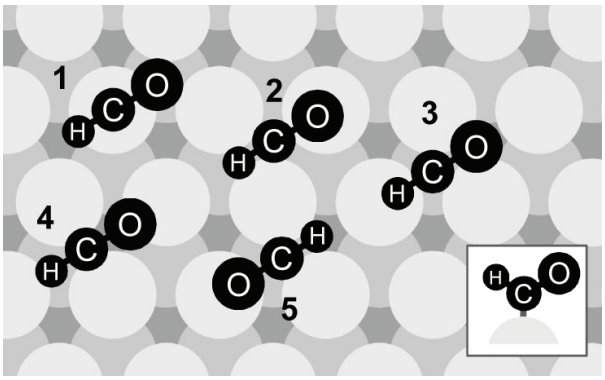

Fig. 4.18. (a) Top view of initial geometries for HCO adsorption calculations. The carbon atom is placed (**1**) on a top site, (**2**) on an fcc hollow site, (**3**) hcp, (**4**) bridge site. The geometry in (**5**) is similar to that used in J. R. B. Gomes et al., J. Electroanal. Chem. 483, 180 (2000). The corresponding adsorption energies are –1.93 eV, –0.85 eV, –1.10 eV, –1.05 eV, and –0.85 eV, respectively. Inset: side view (HCO plane) for configuration **1**.

for this high-coverage coadsorption system (Fig. 4.17) – on top and bridge sites between CO admolecules – and indeed, with significantly weaker adsorption strengths (1.78 eV and 1.62 eV, respectively) due to the stronger repulsion between the adsorbed species. Assuming the repulsion radius for H adatoms does not change drastically from that in Fig. 4.14 (~1 Å), one can infer the possibility of having a mixed overlayer, even to the reportedly favored local CO coverage of 0.5, which has CO-CO separations as close as 3.67 Å.

The lowest energy barrier to surface diffusion calculated from DFT is much increased – to 195 meV, specific to the benchmark model used in this study, from ~60 meV on the clean Pt(111) surface [75, 76, 81], which has easier access to minimum-potential canals connecting the surface threefold hollow sites. Clear delocalization of the H atom motion wave function on the other hand is apparent at states from about 186 meV above the ground state (Fig. 4.16(f)). Higher states expectedly exhibit even greater delocalization across the surface while steering clear of CO due to the repulsion. Lower coverages of CO are expected to substantially reduce the difficulty in surface diffusion.

Finally, I briefly discuss H-CO interaction with respect to the stability of adsorbed formyl on platinum. For this purpose, a reasonable estimate of the binding energy of formyl on the Pt surface was obtained by fully relaxing HCO at five different initial positions on Pt (Fig. 4.18), including that used in a previous study on a Pt cluster

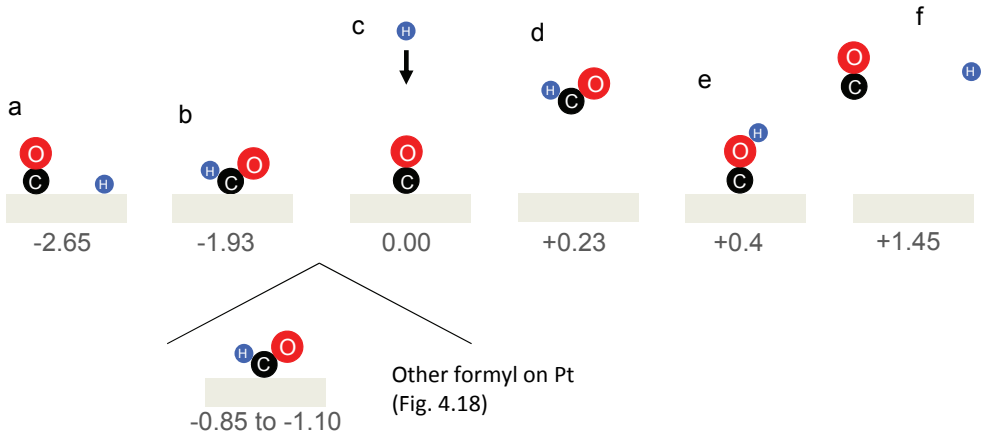

Fig. 4.19. A comparison of H-C-O system states on the platinum surface. All units are in eV.

[155]. The atoms are oriented in a way that the HCO plane is perpendicular to the (111) surface, with the C atom closest to the Pt surface. Formyl slightly rotates in configurations 2 and 5 (configuration 3) due to favorable O-Pt (H-Pt) interaction. Adsorption energies were found to lie within a 0.4 eV of each other, but are all stable to both E_{ref} and the system comprised of the pristine Pt surface and unbound HCO. The lowest-energy configuration (1, Fig. 4.18(a)) in particular is more stable by 1.93 eV and 2.16 eV with respect to these references. Here the formyl molecule is oriented analogous to formaldehyde, in such a way that the top Pt atom replaces the missing hydrogen.

From the standpoint of reactions needed for fuel cells, the formation of adsorbed formyl is unwanted as not only does it decrease available protons, but also since desorption of CO through this complex becomes even harder, as shown in the computational results. It should however be noted that the adsorbed formyl is about 0.7 eV higher in energy with respect to the surface-bound CO molecule and H atom (at f2), and thus corresponds to an unfavorable reaction for adatoms, not to mention a possibly higher energy barrier to the process given the nontrivial geometry changes required. Experimental evidence for the presence of adsorbed formyl [103] originating from CO and hydrogen however suggest that this barrier may not be very high. As a summary for this section, Fig. 4.19 shows the relative stabilities of a system of the three atoms H, C and O on the platinum surface, emphasizing that the separately coadsorbed case for H and CO is most stable.

5 Summary and conclusions

In this work, I firstly discussed the stability and likelihood of the presence of small hydrogen clusters on a face of graphene with a coverage $\theta \approx 0.06$. The most stable adsorbed structures among groups of two and three H atoms were found to be the configurations in which the hydrogen atoms are immediately next to each other, i.e. in the closest possible clustering geometries. In both cases, the adsorption per H atom is stronger as compared with the adsorption of an isolated H atom on graphene, and so favorable cluster formation of H on the graphene surface is ascertained. Other stably adsorbed groups were explicitly pointed out. In all cases, the importance of reconstruction in reaching stable configurations was found. These results show that the H-graphene system is an excellent example of substrate effects being much more important, compared with direct adsorbate interaction, in determining the nature of grouping/ordering of adsorbed species on a surface. The trend of adjacent-adsorption configurations having the strongest bound structures on graphene may still hold for the next larger clusters of bound hydrogen, but this trend is not expected to hold as bound hydrogen is increased infinitely unless both faces of a graphene sheet are hydrogenated. It should be further noted that on the graphite case, inter-sheet interactions may be important in determining the stability of these small hydrogen clusters on the surface and so results presented here may not necessarily be identical.

A hydrogen atom on graphene was shown to be easily identified through its effects on graphene electronic states near the Fermi level. A comparison with effects brought about by pairs having H–H separations less than 2.7 Å show visible differences that make it possible to discriminate the atom from the pairs at a very local level. The adsorption of hydrogen was confirmed to disrupt the π network near the Fermi level of graphene in a rather extended range – an event that affects the material's reactivity to subsequent hydrogen, and hence promotes cluster formation. Calculations for the closest pairing using both faces of graphene suggest not only more strongly adsorbed states, but facile processes for the entry of subsequently adsorbing hydrogen. The ensuing fully hydrogenated material is stable, and has a structure greatly distinct from pristine graphene.

Calculated hydrogen states on Pt(111) within three different numerical treatments were firstly discussed. While the use of analytic fits was found to reduce the difference between top-site and fcc hollow-site occupancy of the H atom, resulting to a premature occupancy of the top site at some of the lowest energy states, the ground state of atomic H on Pt(111) is physically independent of the constructed PES used. The ground state for hydrogen atom motion was found to be much less delocalized than previously reported, showing that the thicker surface slab and denser PES sampling used here improves the description of the quantum mechanical behavior of an H atom on platinum. All calculations support the low barrier to surface diffusion, as delocalization states start just 32 meV above the ground state for atomic H adsorption, and subsequent delocalized states are not much higher in energy. This section's results show excellent agreement with the most recent HREELS data available, and strongly suggest a closer examination of the inconsistent experimental reports regarding hydrogen diffusion at low coverages.

Application on a hypothetical rough Pt surface was also discussed – a benchmark for understanding the role of vacancies on actual surfaces, which should lie between the two extremes for the Pt surface presented in this study. Quantum effects were seen to reduce the barriers on both types of platinum surfaces. While filling up the vacancy seems most logical in order to create a smoother, more stable surface, it was shown that it is the edges of vacancies that trap adsorbed H strongly, and this leads to increased difficulty of hydrogen surface diffusion as compared to that on the ideal surface. A comparison with analogous results for palladium shows that subsurface entry of atomic H is not likely.

Adsorbed CO clearly shows inhibiting effects greater than what can be expected from simple adsorption site exclusion, consistent with the macroscopic effect of lower electrode catalytic activity for 'poisoned' platinum electrodes. It was explicitly shown that the presence of CO decreases the likelihood of H adsorption due to strong repulsion with adsorbed CO, particularly with the oxygen atom. The repulsion furthermore leads to a local decrease in the number of H adsites, affecting the nearest high symmetry sites within 2.77 Å of CO. Farther from this, these results suggest the possibility that H adsorption strength on platinum may not be significantly affected. Considerable weakening of H atom adsorption is on the other hand observed inside more compact CO groups. H diffusion on the surface, given the higher potential energy near CO, understandably favors paths farthest from the

adsorbed CO. Diffusion of H atoms into or within compact CO groups on Pt is expected to be difficult.

Formation of an adsorbed COH complex is highly unlikely given the strong repulsion with oxygen of incoming H, the lack of easy reaction pathways for H adatoms, and the metastable nature of the COH energy minimum. The formation of an adsorbed formyl on the Pt surface is also found to be an endothermic process for interacting coadsorbed species, but is very stable with respect to its unbound state. Stable H atom adsorption has been found even for a high coverage of adsorbed CO, indicating that the existence of H atoms intercalated in CO groups, if not the presence of a more homogeneous mixed overlayer, is not unlikely. However, repulsion between H and CO indicates that regions comprised of mixed adsorbates on Pt are unlikely to spontaneously form.

One future prospect for furthering these studies is a more accurate treatment of weak, noncovalent chemical interactions in implementing density functional theory. Existing implementations of DFT have found a lot of success in explaining physical phenomena and designing new functional materials, but even until today are suggested to still be lacking in areas such as van der Waals interactions and strongly correlated electron systems. In this light, future theoretical work may focus on effectively taking into account physisorption and hydrogen bonding in condensed matter systems by working on post-GGA methods in accounting for nonlocal correlation energy. Another future prospect, more specifically relating to the physical systems of this dissertation, is implementing dynamics for many-hydrogen processes on solid surfaces. It is always beneficial to obtain the temperature dependence of reactions such as collective diffusion of adsorbates, and at least a qualitative description of other factors that affect reaction rates in order to optimize the operational conditions for a desired physical process. While classical molecular dynamics has often been a useful tool in addressing these needs in condensed matter systems, such methods may not be appropriate for dynamics of systems primarily involving hydrogen. It has been made clear that a quantum mechanical treatment is in general necessary for describing individual hydrogen behavior, and this may probably hold as well for a group of hydrogen atoms. I also expect that these studies will contribute to the discussion on the possible breakdown of electronically adiabatic models.

6 References

[1] Kohn W. Nobel Lecture: Electronic structure of matter-wave functions and density functionals. RvMP. 1999 Oct;71(5):1253-66.

[2] Hohenberg P, Kohn W. Inhomogeneous Electron Gas. Phys Rev B. 1964;136(3B):B864.

[3] Kohn W, Sham LJ. Self-Consistent Equations Including Exchange and Correlation Effects. PhRv. 1965;140(4A):1133.

[4] Kisaku M, Rahman M, Kishi T, Matsunaka D, Roman TA, Dino WA, et al. Diameter dependent magnetic and electronic properties of single-walled carbon nanotubes with Fe nanowires. Japanese Journal of Applied Physics Part 1-Regular Papers Brief Communications & Review Papers. 2005 Feb 8;44(2):882-8.

[5] Rahman MM, Kisaku M, Kishi T, Roman TA, Dino WA, Nakanishi H, et al. Electric and magnetic properties of Co-filled carbon nanotube. J Phys Soc Jpn. 2005 Feb 5;74(2):742-5.

[6] Roman T, Diño WA, Nakanishi H, Kasai H. Glycine adsorption on single-walled carbon nanotubes. Thin Solid Films. 2006 Jun 19;509(1-2):218-22.

[7] Roman T, Dino WA, Nakanishi H, Kasai H. Amino acid adsorption on single-walled carbon nanotubes. EPJD. 2006 Feb 21;38(1):117-20.

[8] Roman T, Dino WA, Nakanishi H, Kasai H. Amino acid adsorption effects on nanotube electronics. Journal of the Vacuum Society of Japan. 2006 May 13;49(7):46-8.

[9] David M, Roman T, Diño WA, Nakanishi H, Kasai H, Ando N, et al. Polybutylene terephthalate on metals: a density functional theory and cluster models investigation. Journal of Physics-Condensed Matter. 2006 Feb 1;18(4):1137-42.

[10] David M, Roman T, Dino WA, Nakanishi H, Kasai H, Ando N, et al. Polybutylene terephthalate adhesion on metals: a density functional theory investigation. Journal of the Vacuum Society of Japan. 2006 May 13;49(7):433-6.

[11] David M, Roman T, Dino WA, Nakanishi H, Kasai H, Ando N, et al. A nanoscale understanding of the adhesion of polybutylene terephthalate on aluminum. Surf Sci. 2007 Nov 15;601(22):5241-5.

[12] David M, Roman T, Nakanishi H, Kasai H, Ando N, Naritomi M. A density functional theory-based investigation of adhesion of. poly(butylene terephthalate) on aluminum. Thin Solid Films. 2006 Jun 19;509(1-2):215-7.

[13] Roman T, Diño W, Nakanishi H, Kasai H, Miyako Y, Ando N, et al. Examining poly(phenylene sulfide) adhesion using cluster models. Journal of the Vacuum Society of Japan. 2005 Feb 18;48(3):235-7.

[14] Roman T, Diño WA, Nakanishi H, Kasai H, Miyako Y, Naritomi M. PPS-metal adhesion: a density functional theory-based study. Solid State Commun. 2004 Nov;132(6):405-8.

[15] Dy ES, Roman TA, Kubota Y, Miyamoto K, Kasai H. Exploring haem-based alternatives for oxygen reduction catalysis in fuel cells - a status report of our first principles calculations. Journal of Physics-Condensed Matter. 2007 Nov 7;19(44):445010.

[16] Muhida R, Rahman MM, Tsuda M, Roman TA, Dino WA, Nakanishi H, et al. Change of magnetic properties of benzenes in multiple-decked sandwich clusters: $Mn_n(C_6H_6)_{(n+1)}$ (n=1,2). Journal of Physics-Condensed Matter. 2004 Dec 8;16(48):S5749-S53.

[17] Muhida R, Susanto A, Kishi T, Roman T, Nakanishi H, Kasai H. Density functional calculations for H_2 adsorption on $Fe(OH)_3$ by considering molecular orientation. Journal of the Vacuum Society of Japan. 2005 Jan 8;48(3):199-201.

[18] David M, Muhida R, Roman T, Kunikata S, Diño W, Nakanishi H, et al. Applying computational nanomaterials design to the reactive ion etching of NiO thin films - a preliminary investigation. Journal of Physics-Condensed Matter. 2007 Sep 12;19(36):365210.

[19] David M, Muhida R, Roman T, Nakanishi H, Diño W, Kasai H, et al. First-principles calculations-based model for the reactive ion etching of metal oxide surfaces. Vacuu. 2008 Oct 15;83(3):599-601.

[20] Kishi H, Ozawa N, David M, Roman T, Arboleda NB, Dino WA, et al. Density functional theory based evaluations of the reactive ion etching process model for TiO_2(anatase) thin film. Journal of the Vacuum Society of Japan. 2008 May 10;51(6):63-6.

[21] Ozawa N, Roman T, David M, Kishi H, Kasai H. Modeling the reactive ion etching process for the CoO(001) surface via first principles calculations. Journal of Physics-Condensed Matter. 2008 Sep 3;20(35):355006.

[22] Roman T, Nakanishi H, Kasai H. Halogen-assisted copper atom abstraction: a computational perspective. Jpn J Appl Phys. 2009;48(9).

[23] Takano F, Shima H, Muramatsu H, Kokaze Y, Nishioka Y, Suu K, et al. Reactive Ion Etching Process of Transition-Metal Oxide for Resistance Random Access Memory Device. Jpn J Appl Phys. 2008 Aug 22;47(8):6931-3.

[24] Hartree DR. The wave mechanics of an atom with a non-Coulomb central field Part I theory and methods. Proceedings of the Cambridge Philosophical Society. 1928 Jul;24:89-110.

[25] Perdew JP, Burke K, Ernzerhof M. Generalized gradient approximation made simple. Phys Rev Lett. 1996 Oct 28;77(18):3865-8.

[26] Perdew JP, Burke K, Ernzerhof M. Generalized gradient approximation made simple (errata). Phys Rev Lett. 1997 Feb 17;78(7):1396-.

[27] Perdew JP, Chevary JA, Vosko SH, Jackson KA, Pederson MR, Singh DJ, et al. Atoms, Molecules, Solids, and Surfaces - Applications of the Generalized Gradient Approximation for Exchange and Correlation. Phys Rev B. 1992 Sep 15;46(11):6671-87.

[28] Frisch MJ, Trucks GW, Schlegel HB. Gaussian 03. Pittsburgh, PA: Gaussian, Inc. 2003.

[29] Makov G, Payne MC. Periodic Boundary-Conditions in Ab-Initio Calculations. Phys Rev B. 1995 Feb 15;51(7):4014-22.

[30] Neugebauer J, Scheffler M. Adsorbate-Substrate and Adsorbate-Adsorbate Interactions of Na and K Adlayers on Al(111). Phys Rev B. 1992 Dec 15;46(24):16067-80.

[31] Vanderbilt D. Soft Self-Consistent Pseudopotentials in a Generalized Eigenvalue Formalism. Phys Rev B. 1990 Apr 15;41(11):7892-5.

[32] Chadi DJ, Cohen ML. Special Points in Brillouin Zone. Phys Rev B. 1973;8(12):5747-53.

[33] Monkhorst HJ, Pack JD. Special Points for Brillouin-Zone Integrations. Phys Rev B. 1976;13(12):5188-92.

[34] Chan KT, Neaton JB, Cohen ML. First-principles study of metal adatom adsorption on graphene. Phys Rev B. 2008;77:235430.

[35] Higai S, Honda A, Nishida K, Wada N, Sakabe Y. Alkali-metal lithium on graphite monolayer surface: Theoretical study. J Phys Chem Solids. 2008;69:1158-61.

[36] Sevincli H, Topsakal M, Durgun E, Ciraci S. Electronic and magnetic properties of 3d transition-metal atom adsorbed graphene and graphene nanoribbons. Phys Rev B. 2008;77:195434.

[37] Wu M, Liu E, Ge MY, Jiang JZ. Stability, electronic, and magnetic behaviors of Cu adsorbed graphene: A first-principles study. Appl Phys Lett. 2009;94:102505.

[38] Miura Y, Kasai H, Dino WA, Nakanishi H, Sugimoto T. Effective pathway for hydrogen atom adsorption on graphene. J Phys Soc Jpn. 2003 May;72(5):995-7.

[39] Miura Y, Kasai H, Dino W, Nakanishi H, Sugimoto T. First principles studies for the dissociative adsorption of H2 on graphene. J Appl Phys. 2003 Mar 15;93(6):3395-400.

[40] Zecho T, Guttler A, Sha XW, Jackson B, Kuppers J. Adsorption of hydrogen and deuterium atoms on the (0001) graphite surface. J Chem Phys. 2002 Nov 8;117(18):8486-92.

[41] Zecho T, Guttler A, Kuppers J. A TDS study of D adsorption on terraces and terrace edges of graphite (0001) surfaces. Carbon. 2004;42(3):609-17.

[42] Andree A, Le Lay M, Zecho T, Kupper J. Pair formation and clustering of D on the basal plane of graphite. Chem Phys Lett. 2006 Jul 3;425(1-3):99-104.

[43] Hornekaer L, Sljivancanin Z, Xu W, Otero R, Rauls E, Stensgaard I, et al. Metastable structures and recombination pathways for atomic hydrogen on the graphite (0001) surface. Phys Rev Lett. 2006 Apr 21;96(15):156104.

[44] Allouche A, Ferro Y, Angot T, Thomas C, Layet J-M. Hydrogen adsorption on graphite (0001) surface: A combined spectroscopy-density-functional-theory study. J Chem Phys. 2005 Sep 22;123(12):124701.

[45] Roman T, Dino WA, Nakanishi H, Kasai H, Sugimoto T, Tange K. Hydrogen pairing on graphene. Carbon. 2007 Jan;45(1):218-20.

[46] Roman T, Nakanishi H, Kasai H, Nobuhara K, Sugimoto T, Tange K. Stability of three-hydrogen clusters on graphene. J Phys Soc Jpn. 2009;78(3):035002.

[47] Hammer B, Hansen LB, Norskov JK. Improved adsorption energetics within density-functional theory using revised Perdew-Burke-Ernzerhof functionals. Phys Rev B. 1999 Mar 15;59(11):7413-21.

[48] Kresse G, Furthmuller J. Efficient iterative schemes for ab initio total-energy calculations using a plane-wave basis set. Phys Rev B. 1996 Oct 15;54(16):11169-86.

[49] Blochl PE. Projector Augmented-Wave Method. Phys Rev B. 1994 Dec 15;50(24):17953-79.

[50] Hornekaer L, Rauls E, Xu W, Sljivancanin Z, Otero R, Stensgaard I, et al. Clustering of chemisorbed H(D) atoms on the graphite (0001) surface due to preferential sticking. Phys Rev Lett. 2006 Nov 3;97(18):186102.

[51] Roman T, Diño WA, Nakanishi H, Kasai H, Nobuhara K, Sugimoto T, et al. Identifying hydrogen atoms on graphite. J Phys Soc Jpn. 2007 Nov;76(11):114703.

[52] Ferro Y, Marinelli F, Allouche A. Density functional theory investigation of the diffusion and recombination of H on a graphite surface. Chem Phys Lett. 2003 Jan 24;368(5-6):609-15.

[53] Kelly KF, Halas NJ. Determination of alpha and beta site defects on graphite using C-60-adsorbed STM tips. Surf Sci. 1998 Oct 19;416(1-2):L1085-L9.

[54] Mizes HA, Foster JS. Long-Range Electronic Perturbations Caused by Defects Using Scanning Tunneling Microscopy. Science. 1989 May 5;244(4904):559-62.

[55] Soto MR. The Effect of Point-Defects on the STM Image of Graphite. Surf Sci. 1990 Jan;225(1-2):190-4.

[56] Tersoff J, Hamann DR. Theory of the Scanning Tunneling Microscope. Phys Rev B. 1985;31(2):805-13.

[57] Wiesendanger R, Güntherodt H-J. Scanning Tunneling Microscopy III: Theory of STM and Related Scanning Probe Methods. Berlin 1997.

[58] Ferro Y, Teillet-Billy D, Rougeau N, Sidis V, Morisset S, Allouche A. Stability and magnetism of hydrogen dimers on graphene. Phys Rev B. 2008 Aug;78(8):085417.

[59] Fukunaga T, Itoh K, Orimo S, Aoki M, Fujii H. Location of deuterium atoms absorbed in nanocrystalline graphite prepared by mechanical alloying. J Alloys Compd. 2001 Aug 30;327(1-2):224-9.

[60] Orimo S, Matsushima T, Fujii H, Fukunaga T, Majer G. Hydrogen desorption property of mechanically prepared nanostructured graphite. J Appl Phys. 2001 Aug 1;90(3):1545-9.

[61] Diño W, Nakanishi H, Kasai H, Sugimoto T, Kondo T. H2 Dissociative Adsorption at the Zigzag Edges of Graphite. e-Journal of Surface Science and Nanotechnology. 2004;2:77-80.

[62] Diño WA, Miura Y, Nakanishi H, Kasai H, Sugimoto T, Kondo T. H2 dissociative adsorption at the armchair edges of graphite. Solid State Commun. 2004 Dec;132(10):713-8.

[63] Arboleda NB, Kasai H, Nakanishi H, Diño WA, Sugimoto T. Scattering and dissociative adsorption of H2 on the armchair and zigzag edges of graphite. J Appl Phys. 2004 Dec 1;96(11):6331-6.

[64] Roman T, Diño WA, Nakanishi H, Kasai H, Sugimoto T, Tange K. Realizing a carbon-based hydrogen storage material. Jpn J Appl Phys. 2006 Mar;45(3A):1765-7.

[65] Arboleda NB, Roman T, Kasai H, Nakanishi H, Sugimoto T, Tange K, et al. Absorption of Atomic Hydrogen into Graphite via the Armchair Edge A First Principles Study. in preparation. 2009.

[66] Stojkovic D, Zhang P, Lammert PE, Crespi VH. Collective stabilization of hydrogen chemisorption on graphenic surfaces. Phys Rev B. 2003 Nov;68(19):195406.

[67] Sofo JO, Chaudhari AS, Barber GD. Graphane: A two-dimensional hydrocarbon. Phys Rev B. 2007 Apr;75(15):153401.

[68] Elias DC, Nair RR, Mohiuddin TMG, Morozov SV, Blake P, Halsall MP, et al. Control of Graphene's Properties by Reversible Hydrogenation: Evidence for Graphane. Science. 2009 Jan 30;323(5914):610-3.

[69] Feibelman PJ, Hamann DR. Theory of H-Bonding and Vibration on Pt(111). Surf Sci. 1987 Apr;182(3):411-22.

[70] Legare P. A theoretical study of H surface and subsurface species on Pt(111). Surf Sci. 2004 Jun 20;559(2-3):169-78.

[71] Olsen RA, Kroes GJ, Baerends EJ. Atomic and molecular hydrogen interacting with Pt(111). J Chem Phys. 1999 Dec 22;111(24):11155-63.

[72] Papoian G, Norskov JK, Hoffmann R. A comparative theoretical study of the hydrogen, methyl, and ethyl chemisorption on the Pt(111) surface. J Am Chem Soc. 2000 May 3;122(17):4129-44.

[73] Watson GW, Wells RPK, Willock DJ, Hutchings GJ. A comparison of the adsorption and diffusion of hydrogen on the {111} surfaces of Ni, Pd, and Pt from density functional theory calculations. J Phys Chem B. 2001 May 31;105(21):4889-94.

[74] Badescu SC, Jacobi K, Wang Y, Bedurftig K, Ertl G, Salo P, et al. Vibrational states of a H monolayer on the Pt(111) surface. Phys Rev B. 2003 Nov;68(20):205401.

[75] Badescu SC, Salo P, Ala-Nissila T, Ying SC, Jacobi K, Wang Y, et al. Energetics and vibrational states for hydrogen on Pt(111). Phys Rev Lett. 2002 Apr 1;88(13):136101.

[76] Kallen G, Wahnstrom G. Quantum treatment of H adsorbed on a Pt(111) surface. Phys Rev B. 2002 Jan 15;65(3):033406.

[77] Nobuhara K, Kasai H, Nakanishi H, Okiji A. Vibrational properties of an H atom adsorbed on Pt(111). Surf Sci. 2002 Jun 1;507:82-6.

[78] Nobuhara K, Nakanishi H, Kasai H, Okiji A. Behavior of H atom in adsorption states on metal surfaces - localization and delocalization. Surf Sci. 2001 Nov 1;493(1-3):271-7.

[79] Nobuhara K, Nakanishi H, Kasai H, Okiji A. Quantum mechanical behavior of an H atom on Cu(111) and Pt(111). J Appl Phys. 2002 Feb 15;91(4):1855-9.

[80] Olsen RA, Badescu SC, Ying SC, Baerends EJ. Adsorption and diffusion on a stepped surface: Atomic hydrogen on Pt(211). J Chem Phys. 2004 Jun 22;120(24):11852-63.

[81] Roman T, Dino WA, Nakanishi H, Kasai H. Hydrogen atom quantum migration on platinum. e-Journal of Surface Science and Nanotechnology. 2006 Oct 3;4:619-23.

[82] Difoggio R, Gomer R. Tunneling of Hydrogen in Surface-Diffusion on the Tungsten-(110) Plane. Phys Rev Lett. 1980;44(19):1258-60.

[83] Hsu CH, Larson BE, Elbatanouny M, Willis CR, Martini KM. Evidence of Quantum Motion of Hydrogen on Pd(111) in Helium-Diffraction Data. Phys Rev Lett. 1991 Jun 17;66(24):3164-7.

[84] Mate CM, Somorjai GA. Delocalized Quantum Nature of Hydrogen Adsorbed on the Rh(111) Crystal-Surface. Phys Rev B. 1986 Nov 15;34(10):7417-20.

[85] Takagi N, Yasui Y, Takaoka T, Sawada M, Yanagita H, Aruga T, et al. Quantum delocalization of H on Pd(110): A vibrational study. Phys Rev B. 1996 May 15;53(20):13767-71.

[86] Astaldi C, Bianco A, Modesti S, Tosatti E. Vibrational-Spectra of Atomic H and D on Cu(110) - Evidence for H Quantum Delocalization. Phys Rev Lett. 1992 Jan 6;68(1):90-3.

[87] Lauhon LJ, Ho W. Direct observation of the quantum tunneling of single hydrogen atoms with a scanning tunneling microscope. Phys Rev Lett. 2000 Nov 20;85(21):4566-9.

[88] Fukutani K, Itoh A, Wilde M, Matsumoto M. Zero-point vibration of hydrogen adsorbed on Si and Pt surfaces. Phys Rev Lett. 2002 Mar 18;88(11):116101.

[89] Ozawa N, Arboleda NB, Roman TA, Nakanishi H, Diño WA, Kasai H. Quantum states of hydrogen atom motion on the Pd(111) surface and in the subsurface. Journal of Physics-Condensed Matter. 2007 Sep 12;19(36):365214.

[90] Ozawa N, Roman T, Nakanishi H, Diño WA, Kasai H. Quantum states of a hydrogen atom adsorbed on Cu(100) and (110) surfaces. Phys Rev B. 2007 Mar 26;75(11):115421.

[91] Ozawa N, Roman TA, Nakanishi H, Kasai H. Quantum states of hydrogen (H, D, T) atoms on Cu(100) and (110) surfaces. Surf Sci. 2006 Sep 15;600(18):3550-4.

[92] Ozawa N, Roman TA, Nakanishi H, Kasai H, Arboleda NB, Diño WA. Potential energy of hydrogen atom motion on Pd(111) surface and in subsurface: A first principles calculation. J Appl Phys. 2007 Jun 15;101(12):123530.

[93] Davies JA, Jackson DP, Norton PR, Posner DE, Unertl WN. Surface Relaxation of Clean, and Hydrogen Covered Pt(111). Solid State Commun. 1980;34(1):41-4.

[94] Feder R, Pleyer H, Bauer P, Muller N. Spin Polarization in Low-Energy Electron-Diffraction - Surface-Analysis of Pt(111). Surf Sci. 1981;109(2):419-34.

[95] Hohage M, Michely T, Comsa G. Pt(111) Network Reconstruction - Structure, Growth and Decay. Surf Sci. 1995 Sep 1;337(3):249-67.

[96] Kesmodel LL, Somorjai GA. Structure Determination of Platinum (111) Crystal-Face by Low-Energy-Electron Diffraction. Phys Rev B. 1975;11(2):630-7.

[97] Ogletree DF, Vanhove MA, Somorjai GA. Leed Intensity Analysis of the Structures of Clean Pt(111) and of Co Adsorbed on Pt(111) in the C(4x2) Arrangement. Surf Sci. 1986 Aug;173(2-3):351-65.

[98] Baro AM, Ibach H, Bruchmann HD. Vibrational-Modes of Hydrogen Adsorbed on Pt(111) - Adsorption Site and Excitation Mechanism. Surf Sci. 1979;88(2-3):384-98.

[99] Richter LJ, Ho W. Vibrational Spectroscopy of H on Pt(111) - Evidence for Universally Soft Parallel Modes. Phys Rev B. 1987 Dec 15;36(18):9797-800.

[100] Seebauer EG, Schmidt LD. Surface-Diffusion of Hydrogen on Pt(111) - Laser-Induced Thermal-Desorption Studies. Chem Phys Lett. 1986 Jan 3;123(1-2):129-33.

[101] Graham AP, Menzel A, Toennies JP. Quasielastic helium atom scattering measurements of microscopic diffusional dynamics of H and D on the Pt(111) surface. J Chem Phys. 1999 Jul 22;111(4):1676-85.

[102] Zheng CZ, Yeung CK, Loy MMT, Xiao XD. Step effects and coverage dependence of hydrogen atom diffusion on Pt(111) surfaces. Phys Rev B. 2004 Nov;70(20):205402.

[103] Baldwin VH, Hudson JB. Coadsorption of Hydrogen and Carbon Monoxide on (111) Platinum. Journal of Vacuum Science & Technology. 1971;8(1):49.

[104] Bernasek SL, Lenz K, Poelsema B, Comsa G. Formation of Islands Consisting of Repelling Adsorbates. Surf Sci. 1987 May;183(3):L319-L24.

[105] Craig JH. Adsorption of Hydrogen and Carbon-Monoxide on Platinum. Surf Sci. 1981;111(2):L695-L700.

[106] Hoge D, Tushaus M, Bradshaw AM. Island Formation during Co/H Coadsorption on Pt(111) Studied by Ir Reflection Absorption-Spectroscopy. Surf Sci. 1988 Dec;207(1):L935-L42.

[107] Leiva EPM, Santos E, Iwasita T. The Effect of Adsorbed Carbon-Monoxide on Hydrogen Adsorption and Hydrogen Evolution on Platinum. J Electroanal Chem. 1986 Dec 24;215(1-2):357-67.

[108] Lenz K, Poelsema B, Bernasek SL, Comsa G. Lateral Distribution of Coadsorbed H and Co on Pt(111) Studied by Teas. Surf Sci. 1987 Oct;189:431-7.

[109] Parker DH, Fischer DA, Colbert J, Koel BE, Gland JL. Hydrogen-Induced Low-Temperature Co Displacement from the Pt(111) Surface. Surf Sci. 1990 Oct;236(3):L372-L6.

[110] Parker DH, Fischer DA, Colbert J, Koel BE, Gland JL. Hydrogen-Induced Co Displacement from the Pt(111) Surface - an Isothermal Kinetic-Study. Surf Sci. 1991 Nov;258(1-3):75-81.

[111] Roeterdink WG, Bonn M, Olsen RA. The CO-H interaction on Pt(111) studied using temperature programmed vibrational sum frequency generation. Chem Phys Lett. 2005 Sep 5;412(4-6):482-7.

[112] Stonehart P, Kohlmayr G. Effect of Poisons on Kinetic Parameters for Platinum Electrocatalyst Sites. Electrochim Acta. 1972;17(3):369.

[113] Wang H, Tobin RG, Lamberg DK, Fisher GB, Dimaggio CL. H-CO Interactions on the Terraces and Step Edges of a Stepped Pt Surface. Surf Sci. 1995 Jun 10;330(2):173-81.

[114] Braun W, Steinruck HP, Held G. The surface geometry of carbon monoxide and hydrogen co-adsorbed on Ni{111}. Surf Sci. 2005 Jan 10;574(2-3):193-204.

[115] Mak CH, Deckert AA, George SM. Effects of Coadsorbed Carbon-Monoxide on the Surface-Diffusion of Hydrogen on Ru(001). J Chem Phys. 1988 Oct 15;89(8):5242-50.

[116] Merrill PB, Madix RJ. Hydrogen bonding on iron: Correlation of adsorption and desorption states on Fe(100) and perturbation of the Fe-H bond with coadsorbed CO. Surf Sci. 1996 Feb 20;347(3):249-64.

[117] Mitchell GE, Gland JL, White JM. Vibrational-Spectra of Coadsorbed Co and H on Ni(100) and Ni(111). Surf Sci. 1983;131(1):167-78.

[118] Peebles DE, Schreifels JA, White JM. The Interaction of Coadsorbed Hydrogen and Carbon-Monoxide on Ru(001). Surf Sci. 1982;116(1):117-34.

[119] Riedmuller B, Papageorgopoulos DC, Berenbak B, van Santen RA, Kleyn AW. 'Magic' island formation of CO coadsorbed with H on Ru(0001). Surf Sci. 2002 Sep 1;515(2-3):323-36.

[120] Seebauer EG, Kong ACF, Schmidt LD. Surface-Diffusion of Hydrogen and Co on Rh(111) - Laser-Induced Thermal-Desorption Studies. J Chem Phys. 1988 May 15;88(10):6597-604.

[121] Vorburger TV, Sandstrom DR, Waclawski BJ. Displacement of Hydrogen by Carbon-Monoxide on (100) Face of Tungsten - Photoemission and Thermal Desorption Study. Surf Sci. 1976;60(1):211-30.

[122] Williams ED, Thiel PA, Weinberg WH, Yates JT. Segregation of Co-Adsorbed Species - Hydrogen and Carbon-Monoxide on the (111) Surface of Rhodium. J Chem Phys. 1980;72(6):3496-505.

[123] Aizawa H, Tsuneyuki S. First-principles study of CO bonding to Pt(111): validity of the Blyholder model. Surf Sci. 1998 Mar 10;399(2-3):L364-L70.

[124] Blyholder G. Molecular Orbital View of Chemisorbed Carbon Monoxide. J Phys Chem. 1964;68(10):2772.

[125] Feibelman PJ, Hammer B, Norskov JK, Wagner F, Scheffler M, Stumpf R, et al. The CO/Pt(111) puzzle. J Phys Chem B. 2001 May 10;105(18):4018-25.

[126] Morikawa Y, Mortensen JJ, Hammer B, Norskov JK. CO adsorption and dissociation on Pt(111) and Ni(111) surfaces. Surf Sci. 1997 Oct;386(1-3):67-72.

[127] Orita H, Itoh N, Inada Y. All electron scalar relativistic calculations on adsorption of CO on Pt(111) with full-geometry optimization: a correct estimation for CO site-preference. Chem Phys Lett. 2004 Jan 26;384(4-6):271-6.

[128] Pedersen MO, Bocquet ML, Sautet P, Laegsgaard E, Stensgaard I, Besenbacher F. CO on Pt(111): binding site assignment from the interplay between measured and calculated STM images. Chem Phys Lett. 1999 Jan 16;299(5):403-9.

[129] Tsuda M, Kasai H. Ab initio study of alloying and straining effects on CO interaction with Pt. Phys Rev B. 2006 Apr;73(15):155405.

[130] Adams GF, Bent GD, Purvis GD, Bartlett RJ. Electronic-Structure of the Formyl Radical HCO. J Chem Phys. 1979;71(9):3697-702.

[131] Botschwina P. Unrestricted Hartree-Fock Calculation of Force Constants and Vibrational Frequencies of HCO Radical. Chem Phys Lett. 1974;29(1):98-101.

[132] Bowman JM, Bittman JS, Harding LB. Abinitio Calculations of Electronic and Vibrational Energies of HCO and HOC. J Chem Phys. 1986 Jul 15;85(2):911-21.

[133] Bruna PJ, Buenker RJ, Peyerimhoff SD. Ab initio Study of Structure, Isomers and Vertical Electronic-Spectrum of Formyl Radical HCO. J Mol Struct. 1976;32(2):217-33.

[134] Carter S, Mills IM, Murrell JN. Potential-Energy Functions for Ground-State Surfaces of HCO and HNO. Journal of the Chemical Society-Faraday Transactions II. 1979;75:148-57.

[135] Dunning TH. Theoretical Characterization of the Potential-Energy Surface of the Ground-State of the HCO System. J Chem Phys. 1980;73(5):2304-9.

[136] Geiger LC, Schatz GC, Harding LB. A Quasi-Classical Trajectory Study of Collisions of Fast H-Atoms with CO Using an Accurate Abinitio Potential Surface. Chem Phys Lett. 1985;114(5-6):520-5.

[137] Jursic BS. Computational studies of formaldehyde dissociation and protonated carbon monoxide isomerization with density functional theory methods. Journal of Molecular Structure-Theochem. 1997 Nov 10;418(1):11-6.

[138] Keller HM, Floethmann H, Dobbyn AJ, Schinke R, Werner HJ, Bauer C, et al. Unimolecular dissociation of HCO .2. Comparison of calculated resonance energies and widths with high-resolution spectroscopic data. J Chem Phys. 1996 Sep 22;105(12):4983-5004.

[139] Perez-Juste I, Carballeira L. Theoretical study of the electronic structure of HXY/XYH radicals (X = C,Si; Y = O,S). J Chem Phys. 2007 Oct 28;127(16):164303-1.

[140] Tanaka K, Davidson ER. Theoretical-Study on the Potential Surfaces of the Lower Electronic States of HCO. J Chem Phys. 1979;70(6):2904-13.

[141] Tsuda M, Kasai H. H-2 dissociative adsorption on strained/CO-precovered Pt. Japanese Journal of Applied Physics Part 2-Letters & Express Letters. 2006 Nov;45(42-45):L1219-L21.

[142] Blackman GS, Xu ML, Ogletree DF, Vanhove MA, Somorjai GA. Mix of Molecular Adsorption Sites Detected for Disordered CO on Pt(111) by Diffuse Low-Energy Electron-Diffraction. Phys Rev Lett. 1988 Nov 14;61(20):2352-5.

[143] Chang SC, Weaver MJ. Coverage-Dependent and Potential-Dependent Binding Geometries of Carbon-Monoxide at Ordered Low-Index Platinum Aqueous and Rhodium Aqueous Interfaces - Comparisons with Adsorption in Corresponding Metal Vacuum Environments. Surf Sci. 1990 Nov;238(1-3):142-62.

[144] Ertl G, Neumann M, Streit KM. Chemisorption of CO on Pt(111) Surface. Surf Sci. 1977;64(2):393-410.

[145] Hayden BE, Bradshaw AM. The Adsorption of CO on Pt(111) Studied by Infrared Reflection-Absorption Spectroscopy. Surf Sci. 1983;125(3):787-802.

[146] Hayden BE, Kretzschmar K, Bradshaw AM, Greenler RG. An Infrared Study of the Adsorption of Co on a Stepped Platinum Surface. Surf Sci. 1985;149(2-3):394-406.

[147] Hopster H, Ibach H. Adsorption of Co on Pt(111) and Pt 6(111) X (111) Studied by High-Resolution Electron-Energy Loss Spectroscopy and Thermal Desorption Spectroscopy. Surf Sci. 1978;77(1):109-17.

[148] Kitamura F, Takahashi M, Ito M. Carbon-Monoxide Adsorption on Platinum(111) Single-Crystal Electrode Surface Studied by Infrared Reflection Absorption-Spectroscopy. Surf Sci. 1989 Dec;223(3):493-508.

[149] Lucas CA, Markovic NM, Ross PN. The adsorption and oxidation of carbon monoxide at the Pt(111)/electrolyte interface: atomic structure and surface relaxation. Surf Sci. 1999 Apr 9;425(1):L381-L6.

[150] Schweizer E, Persson BNJ, Tushaus M, Hoge D, Bradshaw AM. The Potential-Energy Surface, Vibrational Phase Relaxation and the Order-Disorder Transition in the Adsorption System Pt(111)-Co. Surf Sci. 1989 Apr;213(1):49-89.

[151] Steininger H, Lehwald S, Ibach H. On the Adsorption of Co on Pt(111). Surf Sci. 1982;123(2-3):264-82.

[152] Villegas I, Weaver MJ. Carbon-Monoxide Adlayer Structures on Platinum(111) Electrodes - a Synergy between in-Situ Scanning-Tunneling-Microscopy and Infrared-Spectroscopy. J Chem Phys. 1994 Jul 15;101(2):1648-60.

[153] Froitzheim H, Schulze M. Surface-Diffusion of Co on Pt(111) - a HREELS Study at High-Temperatures. Surf Sci. 1994 Nov 20;320(1-2):85-92.

[154] Kwasniewski VJ, Schmidt LD. Surface-Diffusion of CO on Pt(111). Surf Sci. 1992 Aug 15;274(3):329-40.

[155] Gomes JRB, Gomes JANF. Adsorption of the formyl species on transition metal surfaces. J Electroanal Chem. 2000 Mar 30;483(1-2):180-7.

7 Acknowledgments

7.1. Academic/research financial support

I am very grateful to the following institutions/programs for the financial assistance I have received during my stay in Osaka: the Japan Society for the Promotion of Science (JSPS), Matsuda Yosahichi Memorial Foreign Student Scholarship, and the Marubun Research Promotion Foundation.

7.2. Personal acknowledgments

A lot of people should be thanked, starting with Prof. Hideaki Kasai and Prof. Hiroshi Nakanishi for the fruitful stay in Osaka.

The lab staff: Reiko Tanaka, Mayuko Ishioka-Takano, Yasuko Kasakawa, Dr. Shigeno Matsumoto, Mayuko Aihara, Keiko Kobayashi, Keiko Furuyama, Akiko Horiguchi, Shin'ichi Kunikata, Ikuko Nojiri, Dr. Nobuaki Shimoji, Dr. Tomoko Ohya, Dr. Mamoru Sakaue for the background support in the lab.

Technical advice: Dr. Tomoya Kishi for advanced technical advice on using Dacapo and VASP, Mr. Masahiro Hanafusa for extremely useful Perl codes and assistance in using Perl, Dr. Nobuki Ozawa and Dr. Hiroshi Nakanishi for real-space data visualization using OpenDX, Dr. Eben Dy for donating his very handy reference on Perl programming to me, and Abdulla Sarhan for help in using Mathematica and Origin.

Mr. Keita Miyamoto, Dr. Emi Minamitani, Mr. Masahiro Hanafusa for all the help with the Japanese language and coursework requirements.

Dr. Nobuki Ozawa for all the research and financial report-related sempai help, which includes hours of fruitful theoretical discussions and tons of reports and financial paperwork.

Mr. Hirofumi Kishi for the extremely valuable help in management of hardware and software, and installing software/packages I needed.

Masanori Tani, Kazuki Kojima, Kuniyuki Miwa and Yuji Kunisada for translation work.

Dr. Thomas Zecho (Bayreuth), Prof. Elod Gyenge (Vancouver), Prof. Loh Kian Ping (Singapore), Prof. Yoshitada Morikawa (Suita), Prof. Katsuyuki Fukutani (Tokyo), Dr. Wilson Agerico Diño (Toyonaka), Dr. Daisuke Matsunaka (Suita), Prof. Branko Gumhalter (Zagreb), Dr. Kunihiro Nobuhara (Toyota), Dr. Tsuyoshi Sugimoto (Toyota), Dr. Kyouichi Tange (Toyota) and Dr. Yoshiyuki Kubota (Kansai Electric) for the tips and discussions.

Mr. Kourou Fujio for the collaborative efforts on coupled-channel quantum dynamics.

Dr. Christopher Que for the sempai help and advice; Dr. Eben Dy, Ms. Clare Escano, Dr. Nelson Arboleda and Dr. Melanie David for the peer advice.

The panelists of this dissertation – Prof. Michio Okada, Prof. Yasuhiro Sugawara, Prof. Yoshihiro Kobayashi, Prof. Yoshitada Morikawa – for their extremely valuable comments and suggestions.

Prof. Ma. Cecilia Galvez and Prof. Edgar Vallar (DLSU Manila) for all that I've learned while in their lab, which have been very useful in my graduate studies research.

My Japanese language instructors: Okazaki-sensei, Takahashi-sensei and Nishiguchi-sensei.

The unnamed peer-reviewers, and the audience of my talks and poster presentations who spent time going over my work, offering valuable comments and suggestions which in most cases helped in improving my papers.

8 Publications in scientific journals

8.1. Refereed publications

1. T. Roman, H. Nakanishi, H. Kasai, *High-uptake graphene hydrogenation: a computational perspective*, J. Phys: Condens. Matter (2009), 21 (2009) 474219.
2. T. Roman, H. Nakanishi, H. Kasai, *Halogen-assisted Copper Atom Abstraction: A Computational Perspective*, Jpn. J. Appl. Phys. 48 (2009) 095501.
3. T. Roman, H. Nakanishi, H. Kasai, K. Nobuhara, T. Sugimoto, K. Tange, *Stability of three-hydrogen clusters on graphene*, J. Phys. Soc. Jpn. 78 (2009) 035002.
4. T. Roman, H. Nakanishi, H. Kasai, *Coadsorbed H and CO interaction on platinum*, Physical Chemistry Chemical Physics. 10 (2008) 6052.
5. T. Roman, W.A. Diño, H. Nakanishi, H. Kasai, K. Nobuhara, T. Sugimoto, K. Tange, *Identifying hydrogen atoms on graphite*, Journal of the Physical Society of Japan 76 (2007) 114703.
6. T. Roman, W. A. Diño, H. Nakanishi, H. Kasai, T. Sugimoto, K. Tange, *Hydrogen pairing on graphene*, Carbon 45 (2007) 218-220.
7. T. Roman, H. Nakanishi, W. A. Diño, H. Kasai, *Hydrogen atom quantum migration on platinum*, e-Journal of Surface Science and Nanotechnology 4 (2006) 619-623.
8. T. Roman, W. A. Diño, H. Nakanishi, H. Kasai, T. Sugimoto, K. Tange, *Realizing a carbon-based storage material*, Japanese Journal of Applied Physics, Vol. 45, No. 3A (2006) 1765-1767.
9. T. Roman, W.A. Diño, H. Nakanishi, H. Kasai, T. Sugimoto, K. Tange, *Graphite Utilization in Hydrogen Storage: A Computational Perspective*, International Journal of Energy, Environment and Economics 14 (2007) 163-171.
10. T. Roman, W. A. Diño, H. Nakanishi, H. Kasai, *Amino acid adsorption on single-walled carbon nanotubes*, Eur. Phys. J. D, 38 (2006) 117-120.
11. T. Roman, W.A. Diño, H. Nakanishi, H. Kasai, *Amino acid adsorption effects on nanotube electronics*, J. Vac. Soc. Jpn 49 (2006) 46-48.
12. T. Roman, W. A. Diño, H. Nakanishi, H. Kasai, *Glycine adsorption on single-walled carbon nanotubes*, Thin Solid Films, 509 (2006) 218-222.
13. T. Roman, W. A. Diño, H. Nakanishi, H. Kasai, Y. Miyako, N. Ando, M. Naritomi, *Examining Poly(Phenylene Sulfide) Adhesion using Cluster Models*, J. Vac. Soc. Jpn, 48 (2005) 235-237.
14. T. Roman, W. A. Diño, H. Nakanishi, H. Kasai, Y. Miyako, M. Naritomi, *PPS-metal adhesion: a density functional theory-based study*, Solid State Commun. 132 (2004) 405- 408.
15. K. Fujio, T. Roman, W. A. Diño, H. Kasai, *O_2 dissociative adsorption from the standpoint of quantum dynamics calculations*, (2009), in preparation.
16. M. David, R. Muhida, T. Roman, H.Nakanishi, W. Diño, H. Kasai, F. Takano, H.Shima, H. Akinaga, *First principles calculations-based model for the reactive ion etching of metal oxide surfaces*, Vacuum 83 (2009) 599-601.
17. N. Ozawa, T. Roman, M. David, H. Kishi, H. Kasai, *Modeling the reactive ion etching process for the CoO(001) surface via first principles calculations,* Journal of Physics: Condensed Matter 20

(2008) 355006.

18. F. Takano, H. Shima, H. Muramatsu, Y. Kokaze, Y. Nishioka, K. Suu, H. Kishi, N. B. Arboleda, Jr., M. David, T. Roman, H. Kasai, H. Akinaga, *Reactive Ion Etching Process of Transition-Metal Oxide for Resistance Random Access Memory Device*, Japanese Journal of Applied Physics 47 (2008) 6931-6933.
19. H. Kishi, N. Ozawa, M. Y. David, T. A. Roman, N. B. Arboleda Jr., W. A. T. Dino, H. Nakanishi, H. Kasai, F. Takano, H. Shima, H. Akinaga, *Density functional theory based evaluations of the reactive ion etching process model for TiO_2(anatase) thin film*, Journal of the Vacuum Society of Japan 51 No. 6 (2008) 397-400.
20. M. David, R. Muhida, T. Roman, S. Kunikata, W. A. Diño, H. Nakanishi, H. Kasai, F. Takano, H. Shima, H. Akinaga, *Applying computational nanomaterials design to the reactive ion etching of NiO thin films—a preliminary investigation*, Journal of Physics: Condensed Matter 19 (2007) 365210
21. E.S. Dy, T.A. Roman, Y. Kubota , K. Miyamoto, H. Kasai, *Exploring heme-based alternatives for oxygen reduction catalysis in fuel cells*, Journal of Physics: Condensed Matter 19 (2007) 445010.
22. N. Ozawa, N. B. Arboleda Jr, T. Roman, W. A. Diño, H. Nakanishi, H. Kasai, *Quantum states of a hydrogen atom motion on the Pd(111) surface and in the subsurface*, Journal of Physics: Condensed Matter 19 (2007) 365214.
23. N. Ozawa, N. B. Arboleda Jr., T. Roman, W. A. Diño, H. Nakanishi, H. Kasai, *Potential energy of hydrogen atom motion on Pd(111) surface and in subsurface: A first principles calculation*, Journal of Applied Physics 101 (2007) 123530.
24. N. Ozawa, T. Roman, H. Nakanishi, W. A. Diño, H. Kasai, *Quantum states of a hydrogen atom adsorbed on Cu(100) and (110) surfaces*, Physical Review B Vol.75, No.11, pp. 115421 (2007).
25. N. Ozawa, T. Roman, H. Nakanishi, H. Kasai, *Quantum states of hydrogen (H, D, T) atoms on Cu(100)*, Surface Science, Vol. 600, No. 18, pp. 3550-3554 (2006).
26. M. David, T. Roman, H. Nakanishi, H. Kasai, N. Ando, M. Naritomi, *A Density Functional Theory-Based Investigation of Adhesion of Polybutylene Terephthalate on Aluminum*, Thin Solid Films 509 (2006) 215-217.
27. M. David, T. Roman, W.A. Diño, H. Nakanishi, H. Kasai, N. Ando, M. Naritomi, *Polybutylene terephthalate adhesion on metals: a density functional theory investigation*, Journal of the Vacuum Society of Japan 49 (2006) 433-436.
28. M. David, T. Roman, W. A. Diño, H. Nakanishi, H. Kasai, N. Ando, M. Naritomi, *Polybutylene Terephthalate on Metals: A Density Functional Theory and Cluster Models Investigation*, J. Phys. Cond. Matt., 18 (2006) 1137-1142.
29. M. David, T. Roman, W. A. Diño, H. Nakanishi, H. Kasai, N. Ando, M. Naritomi, *Nanoscale understanding of the adhesion of polybutylene terephthalate on aluminum*, Surface Science 601 (2007) 5241-5245.
30. R. Muhida, A. Susanto, T. Kishi, T. Roman, H. Nakanishi, H. Kasai, *Density functional calculations for H_2 adsorption on $Fe(OH)_3$ by considering molecular orientation*, Journal of the Vacuum Society of Japan 48 (2005) 199-201.

31. M. Kisaku, M. M. Rahman, T. Roman, W. A. Diño, H. Nakanishi, H. Kasai, *Diameter size-dependent magnetic and electronic properties of single-walled carbon nanotubes with Fe nanowires*, Japanese Journal of Applied Physics 44 (2005) 882-888.
32. M.M. Rahman, M. Kisaku, T. Kishi, T. Roman, W.A. Dino, H. Nakanishi, H. Kasai, *Electric and magnetic properties of Co-filled carbon nanotube*, Journal of the Physical Society of Japan 74 (2005) 742-745.
33. R. Muhida, M. M. Rahman, M. Tsuda, T. Roman, W. A. Diño, H. Nakanishi, H. Kasai, *Change of magnetic properties of benzenes in multiple-decked sandwich clusters:* $Mn_n(C_6H_6)_{n+1}$ *(n = 1,2)*, Journal of Physics: Condensed Matter 16 (2004) S5749-S5753.

8.2. Proceedings papers

1. T. Roman, H. Kishi, H. Nakanishi, and H. Kasai, *Halogen-Based Copper Etching Dynamics: Potential Energy Surfaces*, Proceedings of the Osaka University - De La Salle University Science Research Workshops 9 (2007) 300.
2. T. Roman, H. Nakanishi, H. Kasai, *On fuel cells: H-Pt(111) revisited*, Proceedings of the Osaka University - De La Salle University Science Research Workshops 7 (2006) 148.
3. T. Roman, H. Nakanishi, H. Kasai, W. A. Diño, T. Sugimoto and K. Tange, *Controlling graphite for hydrogen storage*, Proceedings of the Osaka University - De La Salle University Science Research Workshops 3 (2004) 55.
4. T. Roman, W. A. Diño, H. Nakanishi, H. Kishi and H. Kasai, *Halogen-assisted copper atom abstraction dynamics*, Proceedings of the 9th International Symposium on Sputtering and Plasma Processes, Kanazawa, Japan (2007).
5. N. B. Arboleda Jr., H. Kasai, H. Nakanishi, T. Roman, T. Sugimoto, K. Tange, K. Nobuhara, *Pathways for H Absorption into Graphite via the Edges: A Preliminary Study*, Proceedings of the Osaka University - De La Salle University Science Research Workshops 11 (2008), in press.
6. M. David, T. Roman, W. A. Diño, H. Nakanishi, H. Kasai, N. Ando, M. Naritomi, *A study on the adhesion of polybutylene terephthalate on aluminum*, Proceedings of the Osaka University - De La Salle University Science Research Workshops 4 (2005) 12.

9 Presentations at scientific meetings (selected)

(*presenting author)

1. *T. Roman, H. Nakanishi, H. Kasai, *Hydrogen interaction with graphene and platinum*: *a computational perspective*, The 3rd UT Horiba International Symposium and The 11th ISSP International Symposium (ISSP-11) on Hydrogen and Water in Condensed Matter Physics, Seimei no mori Resort, Chiba, Japan, 2009/10/12-10/16
2. *T. Roman, H. Nakanishi, H. Kasai, K. Nobuhara, T. Sugimoto, K. Tange, *Saturating Graphene With Chemisorbed Hydrogen*, 20th European Conference on Diamond, Diamond- Like Materials, Carbon Nanotubes, and Nitrides, Athens Ledra Marriott, Athens, Greece, 2009/9/6-9/10
3. *T. Roman, H. Nakanishi, H. Kasai, K. Nobuhara, T. Sugimoto, K. Tange, *Stability of Three-Hydrogen Clusters on Graphene*, Physical Society of Japan 64th Annual Meeting, Rikkyo University, Tokyo, Japan, 2009/3/27-3/30
4. *T. Roman, H. Nakanishi, H. Kasai, *Coadsorbed H and CO interaction on Pt(111)*, The 4th Vacuum and Surface Sciences Conference of Asia and Australia (VASSCAA-4), Kunibiki Messe, Shimane, Japan, 2008/10/28-31
5. N. B. Arboleda Jr., *T. Roman, H. Kasai, H. Nakanishi, T. Sugimoto, K. Tange, K. Nobuhara, *First principles studies on the absorption of H into graphite via the armchair edge*, The 4th Vacuum and Surface Sciences Conference of Asia and Australia (VASSCAA-4), Kunibiki Messe, Shimane, Japan, 2008/10/28-31
6. *T. Roman, H. Nakanishi, H. Kasai, *A closer look at H-CO interaction on the platinum surface*, AVS 55th International Symposium and Exhibition, Hynes Convention Center, Boston, Massachusetts, USA, 2008/10/19-10/24
7. *T. Roman, H. Nakanishi, H. Kasai, *Elucidating H-CO repulsion on metal surfaces*, 11th Osaka University-De La Salle University Academic Workshop, De La Salle University-Manila, Philippines, 2008/9/1-9/3
8. *T. Roman, H. Nakanishi, H. Kasai, *Quantum simulation case studies for solid surface-bound hydrogen atom states: potential energy treatment for H on Pt*, International Conference on Quantum Simulators and Design 2008, National Museum of Emerging Science and Innovation, Tokyo, Japan, 2008/5/31-6/3
9. *T. Roman, H. Nakanishi, H. Kasai, W. A. Diño, K. Nobuhara, T. Sugimoto, K. Tange, *Discriminating hydrogen structures on graphite*, Physical Society of Japan 63rd Annual Meeting, Kinki University, Osaka, Japan, 2008/3/22-26
10. *T. Roman, H. Kishi, H. Nakanishi, H. Kasai, *Surface etching dynamics: on the vibrational heating of desorbing copper monohalides*, 2nd International Workshop on "Materials Science and Nano-Engineering", Awaji Island, Japan, 2007/12/1-5
11. *T. Roman, H. Kishi, H. Nakanishi, H. Kasai, *On the vibrational heating of desorbing etching by-products: copper monohalides*, International 21st Century COE Symposium for Atomistic

Nanofabrication Technology, Osaka University, Osaka, Japan, 2007/10/15-10/17

12. *T. Roman, H. Nakanishi, H. Kasai, *Hydrogen migration on CO-covered Pt(111),* Physical Society of Japan 62nd Autumn Meeting, Hokkaido University, Sapporo, Hokkaido, Japan, 2007/9/21-24
13. H. Kasai, *T. Roman, W. A. Diño, E. S. Dy, M. Tsuda, *Computational nanomaterials design: Recent progress in fuel cell research*, American Chemical Society 234th National Meeting & Exposition, Boston, Massachusetts, USA, 2007/8/19-8/23
14. *T. Roman, W. A. Diño, H. Nakanishi, H. Kasai, *Dynamics of halogen-assisted Cu atom abstraction from Cu(111) and CuO(100)*, IVC-17/ICSS-13 and ICN+T 2007 Congress, Stockholmsmässan, Stockholm, Sweden, 2007/7/2-7/6
15. *T. Roman, W. A. Diño, H. Nakanishi, H. Kasai, *Halogen-assisted copper atom abstraction dynamics*, ISSP 2007- The 9th International Symposium on Sputtering and Plasma Processes, Kanazawa Kokusai Hotel, Kanazawa, Ishikawa, Japan, 2007/6/6-6/8
16. *T. Roman, W. A. Diño, H. Nakanishi, H. Kasai, *Halogen-based copper/copper oxide etching*, Physical Society of Japan 2007 Spring Meeting, Kagoshima University Kohrimoto Campus, Kagoshima, Japan, 2007/3/18-3/21
17. *T. Roman, W. A. Diño, H. Nakanishi, H. Kasai, *Quantum dynamics of halogen-based copper etching*, International Conference on Quantum Simulation and Design (ICQSD2006), Hiroshima University, Hiroshima, Japan, 2006/12/3-12/6
18. *T. Roman, H. Nakanishi, H. Kasai, *The role of vacancies on hydrogen diffusion on platinum*, Vacuum Society of Japan 47th Annual Meeting, Osaka University, Osaka, Japan, 2006/11/6-11/9
19. *T. Roman, W.A. Diño, H. Nakanishi, H. Kasai, T. Sugimoto, K. Tange, *Forming groups of hydrogen on graphite*, The 10th Institute for Solid State Physics (ISSP) International Symposium, Kashiwa, Chiba, Japan, October 9-13, 2006
20. *T. Roman, H. Kasai, H. Nakanishi, *Hydrogen atom quantum scattering on platinum*, Physical Society of Japan 2006 Autumn Meeting, Chiba, Japan, September 23-26, 2006
21. *T. Roman, H. Kasai, *First-principles study of halogen-assisted atom abstraction from Cu(111)*, Physical Society of Japan 2006 Autumn Meeting, Chiba, Japan, September 23-26, 2006
22. *T. Roman, H. Nakanishi, H. Kasai, *Hydrogen atom quantum migration and scattering on platinum*, 24th European Conference on Surface Science (ECOSS24), Universite Pierre & Marie Curie, Paris, France, September 4-8, 2006
23. *T. Roman, H. Nakanishi, H. Kasai, *Hot-atom hydrogen dynamics on Pt(111)*, Physical Society of Japan 61st Annual Meeting, Matsuyama, Ehime, Japan, March 27, 2006
24. *T. Roman, H. Nakanishi, H. Kasai, *Fuel cell basics revisited: the migration of hydrogen on platinum*, The 3rd Workshop on Environment and Energy, Osaka University Nakanoshima Center, March 8-9, 2006
25. *T. Roman, W. A. Diño, H. Nakanishi, H. Kasai, *Effects of amino acid adsorption on nanotube electronics*, Vacuum Society of Japan Annual Meeting, Tokyo, Japan, November 9-11, 2005
26. *T. Roman, W. A. Diño, H. Nakanishi, H. Kasai, *Amino acids on carbon nanotubes: a first-principles examination*, International Congress on Nanotechnology, San Francisco, California, USA, October 31-November 4, 2005

27. *T. Roman, H. Nakanishi, H. Kasai, *On Fuel Cell Applications: the H-Pt(111) Case Revisited*, 4th International Fuel Cell Workshop, Kofu, Yamanashi, Japan, September 23-24, 2005
28. *T. Roman, H. Nakanishi, H. Kasai, *Fuel cell design: the diffusion of hydrogen on platinum*, Physical Society of Japan 2005 Autumn Meeting, Doshisha University Kyotanabe Campus, Kyoto, Japan, September 19, 2005
29. *T. Roman, W. A. Diño, H. Nakanishi, H. Kasai, *On the employment of nanoscale carbon-based components for biological applications: a density functional theory-based analysis*, International Symposium on the Manipulation of Advanced Smart Materials, Nara-ken Public Hall, Nara, Japan, May 26-27, 2005
30. *T. Roman, W. A. Diño, H. Kasai, *Amino acid adsorption on single-walled carbon nanotubes*, Physical Society of Japan 60th Annual Meeting, Tokyo University of Science, Noda, Chiba, Japan, March 24-27, 2005
31. *T. Roman, Melanie David, H. Kasai, W. A. Diño, H. Nakanishi, Y. Miyako, N. Ando, M. Naritomi, *A nanoscale inspection on the adhesion of some thermoplastics on aluminum*, Physical Society of Japan 60th Annual Meeting, Tokyo University of Science, Noda, Chiba, Japan, March 24-27, 2005
32. *T. Roman, W. A. Diño, H. Nakanishi, H. Kasai, Y. Miyako, N. Ando, M. Naritomi, *A closer look at poly (phenylene sulfide) adhesion onto metal surfaces*, International Workshop on Materials Science and Nano-Engineering, Osaka, Japan, December 2004.
33. *T. Roman, W. A. Diño, H. Kasai, *Glycine adsorption on carbon nanotubes: a density functional theory-based investigation*, International Symposium on Stereodynamics of Chemical Reactions 2004, Osaka University, Osaka, Japan, November 28 to December 3, 2004
34. *T. Roman, W. A. Diño, H. Nakanishi, H. Kasai, Y. Miyako, M. Naritomi, *PPS interaction with various metals: A density functional theory-based study*, Vacuum Society of Japan Annual Meeting, Osaka University, Osaka, Japan, October 27-29, 2004
35. W. A. Diño, *T. Roman, H. Nakanishi, H. Kasai, T. Sugimoto, K. Tange, *Hydrogen Interaction with Various Surfaces of Graphite*, Vacuum Society of Japan Annual Meeting, Osaka University, Osaka, Japan, October 27-29, 2004
36. W. A. Diño, *T. Roman, H. Nakanishi, H. Kasai, T. Sugimoto, *Surface-Science Based Material/Reaction Design: Storing Hydrogen in Graphite, A Case Study*, Donostia International Physics Center Workshop, "Molecule-surface interactions: elementary reactive processes", Palacio Miramar, San Sebastián, Spain, September 7–11, 2004
37. *T. Roman, W. A. Diño, H. Kasai, H. Nakanishi, *Interaction of glycine with single-walled carbon nanotubes*, Physical Society of Japan 2004 Autumn Meeting, Aomori, Japan, September 12-16, 2004
38. *Nobuki Ozawa, Tanglaw Roman, Hiroshi Nakanishi, Hideaki Kasai, *Quantum states of hydrogen (H, D, T) atoms on Cu(100) and Cu(110) surfaces*, European Conference on Surface Science, Berlin, Germany, September 2005.
39. *Nobuki Ozawa, Tanglaw Roman, Hiroshi Nakanishi, Hideaki Kasai, *Quantum states of hydrogen on the Pd(111) surface and in the subsurface*, The 24th European Conference On Surface Science, Paris, France, September 2006.

40. *Nobuki Ozawa, Tanglaw Roman, Hiroshi Nakanishi, Hideaki Kasai, *Hydrogen atom absorption and diffusion on the Pd(111) surface and in the subsurface within the framework of quantum method*, The 10th ISSP International Symposium on Nanoscience at Surfaces, Institute for Solid State Physics, Institute for Solid State Physics, Japan, October 2006.
41. *Nobuki Ozawa, Tanglaw Roman, Hiroshi Nakanishi, Wilson A. T. Diño, Hideaki Kasai, *Behavior of a hydrogen atom on the Pd(111) surface and in the subsurface*, International Conference on Quantum Simulators and Design 2006, Hiroshima University, Japan, December 2006.
42. *Nobuki Ozawa, Tanglaw Roman, Hiroshi Nakanishi, Hideaki Kasai, *A theoretical study on quantum behaviors of a hydrogen atom on the Pd and Pd alloy surfaces*, International Conference on Quantum Simulators and Design 2008, National Museum of Emerging Science and Innovation, Tokyo, Japan, May 2008.
43. *Nobuki Ozawa, Tanglaw Roman, Hiroshi Nakanishi, Hideaki Kasai, *A study of the hydrogen on Pd-Ag alloy surfaces via the first principles calculation*, AVS 55th International Symposium and Exhibition, Hynes Convention Center, Boston, USA, October 2008.
44. *Nobuki Ozawa, Tanglaw Roman, Hiroshi Nakanishi, Hideaki Kasai, *A systematic study of hydrogen atom behaviors on various Pd alloy surfaces with the aid of the first principles calculations*, The 4th Vacuum and Surface Sciences Conference of Asia and Australia, Kunibiki Messe, Shimane, Japan, December 2008.
45. *Nobuki Ozawa, Tanglaw Roman, Hiroshi Nakanishi, Hideaki Kasai, *Adsorption and diffusion of a hydrogen atom on Pd alloy surfaces via quantum manners*, International Symposium on Surface Science and Nanotechnology, Waseda University, Tokyo, Japan, November 2008.